ANALYSIS OF THE PANTOGRAPH ARCING AND ITS EFFECTS ON THE RAILWAY VEHICLE

A THESIS SUBMITTED TO
THE GRADUATE SCHOOL OF NATURAL AND APPLIED SCIENCES
OF
MIDDLE EAST TECHNICAL UNIVERSITY

BY

MUSTAFA KARAGÖZ

IN PARTIAL FULLFILLMENT OF THE REQUIREMENTS
FOR
THE DEGREE OF MASTER OF SCIENCE
IN
ELECTRICAL AND ELECTRONICS ENGINEERING

JANUARY 2014

Approval of the thesis:

ANALYSIS OF THE PANTOGRAPH ARCING AND ITS EFFECTS ON THE RAILWAY VEHICLE

submitted by MUSTAFA KARAGÖZ in partial fulfillment of the requirements for the degree of Master of Science in Electrical and Electronics Engineering Department, Middle East Technical University by,

Prof. Dr. Canan ÖZGEN
Dean, Graduate School of Natural and Applied Sciences _____

Prof. Dr. Gönül TURHAN SAYAN
Head of Department, Electrical and Electronics Engineering _____

Prof. Dr. Osman SEVAİOĞLU
Supervisor, Electrical and Electronics Engineering Dept., METU _____

Prof. Dr. Mirzahan HIZAL
Co-supervisor, Electrical and Electronics Engineering Dept., METU _____

Examining Committee Members:

Prof. Dr. Ahmet RUMELİ
Electrical and Electronics Engineering Dept., METU _____

Prof. Dr. Osman SEVAİOĞLU
Electrical and Electronics Engineering Dept., METU _____

Prof. Dr. Mirzahan HIZAL
Electrical and Electronics Engineering Dept., METU _____

Prof. Dr. Muammer ERMİŞ
Electrical and Electronics Engineering Dept., METU _____

Hüseyin MEŞE, M.Sc. in EEE
SST, ASELSAN _____

Date: 16.01.2014

I hereby declare that all information in this document has been obtained and presented in accordance with academic rules and ethical conduct. I also declare that, as required by these rules and conduct, I have fully cited and referenced all material and results that are not original to this work.

Name, Last name : MUSTAFA KARAGÖZ

Signature :

ABSTRACT

ANALYSIS OF THE PANTOGRAPH ARCING AND ITS EFFECTS ON THE RAILWAY VEHICLE

KARAGÖZ, Mustafa

M. Sc., Department of Electrical and Electronics Engineering

Supervisor: Prof. Dr. Osman SEVAİOĞLU

Co-supervisor: Prof. Dr. Mirzahan HIZAL

January 2014, 108 pages

In this work, pantograph arcing and effects of pantograph arcing on the railway vehicles are investigated. Sliding contact between the pantograph contact strips and the catenary contact wire is described with the emphasis on the pantograph arcing. Electric arc is examined in details. Arc characteristics, formation methods, extinction and reignition of the arc are studied. An experimental test setup is designed and implemented to be used in this work. Outputs of the experiments are presented and discussed. Arc models and theories are examined in details. Basic arc models in ATP-EMTP are studied and a suitable arc model for pantograph arcing is generated and validated with experimental results. Contactless inductive power transfer and usage of super capacitors in electric trains are also discussed.

Keywords: Pantograph arcing, arc discharge, railway traction system, arc model

ÖZ

PANTOGRAF ARKININ VE ONUN DEMİRYOLU ARACI ÜZERİNDEKİ ETKİLERİNİN ANALİZİ

KARAGÖZ, Mustafa

Yüksek Lisans, Elektrik Elektronik Mühendisliği Bölümü

Tez Yöneticisi: Prof. Dr. Osman SEVAİOĞLU

Ortak Tez Yöneticisi: Prof. Dr. Mirzahan HIZAL

Ocak 2014, 108 sayfa

Bu çalışmada pantograf arkları ve bu arkların demiryolu araçlarına etkileri incelendi. Pantograf kontak şeritleri ile katener kontak teli arasındaki kayan kontak pantograf arkları vurgulanarak tanımlandı. Elektik arkları detaylı bir şekilde incelendi. Bu çalışmada kullanılmak üzere bir deney düzeneği tasarlandı ve kuruldu. Deneylerin sonuçları sunuldu ve tartışıldı. Ark modelleri ve teorileri detaylı bir şekilde tartışıldı. ATP-EMTP benzetim programında temel ark modelleri incelendi ve pantograf arkları için uygun bir model yaratılarak bu model deneysel sonuçlar ile doğrulandı. Bunların yanında elektrikli trenlerde kontaksız enerji transferi ve trenlerde süper kondansatör kullanımı konuları da incelendi.

Anahtar Kelimeler: Pantograf arkları, ark deşarjları, tren çekiş sistemleri, ark modeli

to the memory of Faik Alpay Kocabıyık,

ACKNOWLEDGEMENTS

I would like to express my sincere thanks to my supervisor Prof. Dr. Osman Sevaioğlu and co-supervisor Prof. Dr. Mirzahan HIZAL for his guidance, encouragement, suggestions and support throughout the thesis study.

Also, I would like to express my gratitude to my family and friends for their encouragement and support.

TABLE OF CONTENTS

ABSTRACT ..... **V**

ÖZ ..... **VI**

ACKNOWLEDGEMENTS ..... **VIII**

TABLE OF CONTENTS ..... **IX**

LIST OF TABLES ..... **XIII**

LIST OF FIGURES ..... **XIV**

CHAPTERS

1 INTRODUCTION **1**

1.1 Electric Railway History 1

1.2 Traction Power Supply 4

1.3 Scope and Outline of the Thesis 5

2 SLIDING CONTACT **7**

2.1 Introduction 7

2.2 Pantograph 7

2.3 Overhead Contact Line 9

2.4 Interaction between Pantograph and Contact Line 9

2.4.1 Contact Force between the Pantograph and the Overhead Contact Line 9

2.4.1.1 Static Contact Force 9

2.4.1.2 Aerodynamic Contact Force 10

2.4.1.3 Dynamic Contact Force 10

2.4.2 Wave Propagation Velocity of Contact Wires and Uplift of Contact Wire Caused by Lift 10

2.4.3 Pantograph Contact Resistance 13

2.5 ICE ON THE OVERHEAD CONTACT LINE 14

2.6 PANTOGRAPH ARCING 14

3 ELECTRIC ARC 17

3.1 INTRODUCTION 17

3.2 CHARACTERISTICS OF THE ARC 17

3.3 ARC FORMATION METHODS 18

3.4 EXTINCTION OF THE ARC 19

3.4.1 Extinction of the Arc Controlled by Electrode Voltage 20

3.4.2 Blowing the Arc 20

3.4.3 Death of the Cathodic Spot 20

3.4.4 Destruction of the Arc System 20

3.5 REIGNITION OF THE ARC 21

3.6 THE ELECTRIC ARC IN AC 21

3.7 THE SWITCHING ARC 22

3.8 PANTOGRAPH ARCING 22

4 PANTOGRAPH ARCING EXPERIMENTS 25

4.1 INTRODUCTION 25

4.2 EXPERIMENTAL SETUP CONFIGURATION 25

4.3 EFFECTS OF TRANSFORMER ON THE VOLTAGE HARMONICS 29

4.4 PANTOGRAPH ARCING TESTS 30

4.4.1 Test-1 31

4.4.2 Test-2 33
4.4.3 Test-3 34
4.4.4 Test-4 36
4.4.5 Test-5 37
4.5 PANTOGRAPH ARCING TESTS DISCUSSIONS 39
4.5.1 Influence of Contact Distance 42
4.5.2 Influence of Load Current 46
4.5.3 Influence of Load Power Factor 49
5 ARC MODELS 53
5.1 INTRODUCTION 53
5.2 ARC MODELLING 53
5.2.1 Black Box Arc Models 54
5.2.2 Black Box Arc Theories 55
5.2.2.1 Slepian Theory 55
5.2.2.2 Cassie's Theory 55
5.2.2.3 Mayr's Theory 57
5.2.2.4 Cassie Mayr Theory 57
6 ARC MODEL SIMULATIONS 59
6.1 INTRODUCTION 59
6.2 ARC MODELS IN ATP-EMTP 60
6.2.1 Universal Arc Resistance Model "ZAGREB" for ATP-EMTP 60
6.2.2 Static "AirArc" EMTP Model of Long Arc in Free Air 62
6.3 MODELING OF PANTOGRAPH ARCING EXPERIMENTAL SETUP 65
6.3.1 Transformer Parameter Tests and Transformer Model 66

6.3.2 Pantograph Arc Model 69

7 FUTURE OF RAIL TRANSFER 73

7.1 INTRODUCTION 73

7.2 CONTACTLESS INDUCTIVE POWER TRANSFER 73

7.2.1 Model of Magnetic System 74

7.2.2 High Frequency Inverter 75

7.2.3 Contactless Inductive Power Transferred Trains 76

7.3 SUPER CAPACITORS IN TRAINS 78

7.3.1 Super Capacitors in Electrical Braking 78

7.3.2 Super Capacitor Train 78

8 CONCLUSION AND COMMENTS 81

8.1 CONCLUSION 81

8.2 COMMENTS 85

REFERENCES 87

APPENDICES

A CARBON DATASHEET 91

B EXPERIMENT RESULTS 93

C ZAGREB ARC MODEL 99

D AIRARC ARC MODEL 101

E MAYR ARC MODEL 103

F CASSIE ARC MODEL 105

G HYBRID ARC MODEL 107

LIST OF TABLES

TABLES

Table 1-1 Length of high speed lines in the world 3

Table 1-2 Nominal voltages and operational limits for electric railways according to 5

Table 2-1 Limits for dynamic contact forces according to EN 50119..... 10

Table 3-1 Thermoionic properties of selected materials (adopted from [22])..... 23

Table 4-1 Instruments' measurement ratios..... 26

Table 4-2 Measured parameters..... 26

Table 4-3 Harmonic contents of HV input and LV output signals of transformer 29

Table 4-4 Oscilloscope channels of measured parameters 30

Table 4-5 Test-1 parameters 31

Table 4-6 Test-2 parameters 33

Table 4-7 Test-3 parameters 34

Table 4-8 Test-4 parameters 36

Table 4-9 Test-5 parameters 37

Table 4-10 Test parameters with different contact distances..... 42

Table 4-11 Test parameters with different load currents 46

Table 4-12 Test parameters with different load power factors 49

Table 6-1 Transformer measurements and equivalent circuit parameters 69

LIST OF FIGURES

FIGURES

Figure 1-1 Berlin Trade Fair of 1879 (adopted from [2]) 1

Figure 2-1 Pantograph SSS400 (adopted from [4]) 8

Figure 2-2 Contact wire installation 8

Figure 2-3 Contact loss of pantographs (adopted from [7]) 12

Figure 2-4 Rough surfaces in contact (adopted from [8]) 13

Figure 3-1 Variation in potential with position between two electrodes in a gas which a sufficiently high current is flowing for the influence of space charge to be appreciable (adopted from [17]) 18

Figure 3-2 Static voltage-current diagram of a discharge at low pressure≈(1 mm Hg) in which the current is maintained at a given value with the aid of a current-limiting series resistance (adopted from [17]) 18

Figure 3-3 Variation in time of current and voltage between two electrodes in a gas at high pressure (≈1 Atm) shortly after breakdown has taken place (adopted from [17]) 19

Figure 4-1 Schematic of pantograph arcing experimental setup 27

Figure 4-2 Pantograph arcing test setup photographs 28

Figure 4-3 Harmonic frequency histograms of HV input and LV output of transformer .. 30

Figure 4-4 Photograph arcing experimental setup when the arc is at the corner of carbon contact strip 31

Figure 4-5 Test-1 voltage and current waveforms 32

Figure 4-6 Harmonic frequency histograms of measured voltages and current for test-1 . 32

Figure 4-7 Test-2 voltage and current waveforms 33

Figure 4-8 Harmonic frequency histograms of measured voltages and current for test-2 . 34

Figure 4-9 Test-3 voltage and current waveforms 35

Figure 4-10 Harmonic frequency histograms of measured voltages and current for test-335

Figure 4-11 Test-4 voltage and current waveforms 36

Figure 4-12 Harmonic frequency histograms of measured voltages and current for test-437

Figure 4-13 Test-5 voltage and current waveforms 38

Figure 4-14 Harmonic frequency histograms of measured voltages and current for test-538

Figure 4-15 Harmonic frequency histograms of measured currents for tests 1 to 5 39

Figure 4-16 Harmonic frequency histograms of step down transformer output voltage for tests 1 to 5 40

Figure 4-17 Pantograph arcing current of test-2 41

Figure 4-18 Arc voltage in test-2 42

Figure 4-19 Change in arc voltage (blue) due to increased contact distance 43

Figure 4-20 Harmonic frequency histograms of measured currents for Test-1, 2 & 5 45

Figure 4-21 Harmonic frequency histograms of step down transformer LV output voltage for Test-1, 2 & 5 45

Figure 4-22 Change in arc voltage (blue) due to increased load current 47

Figure 4-23 Harmonic frequency histograms of measured currents for Test-2 & 4 48

Figure 4-24 Harmonic frequency histograms of step down transformer LV output voltage for Test-2 & 4 48

Figure 4-25 Change in arc voltage (blue) due to increased load power factor 50

Figure 4-26 Harmonic frequency histograms of measured currents for Test-3 & 4 51

Figure 4-27 Harmonic frequency histograms of step down transformer LV output voltage for Test-3 & 4 51

Figure 6-1 Test circuit 61

Figure 6-2 Test circuit schematic in ATP-EMTP 61

Figure 6-3 Test circuit arc voltage and current simulation in ATP-EMTP 62

Figure 6-4 “AirArc” test circuit (adopted from [21]) 63

Figure 6-5 Representation of “AirArc” test circuit in ATP-EMTP 63

Figure 6-6 Test circuit arc voltage and current simulation in ATP-EMTP 64

Figure 6-7 Pantograph arcing experimental setup configuration used for ATP-EMTP model 65

Figure 6-8 Pantograph arcing experimental setup model in ATP-EMTP 66

Figure 6-9 Equivalent circuit of transformer with short-circuited secondary 67

Figure 6-10 Equivalent circuit of transformer with open-circuited secondary 68

Figure 6-11 Mayr’s model arc voltage in ATP-EMTP 70

Figure 6-12 Experimental arc voltage 70

Figure 6-13 Cassie’s model arc voltage in EMTP-ATP 71

Figure 6-14 Hybrid model arc voltage in ATP-EMTP 72

Figure 7-1 E-Shape Pick-Up (Flux Simulation) 74

Figure 7-2 Flat Pick-Up (Flux Simulation) 75

Figure 7-3 High frequency inverter for contactless energy transmission 75

Figure 7-4 C core transformer system induction power transfer system (adopted from [33]) 76

Figure 7-5 Structure of the Inductive Power Transfer Test System 77

Figure 7-6 PRIMOVE system (adopted from [34]) 77

Figure 7-7 Electrical drive configuration equipped with super capacitors (adopted from [37]) 78

Figure 7-8 Chinese super capacitor light train (adopted from [38]) 79

CHAPTER 1

INTRODUCTION

1.1 Electric Railway History

The first electric railway is presented at the Berlin Trade Fair of 1879 by Werner von Siemens The electric locomotive pulled a train of three small demonstration carriages around a 300-meter-long circular track at the exhibition site, running at a speed of 7 km/h [1].

Figure 1-1 Berlin Trade Fair of 1879 (adopted from [2])

In 1881, the first electric railway began commercial running in Germany [3]. By the end of the century, electric propulsion had spread to subways, elevated railways, and mining and industrial locomotives.

Originally, direct current was used for electric rail transportation. The reason why it was extremely favorable is hyperbolic traction/speed curve of the series commutator motors used as drives in railway applications. Globally, over half of all electric traction systems

still use direct current. The low voltage is a disadvantage of existing direct current traction systems as it necessitates high currents to transmit the required traction power.

At the beginning of the twentieth century, efforts were made to combine the traction advantages of the series motor with the transforming capability of alternating current. In Germany, development efforts led to a single phase AC supply with a frequency of 16.7 Hz, where the electrical energy is generated and distributed as single phase in a separate railway high voltage network. Three German traction administrations introduced this type of traction power during the years in 1912/1913. This power supply was also adopted by Austria, Switzerland, Norway and Sweden [4]. But the conversion was blocked by World War I and its aftermath [2].

Electric locomotives were much more efficient than steam locomotives and had the additional benefit of being able to produce constant pulling power even throughout serpentine routes. On the other hand, the costs of setting up the electrical system on the rail lines were high. As a result, steam locomotives dominated the tracks up to 1950s. For the same reason, electric locomotives had to compete with diesel locomotives, which still provide service today on non-electrified lines.

In 1964, Japanese National Railways started the era of high-speed railway by “Shinkansen” bullet train for 515km line between Tokyo and Osaka with a speed of 210km/h. Starting with the first Shinkansen line, high-speed rail transport speeds up and above 300 km/h. Almost all the high speed trains in the world are electric railway today.

Japanese National Railways became successful in technical, economical, and safety aspects. Then France, Germany and Italy designed their high-speed railways called “TGV”, “ICE” and “ETR” respectively in 1980-1990s. European systems are even faster (260km/h or more) and more economical than Japanese system. Japan updated his system and these European countries and Japan extended their high speed.

In 1990s, European countries began to expand their high-speed network. Meanwhile, economic growth of Asia such as Korea, Taiwan, and China let these countries to build their own high speed railways [3].

TCDD (Turkish State Railways) started an electrification program in mid 1950's. At first, the suburbs of Istanbul and Ankara have been electrified in order to renovate those lines and make a modern offer to the passengers. Then, in the mid 1980's, the program moved to main line electrification, starting with the Istanbul-Ankara line. In turkey, at the end of 2012, 3216 km (27 %) of the railway network is electrified and 457 km of it is high speed line [40].

The total length of the rail transport network is 1,370,782 km in the world in November 2011 according to International Union of Railways data. Furthermore, 17,166 km of total rail transport network is high speed lines (V>250km/h).

Table 1-1 Length of high speed lines in the world

	In operation	Under construction	Planned	Total country
Europe				
Belgium	209	0	0	209
France	1896	210	2616	4722
Germany	1285	378	670	2333
Italy	923	0	395	1318
The Netherland	120	0	0	120
Poland	0	0	712	712
Portugal	0	0	1006	1006
Russia	0	0	650	650
Spain	2056	1767	1702	5525
Sweden	0	0	750	750
Switzerland	35	72	0	107
United Kingdom	113	0	204	317
Total Europe	**6637**	**2427**	**8705**	**17769**
Asia				
China	6299	4339	2901	13539
Taiwan-China	345	0	0	345
India	0	0	495	495
Iran	0	0	475	475
Japan	2664	378	583	3625
Saudi Arabia	0	550	0	550
South Korea	412	186	49	647
Turkey	457	1396	1716	3569
Total Asia	**10167**	**6211**	**5722**	**22100**
Other countries	0	200	480	680
Morocco	0	0	511	511
Brazil	362	0	900	1262
USA				
Total other countries	**362**	**200**	**1891**	**2453**
Total World	**17166**	**8838**	**16318**	**42322**

1.2 Traction Power Supply

Electric traction has the function of safely transporting people and/or goods with the aid of electrified traction lines. The objective of the traction power supply is to ensure uninterrupted, reliable and safe operation of the electric traction vehicle. The traction power supply can be subdivided into systems of traction power generation, traction power transmission, traction power feeding and traction power collection by mobile electric traction vehicles.

To comply with the requirements for reliable operation of electric traction, the following criteria are applicable, particularly with regard to contact lines:

- The provision of uninterrupted traction power at the pantographs of the traction vehicles.
- The ability of the railway network to continuously absorb regenerated braking energy.
- Compliance with specified and standardized quality parameters for the voltages available at the pantographs of the electric traction vehicles.

Initial experience with an AC 50 Hz traction power supply was gained in Germany in 1940. As a result of progress made in the field of power electronics, AC 25kV 50 Hz traction power is the type of electricity currently preferred in countries now starting to electrify their railways or constructing new high speed lines where DC power supply has been previously used.

The most common traction power systems are;

- Direct current 600 V, 750 V, 1,5 kV, 3 kV
- Alternating current 16,7 Hz 15 kV
- Alternating current 50 Hz 25 kV

In Table 1-2 the nominal voltages are shown with their operational limits. Under normal operational conditions the voltages at the pantograph have to be between U_{min1} and U_{max2}. The duration of the voltages between U_{min1} and U_{min2} should not exceed two minutes. Furthermore, the duration of the voltages between U_{max1} and U_{max2} should not exceed five minutes.

Table 1-2 Nominal voltages and operational limits for electric railways according to EN 50163

Type of power supply	**U_n** **V**	**U_{min2}** **V**	**U_{min1}** **V**	**U_{max1}** **V**	**U_{max2}** **V**	**U_{max3}** **V**
DC 600V	600		400	720	800	-
DC 750V	750		500	900	1000	1270
DC 1,5kV	1500		1000	1800	1950	2540
DC 3,0kV	3000		2000	3600	3900	5075
AC 15kV 16,7 Hz	15000	11000	12000	17250	18000	24300
AC 25kV 50 Hz	25000	17500	19000	27500	29000	38750

U_n :Nominal voltage
U_{min2} : Lowest permanent voltage
U_{min1} : Lowest non-permanent voltage, maximum duration 2 minutes
U_{max1} : Highest permanent voltage
U_{max2} : Highest non-permanent voltage, maximum duration 5 minutes
U_{max3} :Highest long-term overvoltage, a duration more than 20 ms

1.3 Scope and Outline of the Thesis

In this thesis, pantograph arcing and effects of pantograph arcing on the railway vehicles are investigated. A test setup is designed and implemented to understand the pantograph arc phenomena, effects of important parameters like contact distance, load current and power factors on the pantograph arcing and effects of pantograph arcing on the traction system. A pantograph arc model is generated in Alternative Transients Program version of the ElectroMagnetic Transients Program (ATP-EMTP) and validated with the experimental results.

This thesis contains eight chapters. In the second chapter, sliding contact between the pantograph and the catenary contact wire is examined in details. In addition, ice on the contact line and pantograph arcing is discussed.

To understand the pantograph arcing, arc phenomena must be discussed first. In the third chapter, electric arc is examined. Arc characteristics, formation methods, extinction and reignition of arc are studied. Furthermore, electric arc in AC and switching arc are also discussed.

Because of the limitations of railway test facilities, a scaled test setup is designed and implemented to understand the effect of pantograph arcing on the railway vehicles. In the

fourth chapter, pantograph arcing experiments which are conducted with the pantograph arcing test setup, are presented. Firstly, the test setup is described and then the outputs of the experiments are presented and discussed.

Arc model simulations are used for circuit breakers. Since there are different arc models, generating a suitable arc model for pantograph arcing and verifying it with experimental results are useful for power system transient analysis of the electrified trains. In the fifth chapter arc models and theories are examined in details. In the sixth chapter, basic arc models in ATP-EMTP are examined firstly. Later a suitable arc model for pantograph arcing is generated and validated for experimental results.

In the seventh chapter, as the future of the rail transfer, contactless inductive power transfer and super capacitors in electric trains are discussed in details.

The last chapter is a concluding chapter.

CHAPTER 2

SLIDING CONTACT

2.1 Introduction

Power delivery to moving loads usually includes sliding contact by metal-to-metal and carbon brush connection or trailing cable. Problems with the moving components result from wear exposed live conductors, loss of good connection, and thermal cycling [5].

The sliding contact between pantograph and overhead contact wire is a critical interface between train and infrastructure in an electrified railway. As well as requiring correct tensioning and geometry, it is necessary to eliminate imperfections and obstruction from the contact wire. Such discontinuities can be developed due to various reasons and may lead to pantograph arcing [6].

In this chapter, sliding contact between the pantograph and the catenary contact wire is examined in detail. In addition, ice on the contact line and pantograph arcing is discussed.

2.2 Pantograph

The purpose of the pantograph is to transfer power from the contact line to the electric traction unit. The transfer of the power has to be safe and reliable both in a stationary condition for auxiliary and convenience power and for motive power to the operation of the traction vehicle.

The parts of the pantograph are shown in Figure 2-1. The pantograph consists of a main frame, an arm, a pantograph head and a drive.

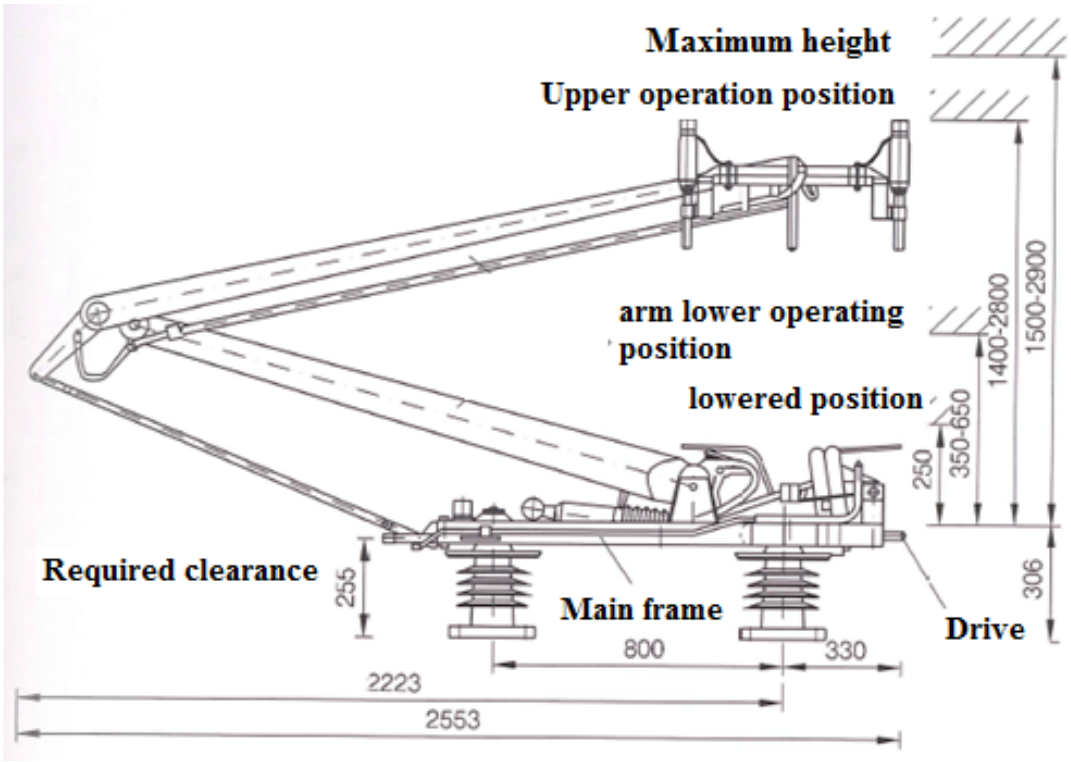

Figure 2-1 Pantograph SSS400 (adopted from [4])

To ensure uniform and low wear of the pantograph collector strips and the contact wire, the contact wire has to be installed with a lateral offset to the projected track centre line. A sample contact wire installation is shown in Figure 2-2.

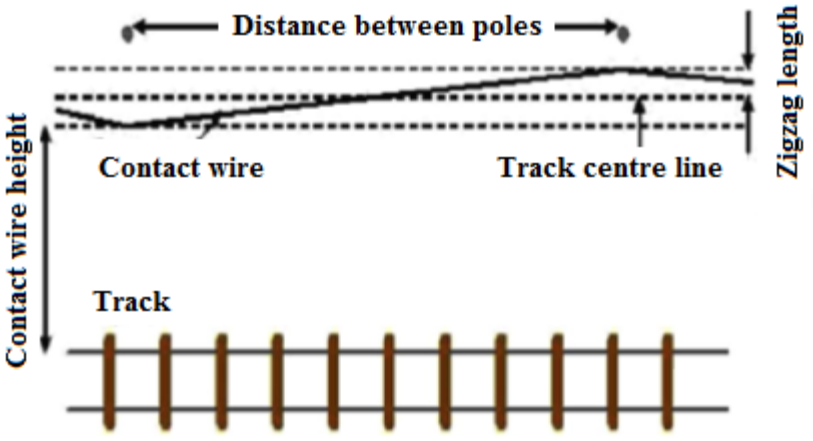

Figure 2-2 Contact wire installation

The collector strips are part of the collector head and directly contact to the contact wire to transfer the power. The collector strips have to be selected and designed to cope with the requirements of current transfer when the vehicle is both running and standstill. In modern trains, the power requirement for convenience and auxiliaries reaches up to 1,000 kVA. This power has to be safely transferred through the pantograph on a vehicle at standstill.

2.3 Overhead Contact Line

For safety reasons, only overhead contact lines are permitted for operation at voltages above AC 1000 V and DC 1500 V. For high running speeds, especially above 100 km/h, energy transmission becomes an increasingly challenging task.

The main purpose of the contact line is to act as a contact slide ensuring uninterrupted transmission of electrical energy to the collectors on a train's pantograph.

High conductivity, tensile strength, hardness and ability to withstand temperature changes and corrosion make electrolytic copper and copper alloys as a global contact wire materials. When copper exposed to air, forms a hard but conductive oxide layer. However aluminum forms an oxide layer of poor conductivity. Therefore all attempts to use aluminum as contact wire material have failed.

Among other factors, the combination of contact materials used for collector strips and contact wires affects the rate of wear of these components. The lowest rates of wear are achieved using a combination of copper contact wire with carbon collector strips. Steel and copper collector strips lead to considerably higher rates of wear [4].

2.4 Interaction between Pantograph and Contact Line

2.4.1 Contact Force between the Pantograph and the Overhead Contact Line

2.4.1.1 Static Contact Force

The static contact force is the force exerted by the collector strips due to the force applied by the pantograph drive on the overhead contact line, measured at a stationary traction unit. To achieve the most consistent working conditions, this should be as equal as possible throughout the entire working range of the pantograph during both upward and downward movements.

2.4.1.2 Aerodynamic Contact Force

The sum of the static contact force and the component resulting from running speed which depends on the aerodynamic effects is designated as the aerodynamic contact force.

2.4.1.3 Dynamic Contact Force

The sum of the aerodynamic contact force and the dynamic components from the interaction between the overhead contact line and the pantograph is designated according to EN 50206-1 as the dynamic contact force. This depends on the speed, the dynamic properties of the overhead contact line, the pantographs and the number of lifted pantographs on a train and their spacing.

Irregularities in the overhead contact line create peaks in the dynamic contact force. The quality of the contact between the overhead contact line and the pantograph can be assessed by dynamic contact forces or by the number and duration of arcs. To avoid arcs and also to limit the uplift of the contact line and wear of components, the dynamic contact forces should comply with the requirement stipulated in the TSI Energy for high-speed lines, in EN 50367 for lines traversed with speeds of 160 km/h and above and in EN 50119 as shown in Table 2-1. The dynamic contact force should be high enough to prevent arcing but also be as low as possible to keep the contact wire uplift minimum and to avoid unnecessary dynamic excitation of the contact line.

Table 2-1 Limits for dynamic contact forces according to EN 50119

System	Speed in km/h	Contact forces in N	
		Minimum	Maximum
AC	≤200	positive	300
AC	>200	positive	350
DC	≤200	positive	300
DC	>200	positive	400

2.4.2 Wave Propagation Velocity of Contact Wires and Uplift of Contact Wire Caused by Lift

When the train approaches wave propagation velocity, the uplift and detachment of pantograph will increase and power transfer becomes difficult. In [7], the contact wire is considered as an elastic supporting-floor and the uplift y_0 of contact wire at the pantograph point is given as

$$y_0 = \frac{P_0}{2\sqrt{k_0 T}\sqrt{1-(V/C)^2}} \tag{2.1}$$

$P_0: The\ lifting\ fource\ of\ the\ pantograph\ at\ stop.$

$T: Tension\ of\ the\ contact\ wire.$

$V: Train\ speed.$

$C: Wave\ propagation\ velocity\ of\ the\ contact\ wire.$

$k_0: Equivalent\ spring\ constant\ of\ the\ elastic\ supporting\ floor.$

As it is seen from the given formula the uplift of the contact wire gets bigger when V approaches the wave propagation velocity of the contact wire. Therefore, type of the wire limits the maximum train speed.

When the pantograph is moving at speed V, the lifting force P of the pantograph can be expressed as

$$P = P_0 + \alpha V^2 \tag{2.2}$$

$P_0: The\ lifting\ fource\ of\ the\ pantograph\ at\ stop$

$\alpha: lift\ coefficient$

Figure 2-3 indicates the measured results of contact losses the CS (composition of copper and steel) and TA (composition of aluminum and steel) contact wires. The measurements are conducted during the high-speed test of test train STAR 21 in 1993 in Japan. The test train has two pantographs. The pantograph of the No. 7 car which is the leading pantograph and the pantograph of the No. 1 car is the rear pantograph. Contact loss of the No. 1 car is larger than the No. 7 car since the rear pantograph has been influenced by the contact line oscillation excited by the leading pantograph.

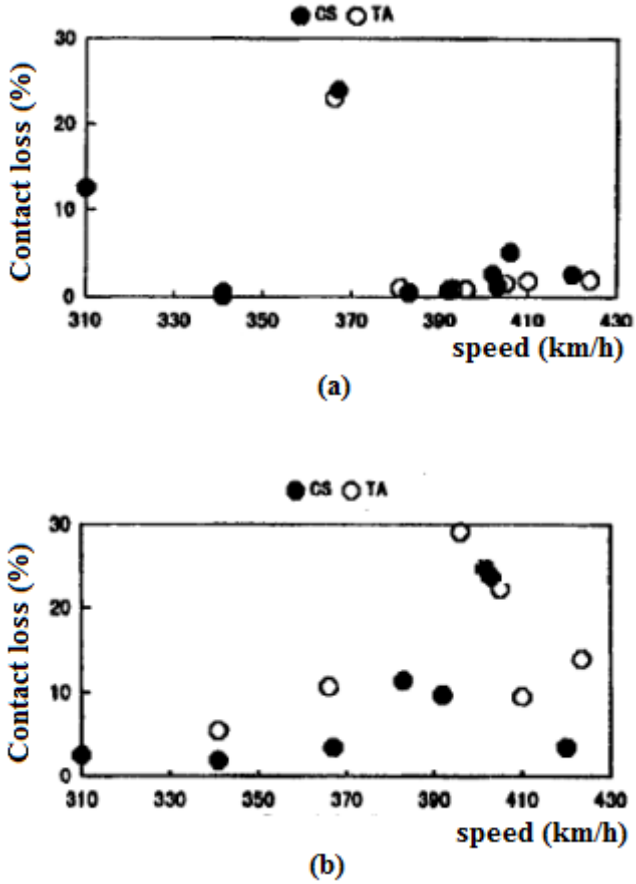

Figure 2-3 Contact loss of pantographs (adopted from [7])
(a) leading pantograph (b) rear pantograph

The interaction between the overhead contact wire and the contacts of a pantograph determines the quality and reliability of the energy transmission to traction units. This interaction depends on the design of the overhead contact line and the pantograph. High speed trials have shown that the pantograph-contact line interaction is of extreme importance because energy transmission is a factor that could limit the maximum speed achieved. In May 1991, an SNCF train of an enhanced TGV-Atlantique type achieved a speed of 515 km/h and set a world speed record for railway vehicles. During preparatory runs the importance of the contact line design became apparent. The trial had to be aborted a speed of approximately 480 km/h due to current interruptions caused by contact wire uplift values of more than 300mm [4]. Pantograph arcing causes interruption of the power supply because of this wire uplift.

2.4.3 Pantograph Contact Resistance

When two surfaces are in contact, the real contact area is much smaller than the nominal one. The contact occurs in a finite number of asperities that are subjected to an elastic, plastic or combined elastic-plastic deformation depending on the normal pressure value, the superficial roughness and the material properties [8], [9], [10].

Real contact area, the total area of micro contacts, is a small fraction of the nominal area, usually a few percent. Macro contact area is formed as a result of surface curvature of the bodies in contact. These micro and macro contacts can be shown in Figure 2-4.

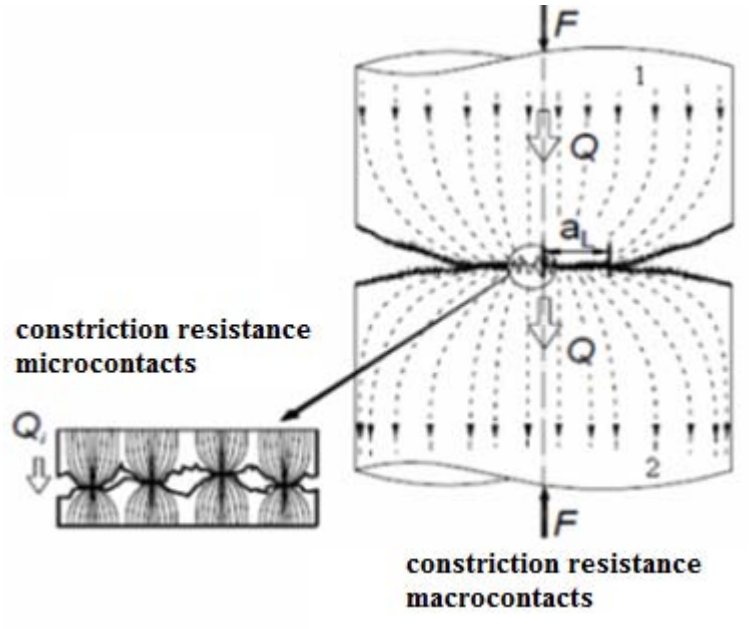

Figure 2-4 Rough surfaces in contact (adopted from [8])

The proper balance between the dynamic characteristics of the pantograph and the contact line depends on the quality of current collectors and on the longevity of the contact wire and inserts. The pantograph must support them with sufficient force to remain in permanent contact with the wire, but not unduly rise which would loose contact after the points of attachment [8].

The estimation of contact wire wear must take into account in the variation of electrical contact resistance together with radius of contact spots and contact force. The increasing contact force reduces the contact resistance and arcing but increases the plate and wire wear rate. The experimental results of [8] and [11] also support this idea.

At increasing walking speed, the separation of the wire from pantograph occurs more frequently which leads to an increase in the contact resistance and arcing. Therefore the contact resistance and arcing increases with the speed of the train. In [12], an experimental setup is used to measure the contact resistance between pantograph and catenary. It is demonstrated that the static contact resistance decreases with the contact force and increasing current. When the contact force becomes larger, the radius of contact spots increase and the contact resistance gets smaller. Also the generation of heat which increases with the traction current, makes the material softer.

2.5 Ice on the Overhead Contact Line

Similarly with overhead transmission line conductors, ice layers with thicknesses up to ten millimeters can be formed on the conductors of overhead traction lines. Ice accretion affects the operation only where the headway between trains with pantographs in contact is more than 15 min. For instance, line without traffic during the night time can accumulate ice of magnitude that would result in disturbing effects.

At temperatures below freezing point hoar frost can form on the conductors when enough moisture is in the air and wind is blowing against the lines. Also super-cooled rain and wet snow can lead to serve ice accretion on the conductors.

2.6 Pantograph Arcing

Arcing from pantograph is commonly observed throughout the year. However, factors like the increase in the train speed, current and especially cold weather conditions contribute in increasing the visibility of the pantograph arcing.

Because of the irregularity of catenary and tracks, the vibration between catenary and pantograph and other factors during the process of power supply, it is inevitable that pantograph will separate from the contact wire. The separation of pantograph and contact wire will lead to pantograph arcing, and simultaneously it will cause the current flowing through the locomotive equipment become discontinuous. On one hand, wear of pantograph strip and catenary wire increases significantly [12], [13].

The ice accretion on contact wires forms an insulating layer which cannot be penetrated by the pantograph. However, the current will not be completely interrupted but flows across arcs between the contact wire and the collector strips and causes erosion and current burn marks at the edges of the contact elements on the contact wire and the collector strips.

The pantograph arc current generates significant low and high frequency current components because of the arc nonlinearity [14]. Pantograph arcing causes radiated interference with the wireless and radio communication services. It also causes conducted interference with railway signaling systems, power supplies and nearby grounded structures through its return path [15]. Saturation of the transformer core is another consequence of pantograph arcing.

The Swiss railways are electrified with 16.7 Hz and are equipped with 100 Hz track circuits. During winter time, Swiss railways have severe problems due to the fact that the existence of a DC current component also leads to even harmonics. In Denmark, during the winter 2001-2002, the operation with new EMUs had to be cancelled at some occasions. The similarity of these trains is that they are equipped with a DC supervision system. At conditions with ice on the contact line, this system reacted and stopped the EMUs [16].

CHAPTER 3

ELECTRIC ARC

3.1 Introduction

Although all gases are normally good electrical insulators, it is well known that the application of a sufficiently high electrical field may cause breakdown of the insulating properties leading to large currents passing through the gas. The phenomena associated with the passage of the current, which is called an electrical discharge through the gas, depend markedly on the nature and pressure of the gas, on the materials of which the electrodes are made, on the geometry of the electrodes and of any containing vessel, and on the magnitude of the current flowing. Various types of discharges with characteristics features are given special names, like dark discharge, corona discharge, glow discharge, and so on. However, if the current is made sufficiently high then, under a very wide range of conditions, discharges are obtained having in common certain important characteristic features which allow them all to be included within a single classification as arc discharges [17].

To understand to pantograph arcing, arc phenomena must be discussed first. In this chapter, electric arc is examined in detail. Arc characteristics, formation methods, extinction and reignition of arc are worked. Finally, electric arc in ac and switching arc are discussed.

3.2 Characteristics of the Arc

In any self-sustained discharge carrying a current of more than a few μA the potential gradient between the electrodes is not uniform. As Figure 3-1 illustrates, there are sharp drops in potential near the electrodes, known as the cathode and anode falls, the former being often much larger than the latter. The existence of the electrode falls is due to space charge accumulations associated with the conditions required for the passage of a current across the junction between a metallic and a gaseous conductor.

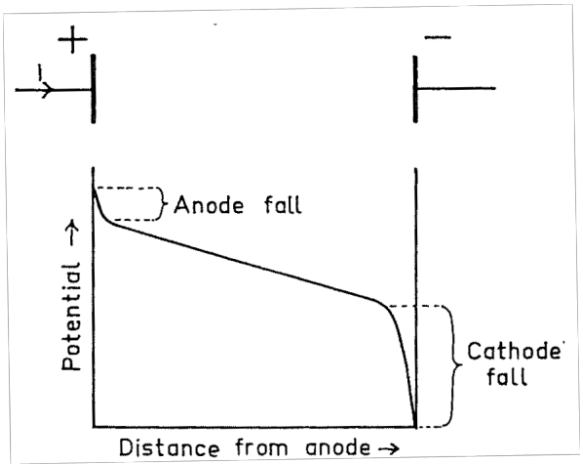

Figure 3-1 Variation in potential with position between two electrodes in a gas which a sufficiently high current is flowing for the influence of space charge to be appreciable (adopted from [17])

3.3 Arc Formation Methods

Formation of an arc may be in several ways. First of all, an arc may be formed by a continuous or discontinuous transition from a lower current stable discharge such as glow. The steps of transition of discharge which leads to an arc are given in Figure 3-2. This diagram is applicable to a discharge between electrodes a few centimeters apart in a tube of a few millimeters of mercury.

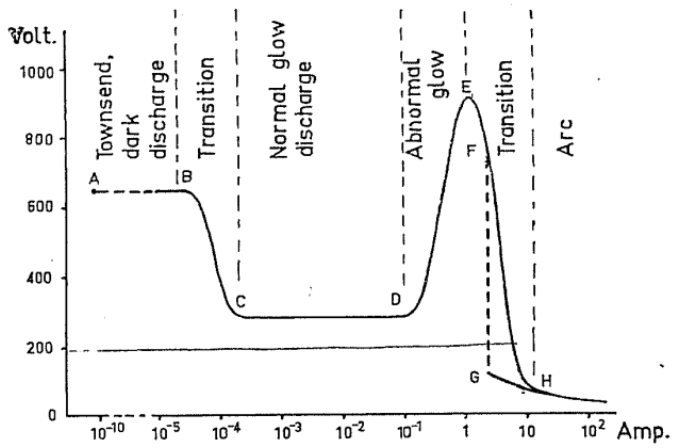

Figure 3-2 Static voltage-current diagram of a discharge at low pressure (≈1 mm Hg) in which the current is maintained at a given value with the aid of a current-limiting series resistance (adopted from [17])

Secondly, an arc may be formed transient from a non-steady spark discharge. Under a pressure of the order of an atmosphere, initiation of a discharge between electrodes by a voltage source capable of breaking down the gap and maintaining a current sufficient for an arc is formed in this way. Before the arc is formed, no stable form of discharge exists. In addition, if the voltage source could not maintain the arc current, the discharge would extinguish. The voltage and current variation of the arc which is formed in this way is presented in Figure 3-3. The voltage collapses suddenly from a value close to the breakdown voltage in a time of the order of 10^{-8} seconds, after which a step may or may not be exist. By about 10^{-6} seconds the voltage is only some tens of volts and thereafter a steady state is gradually approaches, full equilibrium not being attained until the electrodes and the vessel reach thermal equilibrium, a process which may take minutes.

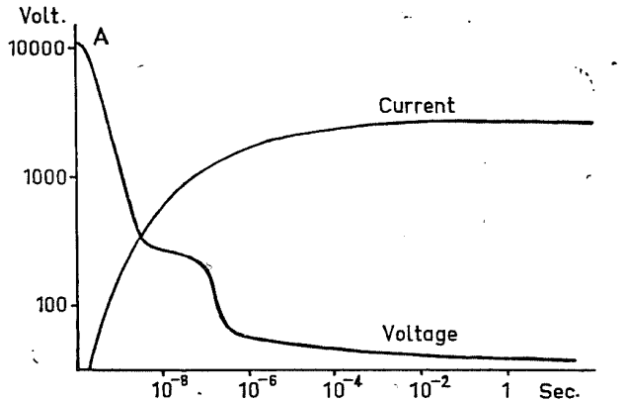

Figure 3-3 Variation in time of current and voltage between two electrodes in a gas at high pressure (≈1 Atm) shortly after breakdown has taken place (adopted from [17])

In Figure 3-3, "A" represents the beginning of the sudden voltage collapse. There may be a relatively long time interval (time lag) between the initial breakdown and the start of the collapse at A. The non-stable discharge, beginning at "A", is called a spark.

Thirdly, an arc may be formed by drawing apart two current carrying electrodes in contact. In this way the ordinary breakdown of the gas between the electrodes becomes unnecessary. Therefore, the voltage source need not be large enough to cause breakdown.

3.4 Extinction of the Arc

The problem of getting rid of an arc, whether it is totally undesirable one like in switching processes or a useful one which has completely fulfilled its purpose and cannot be any further use, is a major problem.

3.4.1 Extinction of the Arc Controlled by Electrode Voltage

This is a natural way of extinguishing an arc. The effect of a lowering in voltage is in general a lowering current. At some voltage, the arc becomes incapable of sustaining itself. Beyond this point and apart from a possible reignition, any further evolution of the voltage between electrodes is in general irrelevant. Whether it goes smoothly to zero, gets reversed, or starts increasing again is unimportant. However, it would be a mistake to consider that there is no plasma any more between the electrodes. Actually, there may still be an appreciable density of charge carrier for some time because of the recombination phenomena. On the other hand, in general, even if strong voltages are reapplied whether direct or reversed the arc does not reignite.

It should be considered that normal behaviour of an arc, the voltage of which has been once lowered below a critical threshold, is to decay completely.

3.4.2 Blowing the Arc

It is known in literature that an arc can be extinguished as a result of some kind of lateral force increasing the length of the arc to such a value that the power supply cannot do it anymore.

3.4.3 Death of the Cathodic Spot

In arcs at relatively low currents in which there is only one cathodic spot, it seems that extinction is possible for purely statistical reasons. A cathodic spot has at each moment a certain probability (infinitesimal in normal conditions) of getting spontaneously extinct. In an arc with many cathodic spots, individual spots appear and disappear without the general stability of the arc being significantly affected. This is not true anymore if there is only one spot and no special precaution is taken for arc maintenance, because if the spot dies, the arc can die also.

3.4.4 Destruction of the Arc System

An arc can become extinguished as a result of the system in which it was created becoming inadequate, due to either of damage caused by the arc itself, or of modifications voluntarily introduced. A major practical cause of this nature is the total destruction of the cathode by evaporation, erosion, or any other processes.

3.5 Reignition of the Arc

There are two major types of reignition, depending upon whether the reignition arises from the resurrection of a pre-existing cathodic spot or the birth of a new one. The second case is, of course, the absolute rule for reignition with an inversion of polarity.

Cathodic spots, whose mechanism is purely or essentially thermo-electronic, reignite on carbon electrode, for instance, with the greatest ease with time constants characteristics of the thermal transfer. Obviously in such a case, reignition is easy as long as the temperature is still above a certain threshold when the conditions favorable to the reignition of an arc are restored. As the hot spot cools down, it is observed that the reignition becomes less and less easy (is characterized by higher and higher voltage peaks during the transient) until the conditions become essentially those of a first ignition.

The generation of a new spot does not differ in principle from a first ignition, except that the extinguished arc may create circumstances which favor new births. For instance, an electrode can be considerably hotter after the arc has operated for some time than it was before the first ignition.

3.6 The Electric Arc in AC

When an electric arc is inserted in an ac rather than dc circuit, a question immediately arises whether the arc rectifies or not.

Reignition at the new cathode is, in general, helped considerably by the heat liberated at the old anode since they are one and the same surface. The importance of the reignition peaks depends considerably upon the time during which the arc is extinct as compared to the thermal time constants of electrode cooling.

The conditions in the case of reignition of a self-sustained discharge by an alternating potential are vastly unlike those existing in the case of the original breakdown of the gap. First, the number of the free ions, both positive and negative ions and electrons, is very much larger than in the fresh gas; second, after one-half cycle of arcing the gas temperature will be considerably higher than it was initially; third, the active portion of the electrodes will be heated, the extent of this heating depends on the current of the discharge; fourth, under certain conditions considerable electrode material will be vaporized into the gas region [19].

The degree of ionization at zero current is a direct function of the arc current. In the absence of a reappearing voltage, the ionization when the current is low will quickly disappear by recombination in the gas and neutralization at the electrode surfaces. For

higher values of current, the volume deionization will be slower, because in the presence of thermal ionization, deionization will proceed at a much slower rate, determined by a time constant characteristic of the gas. Obviously, in the case of small current arcs, the reapplied voltage must be very much higher or must be applied at a much higher rate than those for heavy currents if deionization is to be arrested [19].

3.7 The Switching Arc

The electric arc between the pantograph contact strips and the overhead line is similar to the electric arc in a circuit breaker. In both situations the electric arc is formed by separation of the contacts. Although there are lots of researches and experiments on the electric arc in a circuit breaker, there are a few researches on the pantograph arcs. Therefore, previous studies on the electric arc in circuit breakers may be useful to understand the pantograph arcing.

3.8 Pantograph Arcing

A metal contains mobile electrons in a partially filled band of energy levels—*i.e.*, the conduction band. These electrons, though mobile within the metal, are rather tightly bound to it. The energy that is required to release a mobile electron from the metal varies from about 1.5 to approximately 6 electron volts, depending on the metal. In thermionic emission, some of the electrons acquire enough energy from thermal collisions to escape from the metal. The number of electrons emitted and therefore the thermionic emission current depend critically on temperature [21]. The work function of the metal which is the required energy to remove an electron from the metal denoted W, and it is expressed in joules (eV).

Richardson's law is almost valid for all metals. It is usually expressed in terms of the emission current density (*J*) as

$$J = AT^2 e^{-W/kT} \tag{3.1}$$

in amperes per square meter. The Boltzmann constant "k" has the value 8.62 10^{-5} electron volts per Kelvin, and temperature "T" is in Kelvin. "*A*" is the Richardson constant expressed in $A.m^{-2}K^{-2}$. In theory, the Richardson constant would be equal to 1.2 $MA.m^{-2}K^{-2}$, but in practice, because the work function is also a function of temperature, "*A*" varies over a wide range of magnitude.

Table 3-1 Thermoionic properties of selected materials (adopted from [22])

Material	**Electron work function (W/eV)**	**Richardson constant ($A/kA.m^{-2}.K^{-2}$)**
Carbon	5.0	150
Copper	4.65	1200

When the electron work function and Richardson constants of pantograph contact strip material carbon and overhead contact line material copper compared, it can be said that emission current density of copper is higher than carbon. Therefore, it is easier to liberate electrons from the copper.

CHAPTER 4

PANTOGRAPH ARCING EXPERIMENTS

4.1 Introduction

Electric railway history, sliding contacts and arc characteristics are examined in the previous chapters. Because of the limitations of railway test facilities, a scaled test setup is designed and implemented to understand the effect of pantograph arcing on the railway vehicles. In this chapter pantograph arcing experiments which are conducted with the pantograph arcing test setup, are presented. Firstly, the test setup is described and then the outputs of the experiments are presented and discussed.

4.2 Experimental Setup Configuration

Pantograph arcing experimental setup configuration is shown in Figure 4-1. A brass contact line which is fixed around a wheel is used to simulate the overhead contact line and a carbon strip is used for pantograph contact strip. The setup is designed and implemented to simulate the interaction between a pantograph and over head contact line as similar as the real case. Since the over head contact line is installed with a lateral offset to the projected track centre line, the speed of pantograph has two components, one of them is on longitudinal axis and the other one is on latitudinal axis. Therefore, there are two electric motors in the test setup. One of them is connected to center of the wheel and the other one to the carbon strip with belt-pulley systems. The belt-pulley system of the wheel has four pulleys with different diameters so the speed of the wheel can be arranged. The speed of the motor which drives carbon strip laterally is controlled by a motor controller unit.

In the experimental setup, a rigid carbon strip is used as a pantograph contact strip. The datasheet of the carbon is given in Appendix A.

The high voltage is supplied from a 100V/15000V step-up transformer. The transformer voltage is controlled by a variac which is integrated into the control unit of the high voltage supply. The output voltage of the step up transformer is measured with a resistive voltage divider to arrange the input voltage. Also two capacitive voltage dividers are used

in the test setup. Divider-1 is used to measure the voltage of the contact line and the other one, divider-2, is used to measure the voltage of the carbon strip. In this way, the voltage difference of these two capacitive dividers gives the arc voltage. Furthermore a 10 Ω current shunt resistor is used to measure the current circulated in the circuit. A 15000V/100V step-down transformer which simulates the train transformer, is fed from the carbon strip. An adjustable load is connected to the low voltage side of this step-down transformer. The power factor of load can also be arranged.

A four channel 300 MHZ, 2.5 GS/s digital oscilloscope is used for the voltage and current measurements. The capacitive dividers are designed with a 149 ratio. However, they are calibrated with the help of a high voltage probe and oscilloscope which are both have a valid calibration certificate. The measurement ratios of the instruments are given in Table 4-1. During the tests, the parameters given in Table 4-2 are measured with the oscilloscope.

Table 4-1 Instruments' measurement ratios

Instrument	**Measurement ratio**
Divider-1	147
Divider-2	149
Current Shunt Resistor	0.1 A/V

Table 4-2 Measured parameters

Measured Parameters	**Instrument**
Step-up transformer HV side voltage	Divider-1
Carbon strip voltage	Divider-2
Current	Current shunt resistor
Step-down transformer LV side voltage	Low voltage probe

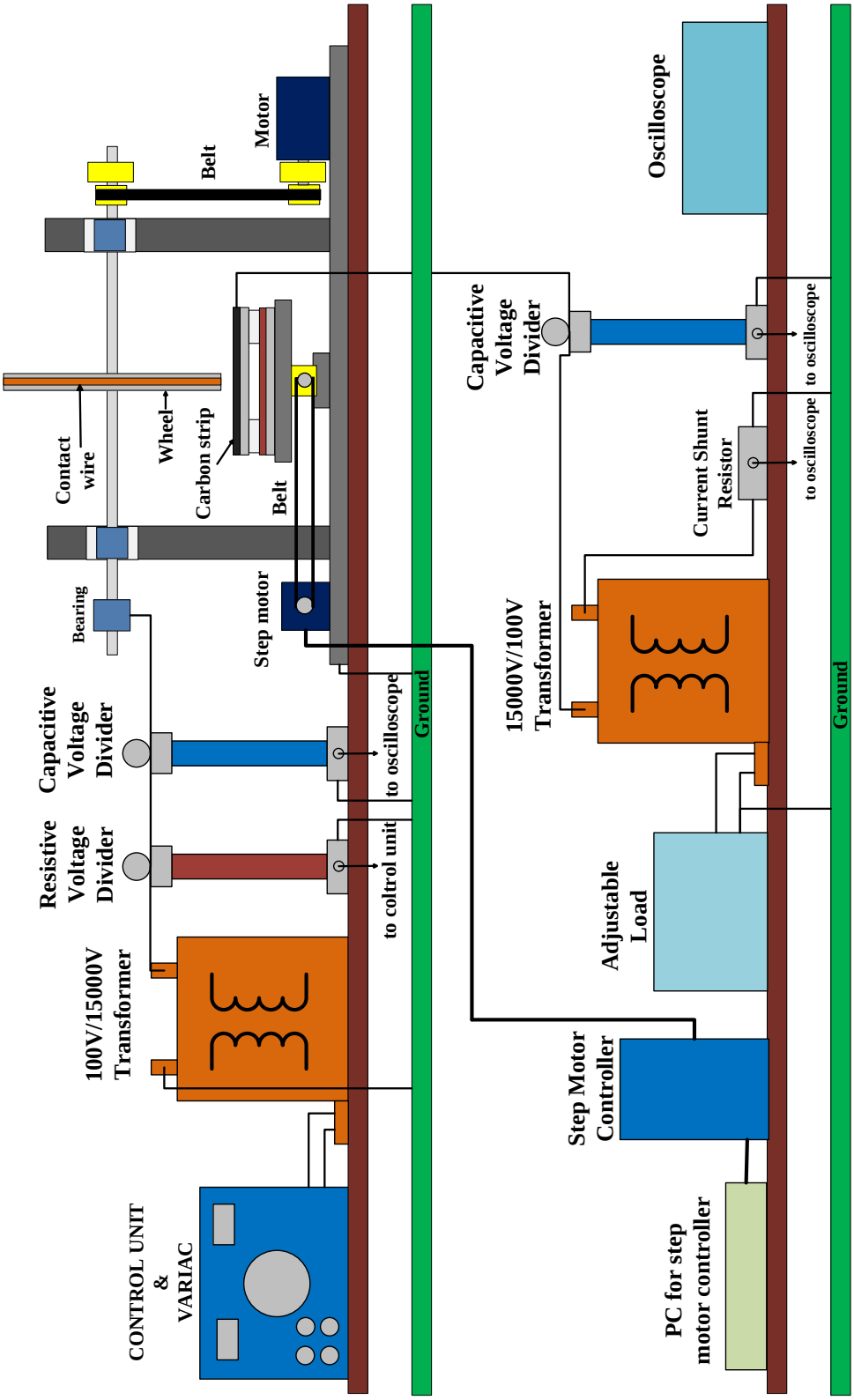

Figure 4-1 Schematic of pantograph arcing experimental setup

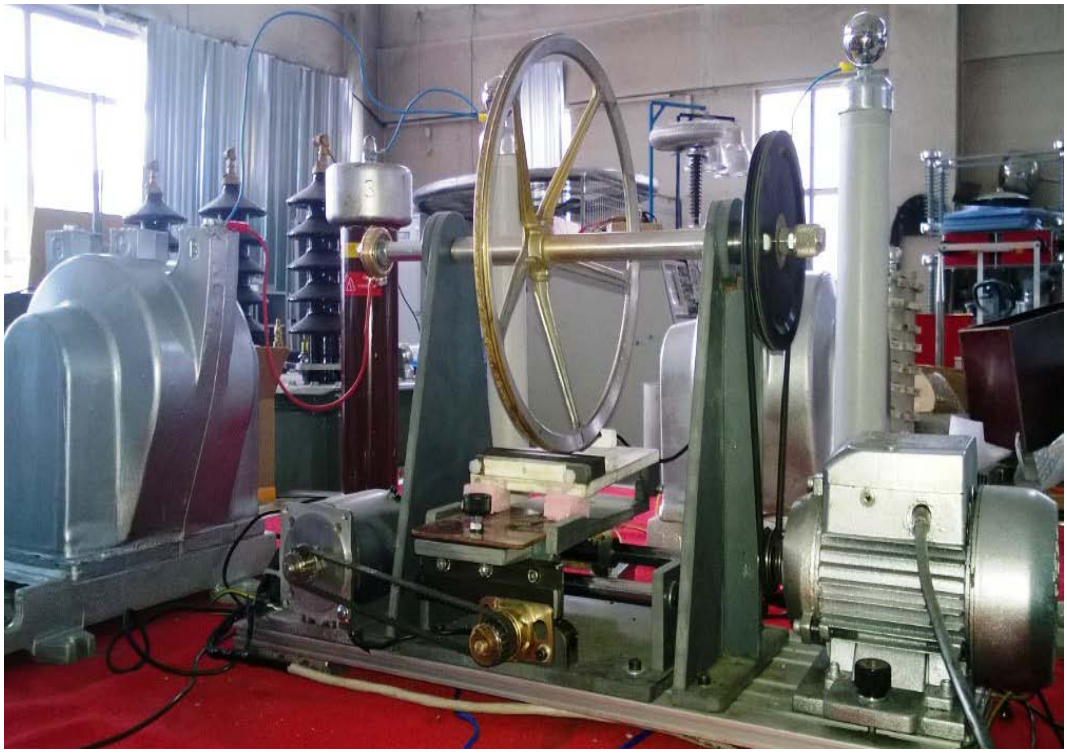

Figure 4-2 Pantograph arcing test setup photographs

4.3 Effects of Transformer on the Voltage Harmonics

To understand the effects of transformer on the voltage, the harmonic contents of the HV input and LV output of the step down transformer is compared using FFT function of the oscilloscope.

The amplitudes of harmonics are given in Table 4-3. In addition, the harmonic frequency histograms of HV input and LV output of transformer are shown in Figure 4-3. Comparing the harmonics of both side of transformer, it can be said that transformer has very little influence on the harmonic content of voltage.

Table 4-3 Harmonic contents of HV input and LV output signals of transformer

	Harmonic content of HV input		Harmonic content of LV output	
Frequency (Hz)	Amplitude (V)	Relative Amplitude	Amplitude (V)	Relative Amplitude
50	66.42	1.00	63.58	1.00
150	0.97	0.02	0.97	0.02
250	0.44	0.01	0.43	0.01
350	0.85	0.01	0.78	0.01
450	0.60	0.01	0.55	0.01
550	0.32	0.01	0.30	0.01
650	0.16	< 0.01	0.14	< 0.01
750	0.28	< 0.01	0.27	< 0.01
850	0.13	< 0.01		

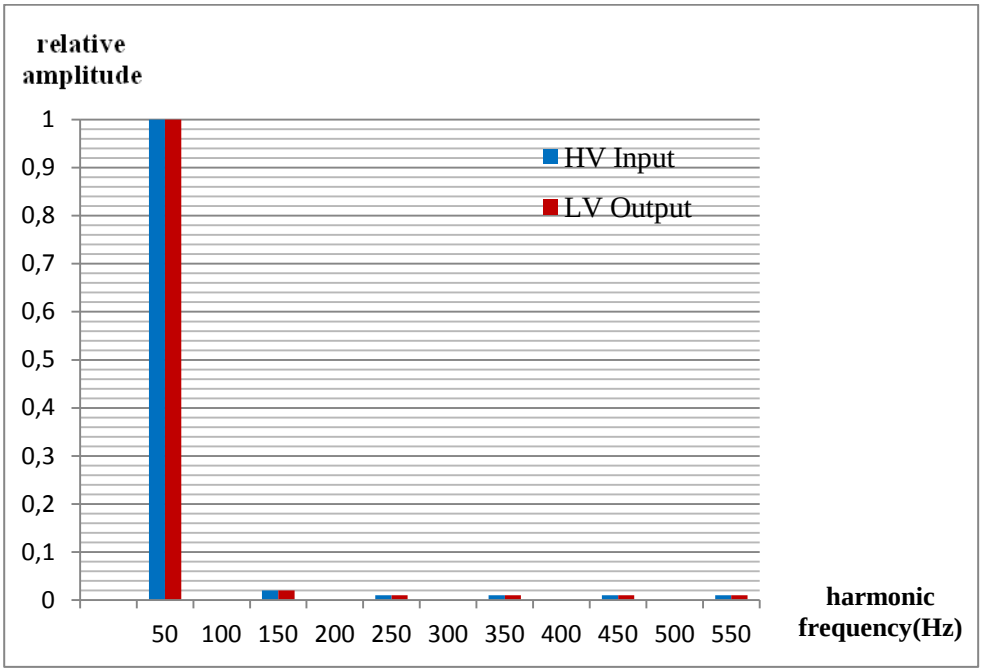

Figure 4-3 Harmonic frequency histograms of HV input and LV output of transformer

4.4 Pantograph Arcing Tests

Throughout this work, the oscilloscope channels which are given in Table 4-4 are used unless otherwise is specified.

Table 4-4 Oscilloscope channels of measured parameters

Measured Parameters	Instrument	Oscilloscope Channel
Step-up transformer HV output voltage /149	Divider-1	CH1
Carbon strip voltage / 149	Divider-2	CH2
Arc voltage / 149	Oscilloscope Math function (Divider1-Divider2)	M (CH1-CH2)
Current * 10 V/A	Current Shunt Resistor	CH3
Step-down transformer LV output voltage	Oscilloscope voltage probe	CH4

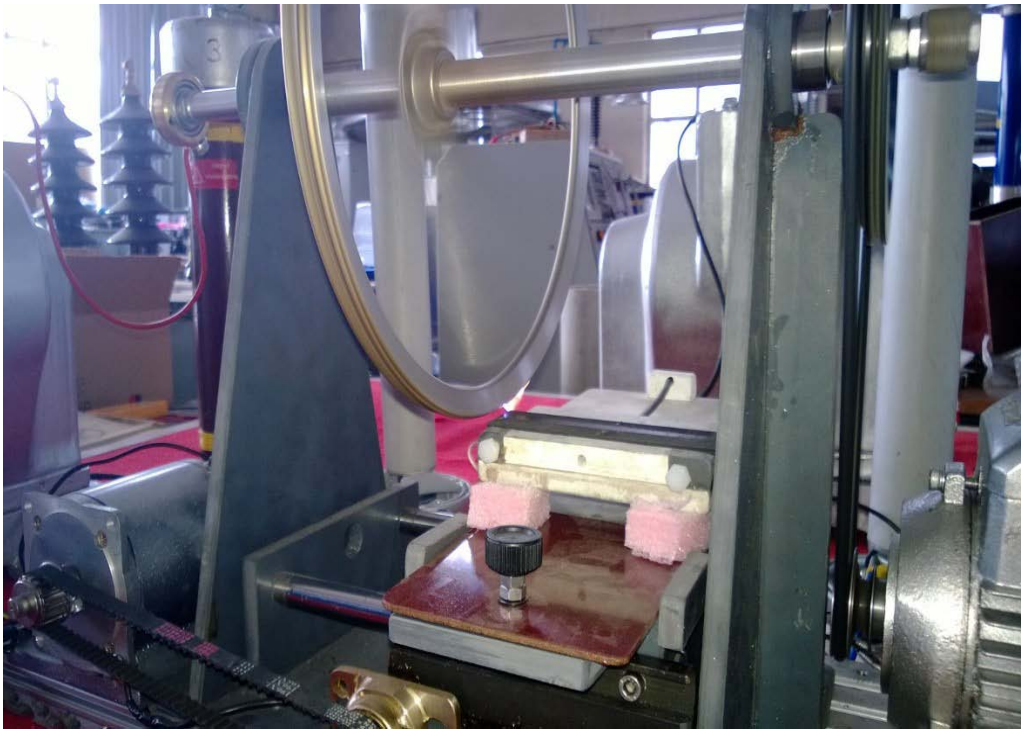

Figure 4-4 Photograph arcing experimental setup when the arc is at the corner of carbon contact strip

Five of the pantograph arcing tests are selected to investigate the effects of parameters on pantograph arcing. Results of these tests are given in the following parts.

4.4.1 Test-1

During Test-1, parameters given in Table 4-5 are adjusted. Voltages and current which are specified in Table 4-4 are measured. These measured waveforms can be shown in Figure 4-5. Also, the harmonic frequency histograms of measured voltage and current waveforms are given in Figure 4-6. Details of measurements are given in Appendix B.

Table 4-5 Test-1 parameters

Test Parameters	**Tested Value**
Step-up transformer HV output voltage	10 kV
Distance between contacts	-
Resistive load	20 Ω
Inductive load	-

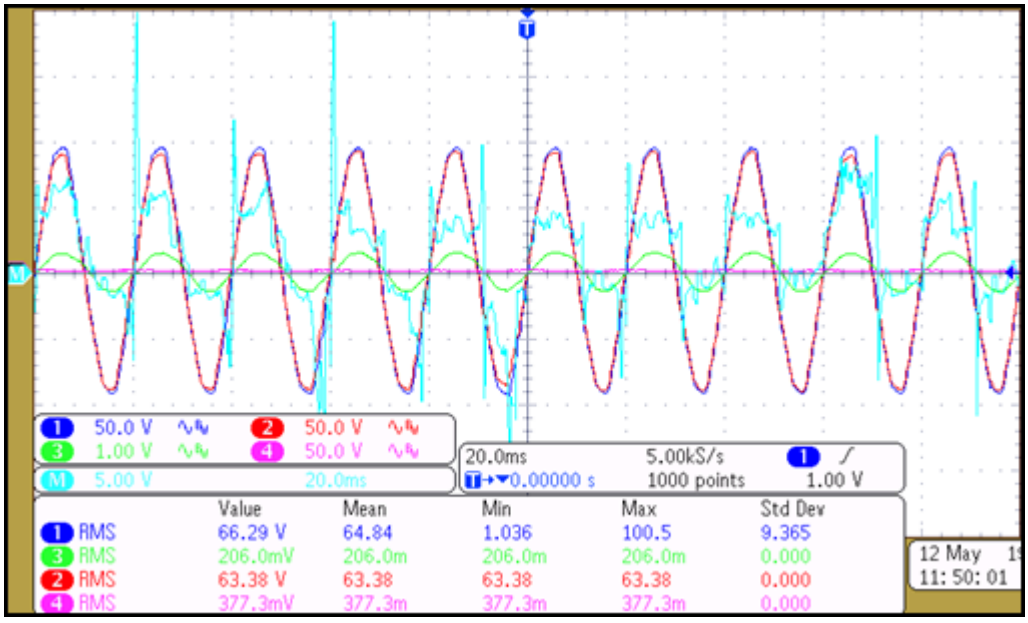

Figure 4-5 Test-1 voltage and current waveforms

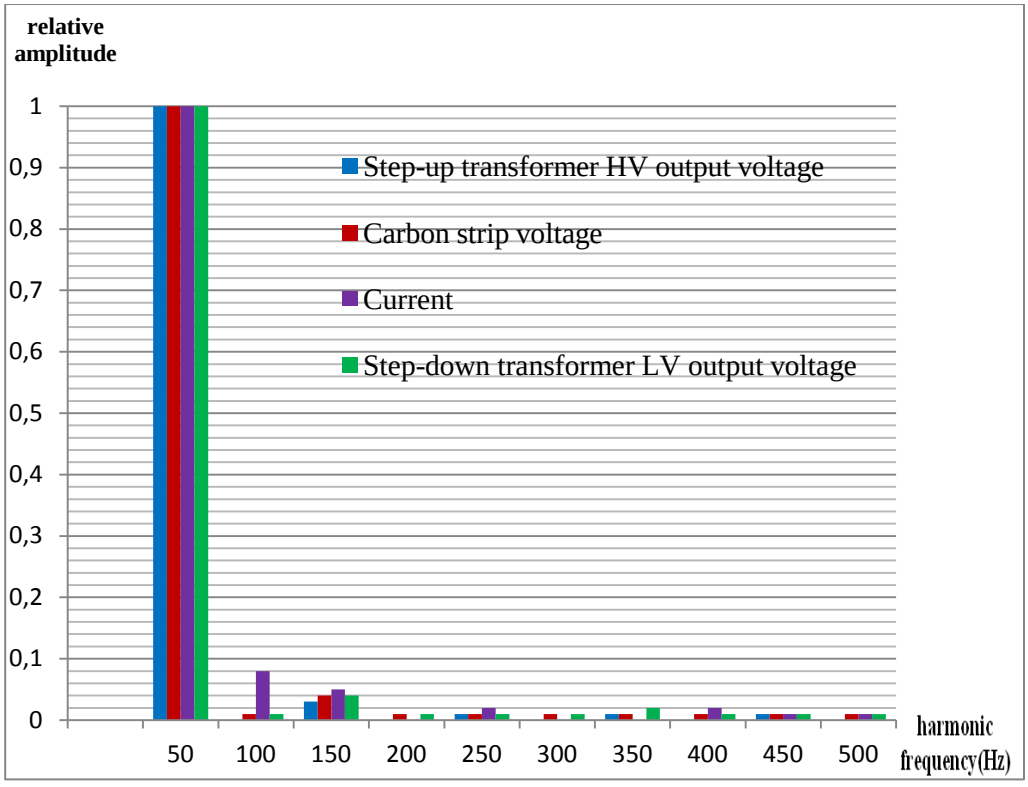

Figure 4-6 Harmonic frequency histograms of measured voltages and current for test-1

4.4.2 Test-2

During Test-2, parameters given in Table 4-6 are adjusted. Voltages and current which are specified in Table 4-4 are measured. These measured waveforms can be shown in Figure 4-7. Also, the harmonic frequency histograms of measured voltages and current are given in Figure 4-8. Details of measurements are given in Appendix B.

Table 4-6 Test-2 parameters

Test Parameters	**Current Test Value**
Step-up transformer HV output voltage	10 kV
Distance between contacts	1 mm
Resistive load	20 Ω
Inductive load	-

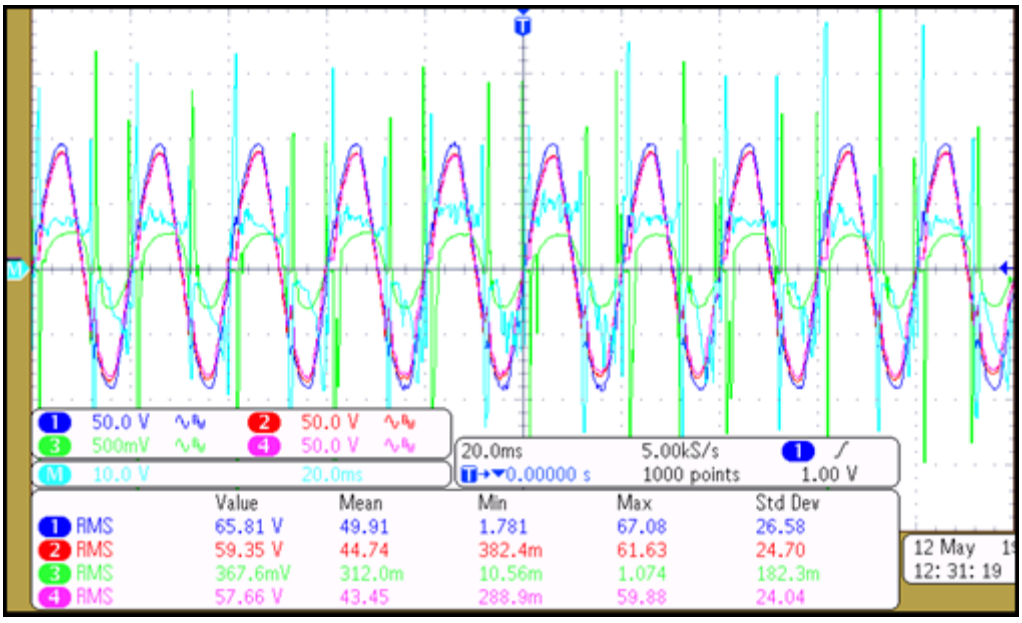

Figure 4-7 Test-2 voltage and current waveforms

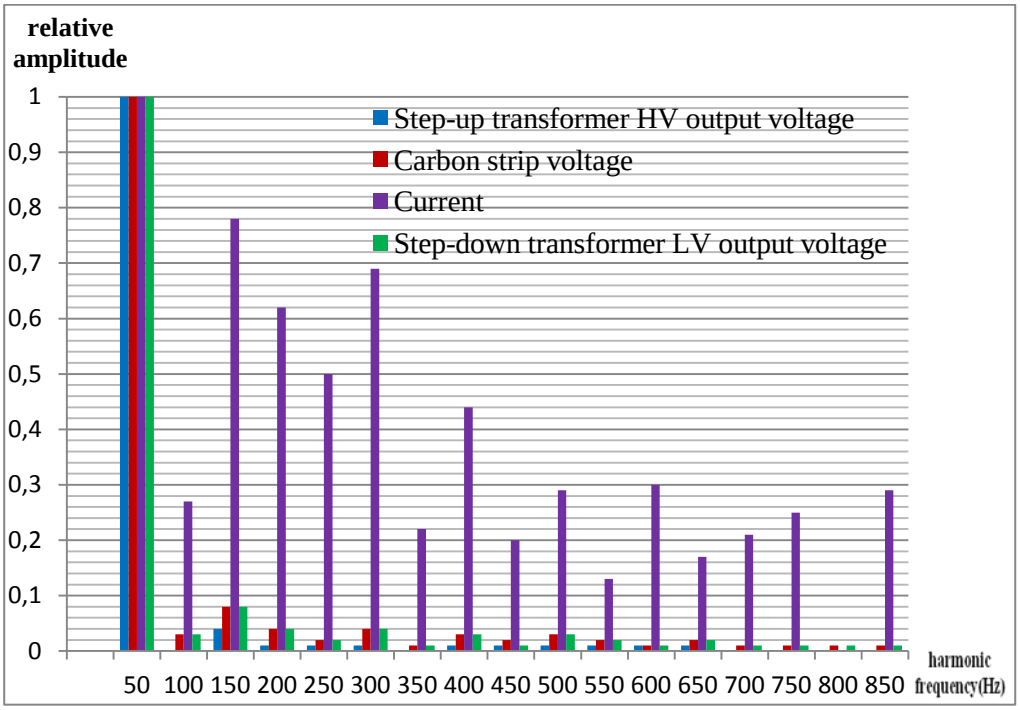

Figure 4-8 Harmonic frequency histograms of measured voltages and current for test-2

4.4.3 Test-3

During Test-3, parameters given in Table 4-7 are adjusted. Voltages and current which are specified in Table 4-4 are measured. These measured waveforms can be shown in Figure 4-9. Also, the harmonic frequency histograms of measured voltages and current are given in Figure 4-10. Details of measurements are given in Appendix B.

Table 4-7 Test-3 parameters

Test Parameters	**Current Test Value**
Step-up transformer HV output voltage	10 kV
Distance between contacts	1 mm
Resistive load	10 Ω
Inductive load	2,34 Ω

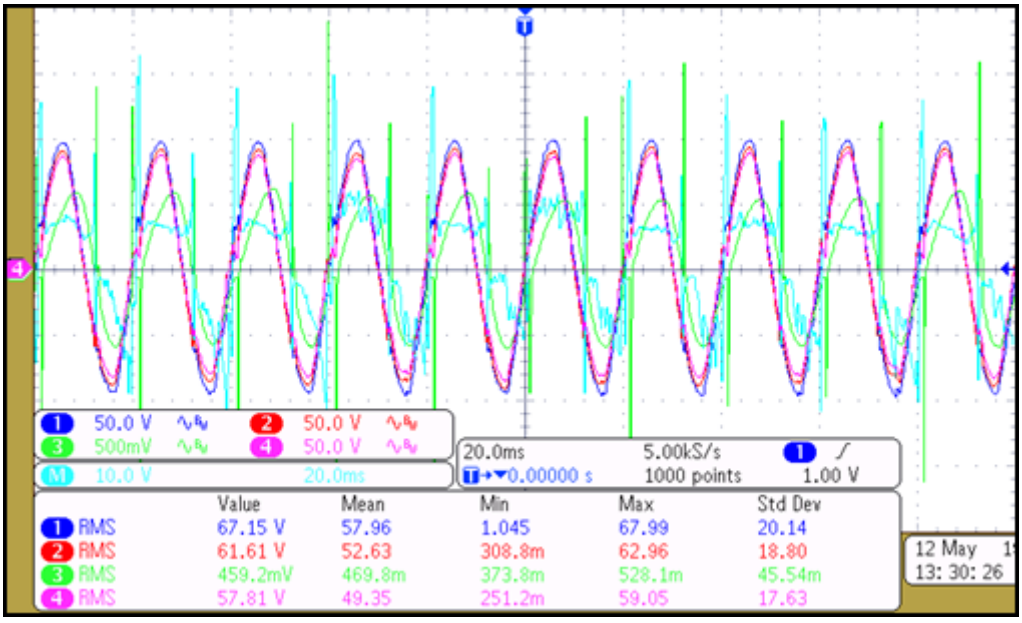

Figure 4-9 Test-3 voltage and current waveforms

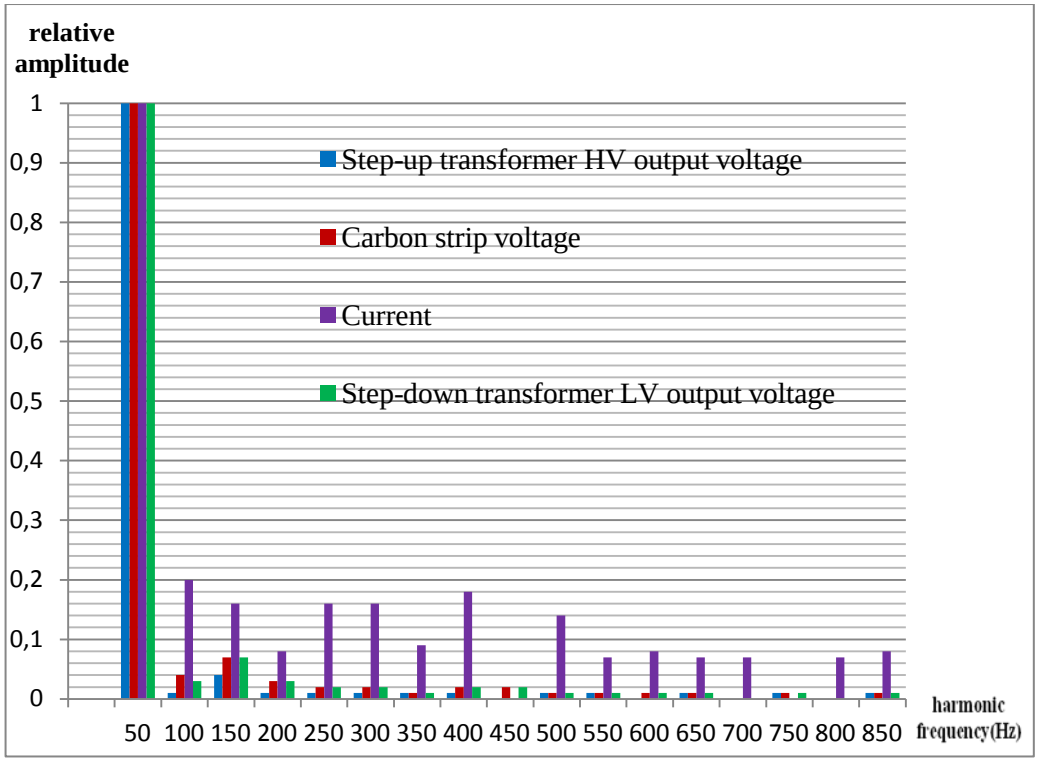

Figure 4-10 Harmonic frequency histograms of measured voltages and current for test-3

4.4.4 Test-4

During Test-4, parameters given in Table 4-8 are adjusted. Voltages and current which are specified in Table 4-4 are measured. These measured waveforms can be shown in Figure 4-11. Also, the harmonic frequency histograms of measured voltages and current are given in Figure 4-12. Details of measurements are given in Appendix B.

Table 4-8 Test-4 parameters

Test Parameters	**Current Test Value**
Step-up transformer HV output voltage	10 kV
Distance between contacts	1 mm
Resistive load	10 Ω
Inductive load	-

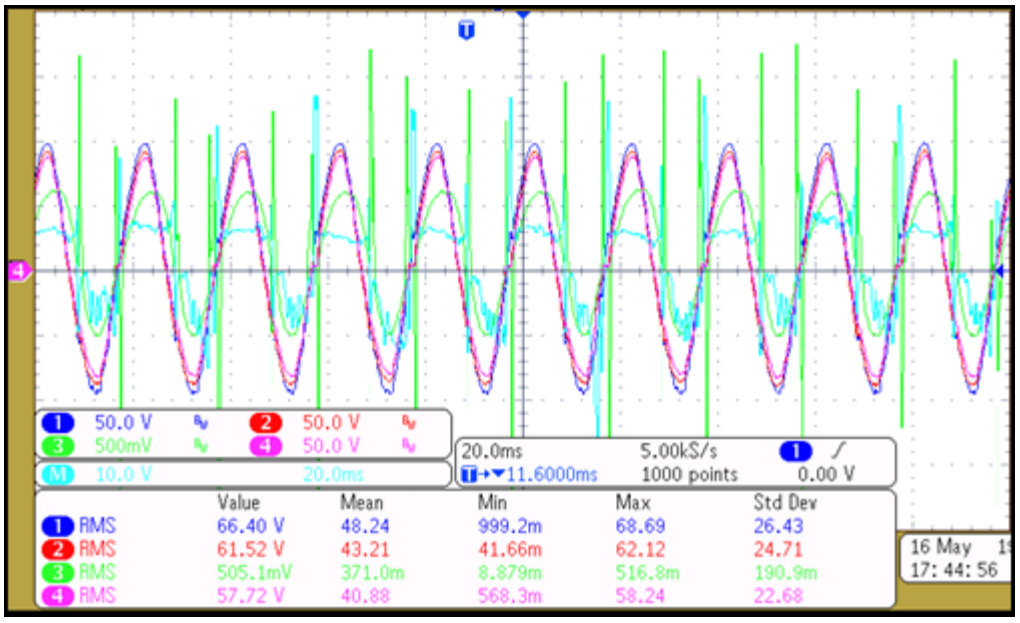

Figure 4-11 Test-4 voltage and current waveforms

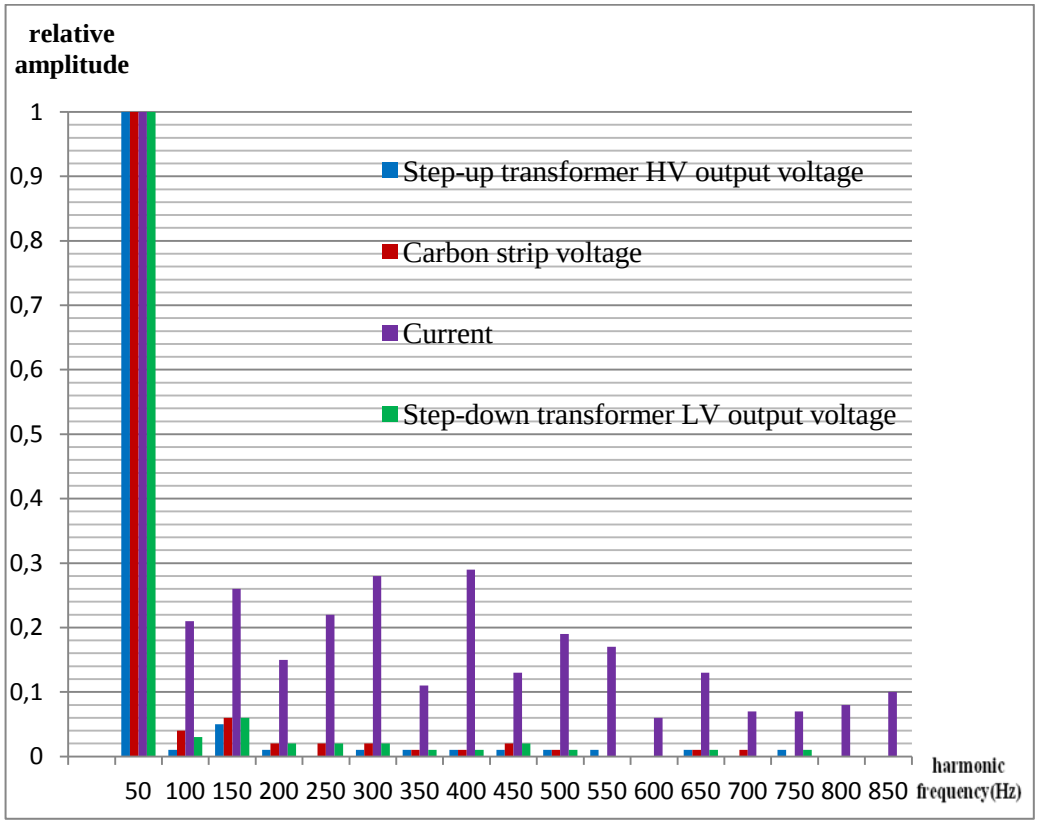

Figure 4-12 Harmonic frequency histograms of measured voltages and current for test-4

4.4.5 Test-5

During Test-5, parameters given in Table 4-9 are adjusted. Voltages and current which are specified in Table 4-4 are measured. These measured waveforms can be shown in Figure 4-13. Also, the harmonic frequency histograms of measured voltages and current are given in Figure 4-14. Details of measurements are given in Appendix B.

Table 4-9 Test-5 parameters

Test Parameters	**Current Test Value**
Step-up transformer HV output voltage	10 kV
Distance between contacts	2 mm
Resistive load	20 Ω
Inductive load	-

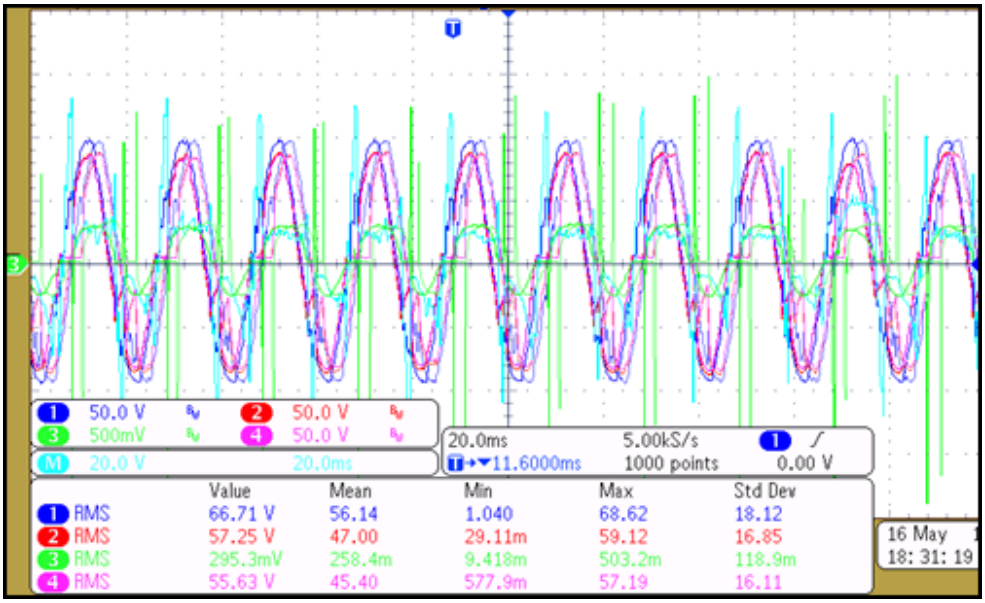

Figure 4-13 Test-5 voltage and current waveforms

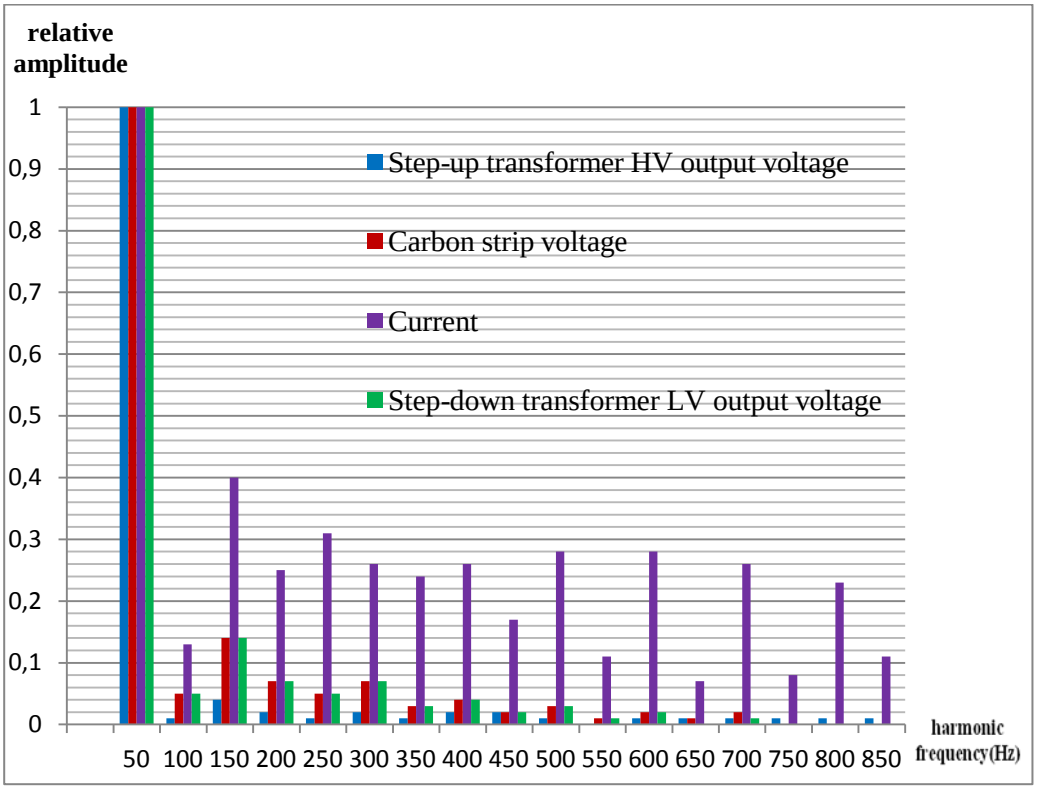

Figure 4-14 Harmonic frequency histograms of measured voltages and current for test-5

4.5 Pantograph Arcing Tests Discussions

A track circuit is a simple electrical device used to detect the absence of a train on rail tracks. Track circuits are used to inform signalers and control relevant signals. The track circuit based signaling systems are operating using the dc or even harmonic of the traction power frequency. Harmonic frequency histograms of measured currents and step down transformer output voltages (pantograph voltages) for test-1 to test-5 are given in Figure 4-15 and Figure 4-16 respectively. Test results shown that current and pantograph voltage both have even and odd harmonics because of arcing. Therefore, pantograph arcing may cause interference with the track signaling systems. False signaling in the railways may cause accidents and delays in the rail operations. Same problems are also focused on in [16]. The operation of the Oeresund Train Unit (OTU) EMUs had to be cancelled at some occasions during the winter 2001-2002. In contrary to other electric trains and locomotives in Denmark, the OTU is equipped with a DC supervision system. At conditions with ice on the OHL, this system reacted and stopped the OTU EMUs. The Swiss 16,7 Hz electrified railways are equipped with 100 Hz track circuits, i.e., they operate at the 6th harmonic. This causes severe problems during winter time, due to the fact that the existence of a DC component in the line current also leads to even harmonics.

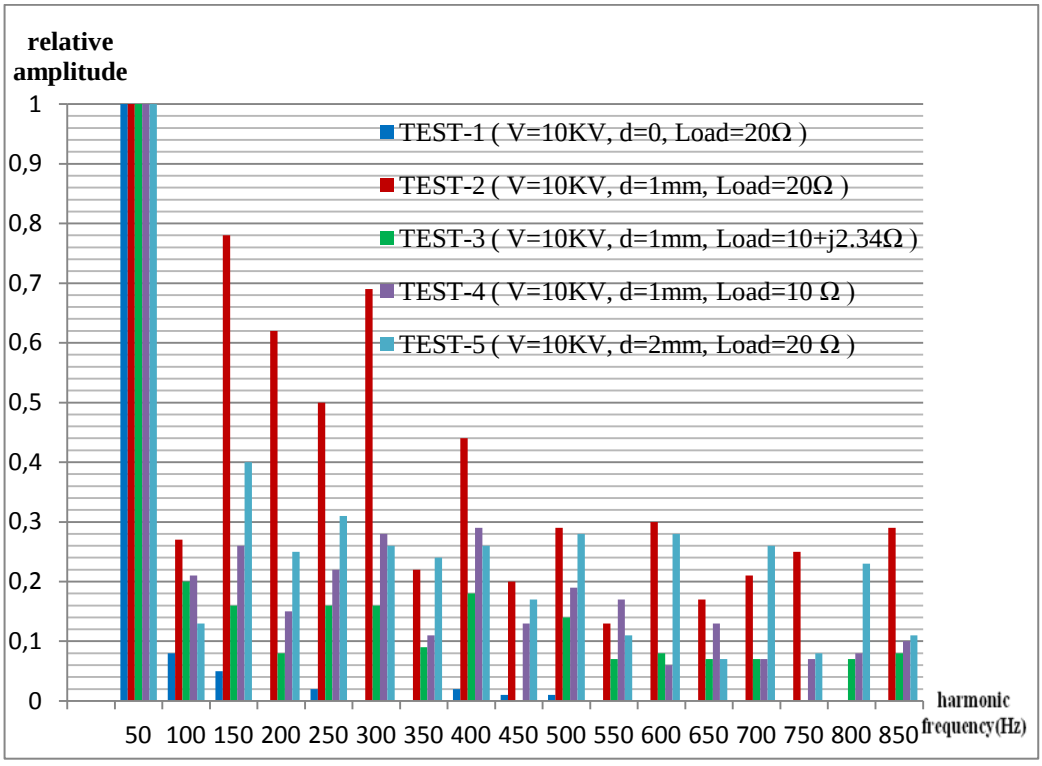

Figure 4-15 Harmonic frequency histograms of measured currents for tests 1 to 5

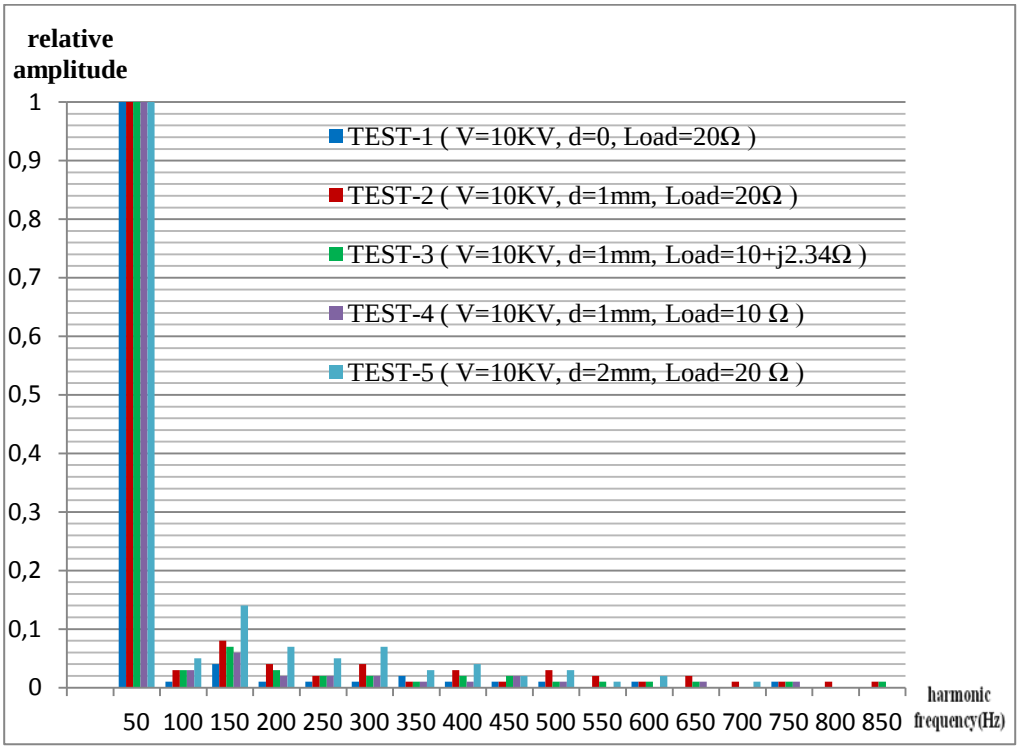

Figure 4-16 Harmonic frequency histograms of step down transformer output voltage for tests 1 to 5

The pantograph arcing current waveform of test-2 is given in Figure 4-17. The current has peaks every half cycle due to arcing. Pantograph arcing may cause the wrong opening of the protective circuit breakers due to these current peaks. This is another problem of pantograph arcing. Similar problems are also mentioned in [41] and [42].

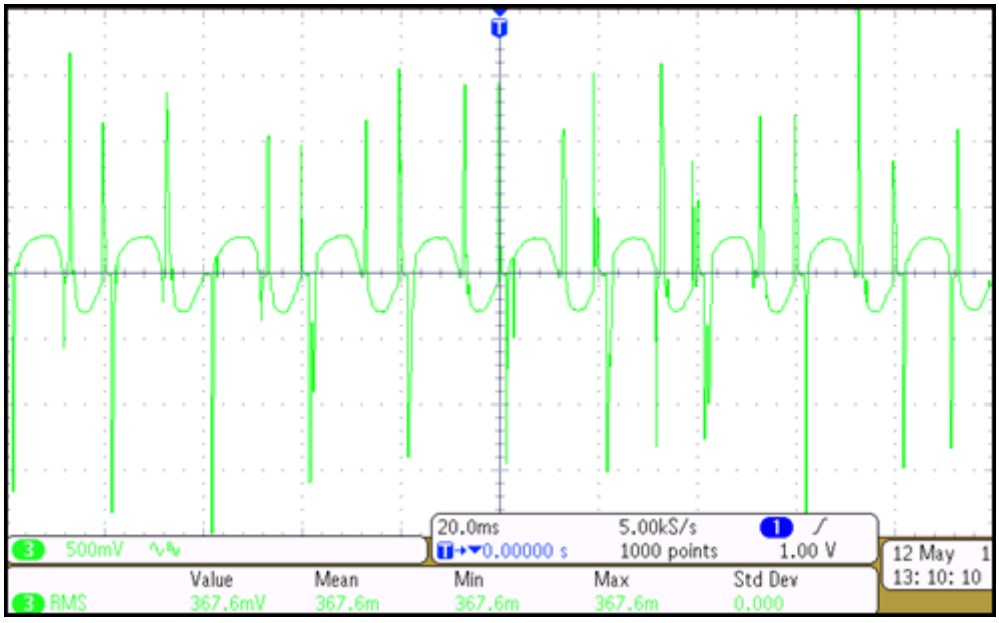

Figure 4-17 Pantograph arcing current of test-2

Arc voltage waveform of test-2 is shown in Figure 4-18. When the experimental results of arc voltages of the positive and negative half cycles are compared, it can be said that they are not symmetrical. The arc voltage at positive half cycle is greater than the negative half cycle in this work. The current is 10 mA in the test setup. Therefore, the line and carbon contact are at the same temperature. With the help of Richardson's law, and thermionic properties of carbon and brass, it can be said that emission current density of brass (copper) is higher than carbon. Therefore, it is easier to liberate electrons from the brass (copper). Results of pantograph arcing experiments conducted by "OHL Ice Team" in Sweden also shows asymmetry between the arc voltages. However, they found that arc voltage is greater at negative half cycle opposite to the results of this work. At negative half cycle, carbon strip is anode and copper contact line is cathode. Since copper contact is always cool, it causes a lower rate of electron emission compared to the heated carbon when it is the cathode. Therefore, it can be concluded that the arc voltage is higher when the copper contact line is the cathode. In [16], experiments conducted by "OHL Ice Team" has a supply current of order of 10 A with the help of a more powerful voltage supply. On the other end, experiments conducted with supply currents order of 10 mA in this work. Therefore, the pantograph contact (carbon) was at a much higher temperature then the copper line in their work. This may cause a higher rate of thermionic emission from the carbon when it is the cathode resulting in a higher conductivity in the arc and a lower arc voltage as observed.

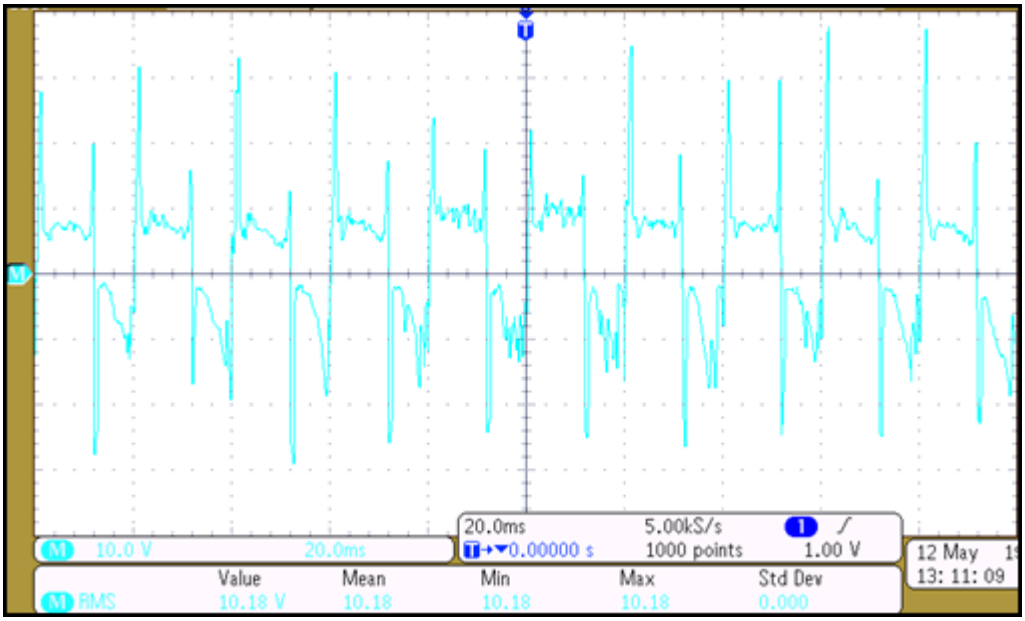

Figure 4-18 Arc voltage in test-2

In the following parts, effects of contact distance, load current and power factor on the test results will be discussed.

4.5.1 Influence of Contact Distance

Table 4-10 Test parameters with different contact distances

Test Parameters	**Test-1**	**Test-2**	**Test-5**
Step-up transformer HV	10 kV	10 kV	10 kV
Distance between contacts	-	1 mm	2 mm
Resistive load	20 Ω	20 Ω	20 Ω
Inductive load	-	-	-

In the tests 1, 2 and 5 contact distances are changed while the other variables are kept constant. The test parameters are given in Table 4-10. The peak values of the arc voltages are measured 1650V, 5700V and 7500V respectively. The arc voltage waveforms can be observed in Figure 4-19. The arc voltage waveforms have a 149 divider ratio.

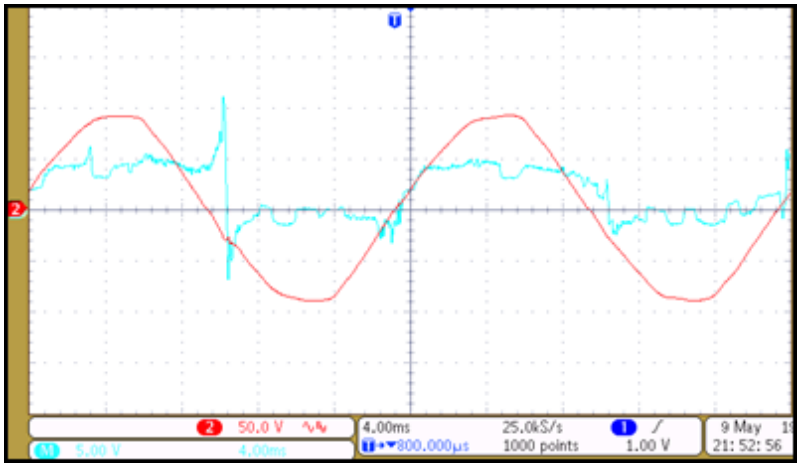

(a)

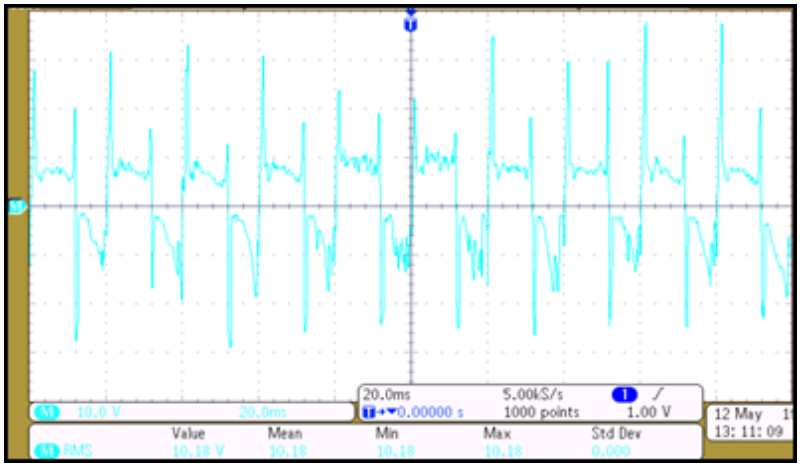

(b)

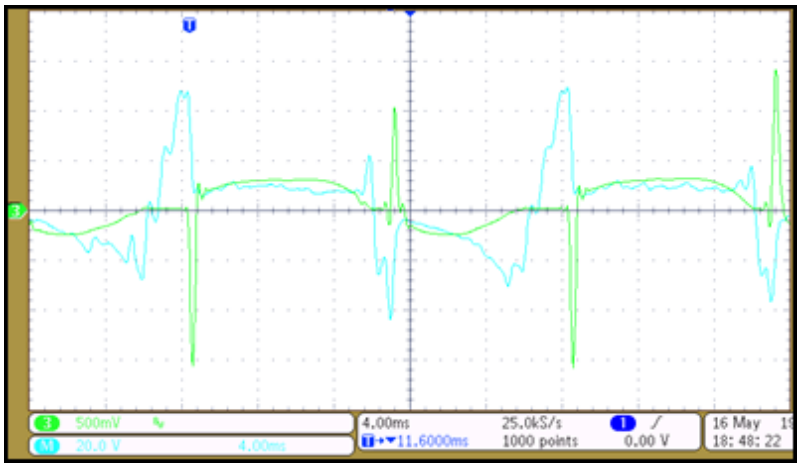

(c)

Figure 4-19 Change in arc voltage (blue) due to increased contact distance
(a) Test-1, d=0mm (b) Test-2, d=1mm (c) Test-5, d=2mm

In 1889 Paschen states a law which gives the relation between the breakdown voltage and the electrodes distance and pressure of the gas. The Paschen equation is

$$V = \frac{apd}{\ln(pd) + b} \tag{4.1}$$

where "V" is the breakdown voltage in volts," p" is the pressure in atmospheres or bar, and "d" is the gap distance in meters. The constants "a" and "b" depend upon the composition of the gas. For air at standard atmospheric pressure of 101 kPa, "a" = 4.36×107 V/(atm·m) and "b" = 12.8.

Using the equation (4.1) breakdown voltages for 1 mm and 2 mm contact distance are found 7400 V and 13240 V respectively. As Paschen law states, breakdown voltages increases with electrode separation. The conditions in the case of reignition of a self-sustained discharge by an alternating potential are vastly unlike those existing in the case of the original breakdown of the gas. In the arc plasma, the number of free ions is larger than in the fresh gas. Therefore in the experiment, reignition voltages are measured smaller than breakdown voltages of the gas for given contact distances. In conclusion, to reignite the arc, the required voltage increases with contact separation.

Harmonic content of the low voltage side of the step-down transformer, shown in Figure 4-21, also increases with the contact separation distance. This is also related with the increase in the arc voltage since the distortion in the voltage waveform is increased with the increase in the arc voltage.

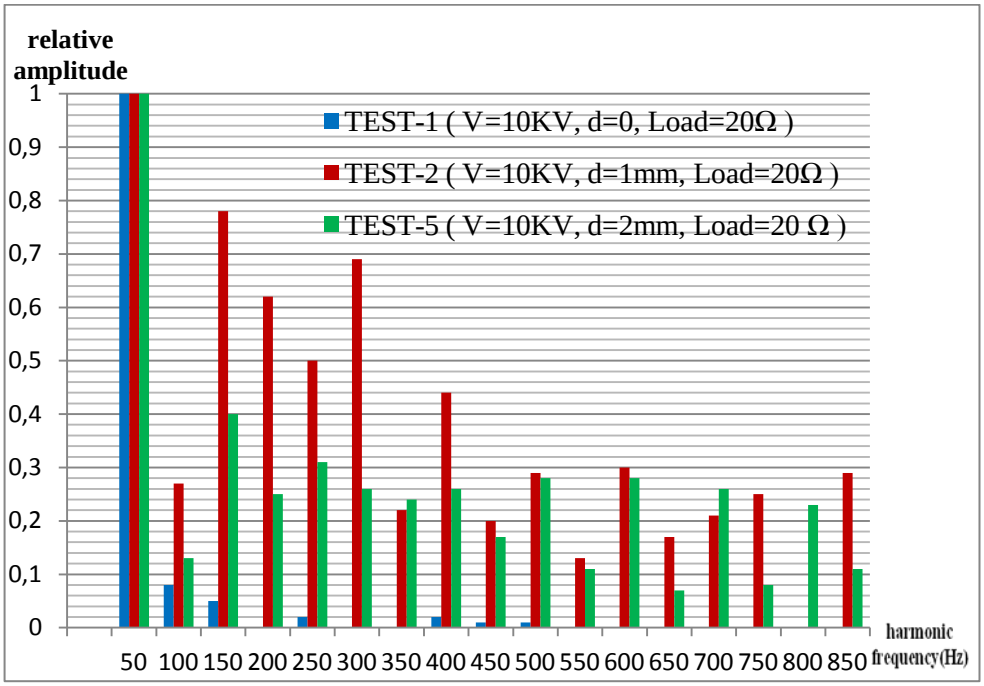

Figure 4-20 Harmonic frequency histograms of measured currents for Test-1, 2 & 5

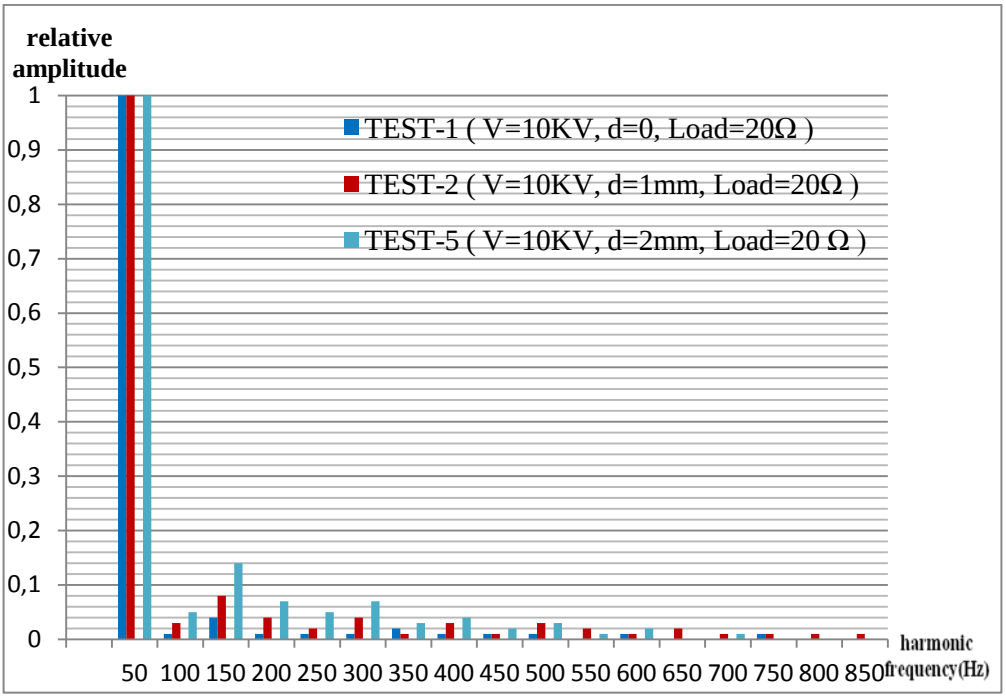

Figure 4-21 Harmonic frequency histograms of step down transformer LV output voltage for Test-1, 2 & 5

4.5.2 Influence of Load Current

Table 4-11 Test parameters with different load currents

Test Parameters	**Test-2**	**Test-4**
Step-up transformer HV	10 kV	10 kV
Distance between contacts	1 mm	1 mm
Resistive load	20 Ω	10 Ω
Inductive load	-	-

In the test-2 and 4 load currents are changed with changing resistive load while the other variables are kept constant. The test parameters are tabulated in Table 4-11. The arc current is doubled in test-4. The peak values of the arc voltages are measured 5700 V and 4050 V, respectively. The arc voltage waveforms can be shown in Figure 4-22. The arc voltage waveforms have a 149 divider ratio.

An AC arc may be extinguished or reignite after each zero current crossing. The arc reignition arises from the birth of a new cathodic spot after zero current crossings. In principle, the generation of a new spot is not different from a first ignition of the arc, except that the extinguished arc may create circumstances which favor new births. For example, an electrode can be considerably hotter after the arc has operated for some time than it was before the first ignition. Mechanism of the cathodic spots is purely or essentially thermo-electronic. Arc reignition is easy as long as the temperature is still above a certain threshold when the conditions favorable to the reignition of an arc are restored. As the hot spot cools down, it is observed that the reignition becomes less and less easy. Reignition at the new cathode is helped considerably by the heat liberated at the old anode since they are one and the same surface. The active portion of the electrodes will be heated, the extent of this heating depends on the current of the discharge. The degree of ionization at zero current is a direct function of the arc current. In the absence of a reappearing voltage, the ionization when the current is low will quickly disappear by recombination in the gas and neutralization at the electrode surfaces. For higher values of current, the volume deionization will be slower, because in the presence of thermal ionization, deionization will proceed at a much slower rate, determined by a time constant characteristic of the gas. Obviously, in the case of small current arcs, the reapplied voltage must be very much higher or must be applied at a much higher rate than for heavy currents if deionization is to be arrested.

In [39] recovery strength characteristics of silver electrodes with a 2 mm distance are measured. Measurements confirmed that the higher the arc current value, the lower the

recovery strength thus the magnitude of the breakdown voltage decreases with higher arc current.

Harmonic contents of the arc current and low voltage side of step-down transformer are shown in

Figure 4-23 and Figure 4-24 respectively. Harmonic contents of the arc current decreases with increase in the current since the zero current crossing times are smaller for higher arc current. Harmonic contents of the low voltage side of the transformer is also decrease with the increase in arc current since the arc voltage peaks are decreased with higher current.

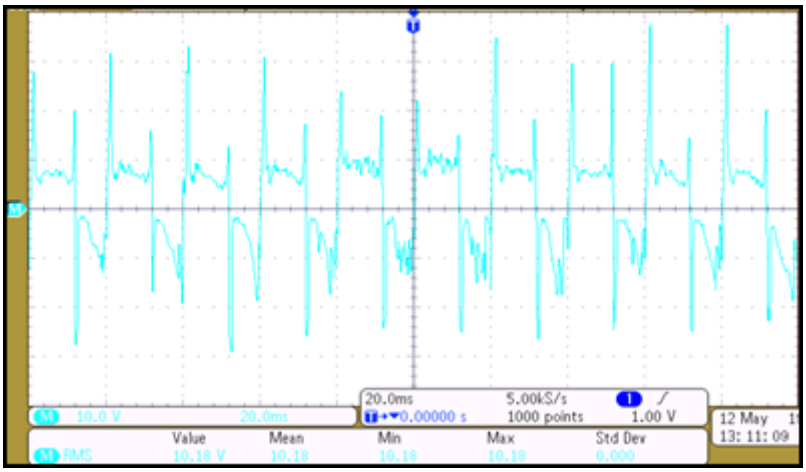

(a)

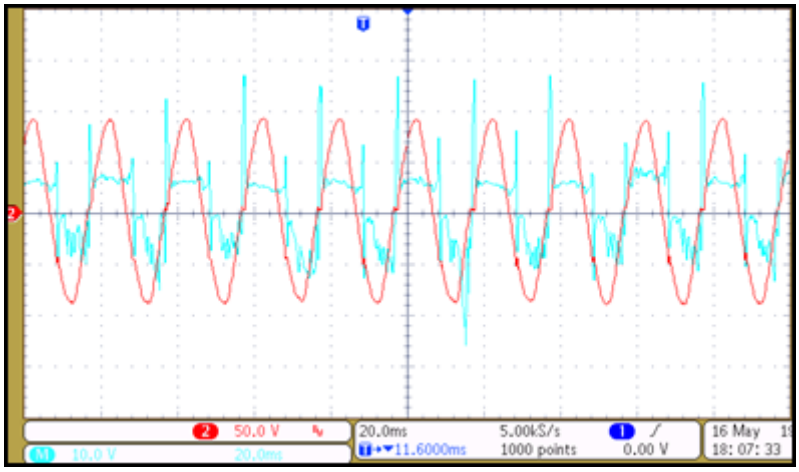

(b)

Figure 4-22 Change in arc voltage (blue) due to increased load current
(a) Test-2 R = 20Ω (b) Test-4, R = 10Ω

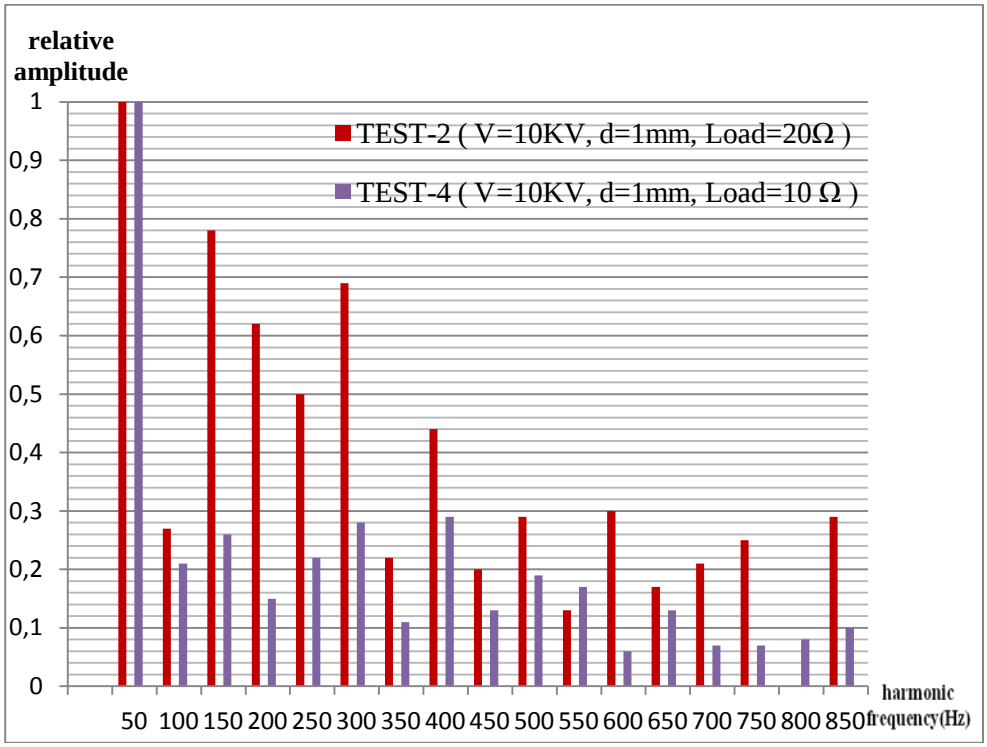

Figure 4-23 Harmonic frequency histograms of measured currents for Test-2 & 4

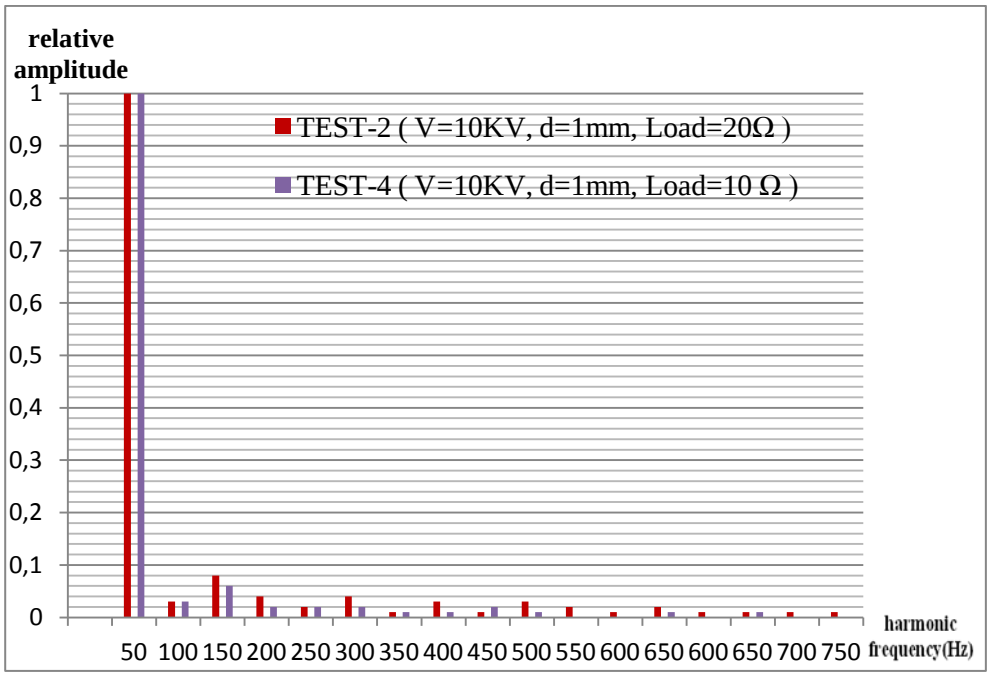

Figure 4-24 Harmonic frequency histograms of step down transformer LV output voltage for Test-2 & 4

4.5.3 Influence of Load Power Factor

Table 4-12 Test parameters with different load power factors

Test Parameters	**Test-3**	**Test-4**
Step-up transformer HV	10 kV	10 kV
Distance between contacts	1 mm	1 mm
Resistive load	10 Ω	10 Ω
Inductive load	2,34 Ω	-

In the test-3 and 4 load power factors are changed with removing the inductive load while the other variables are kept constant. The test parameters are given in Table 4-12. The peak values of the arc voltages are measured 4800V and 4050V respectively for test 3 and 4. The arc voltage waveforms can be shown in Figure 4-25. The arc voltage waveforms have a 149 divider ratio.

The magnetic energy stored in the inductances of the load forces the current to flow. Therefore, zero current crossing times are smaller in inductive circuit. Increasing the power factor by removing the reactance in the load increases the current harmonics. Harmonic content of the arc current is given in Figure 4-26.

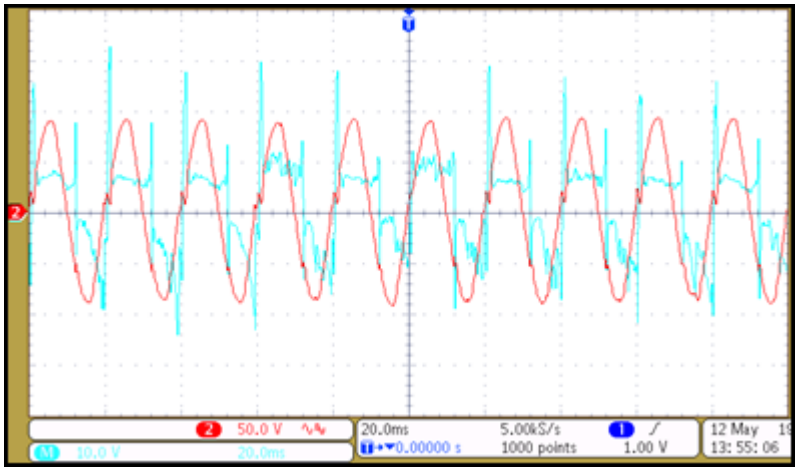

(a)

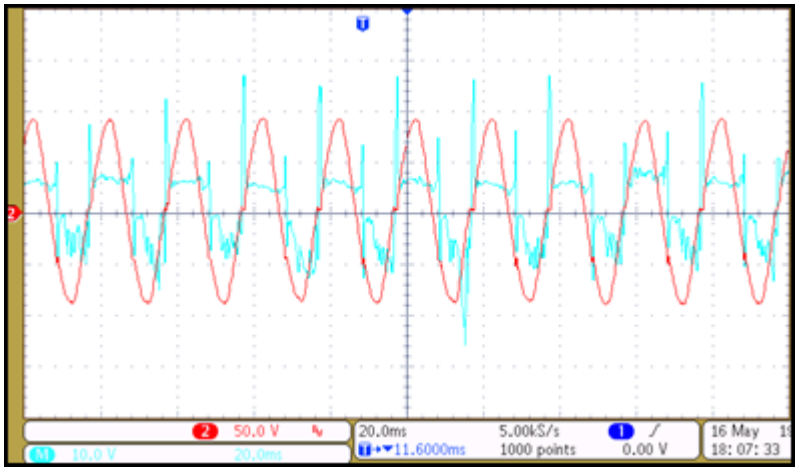

(b)

Figure 4-25 Change in arc voltage (blue) due to increased load power factor
(a) Test-3, R = (10+j2,34) Ω (b) Test-4, R = 10Ω

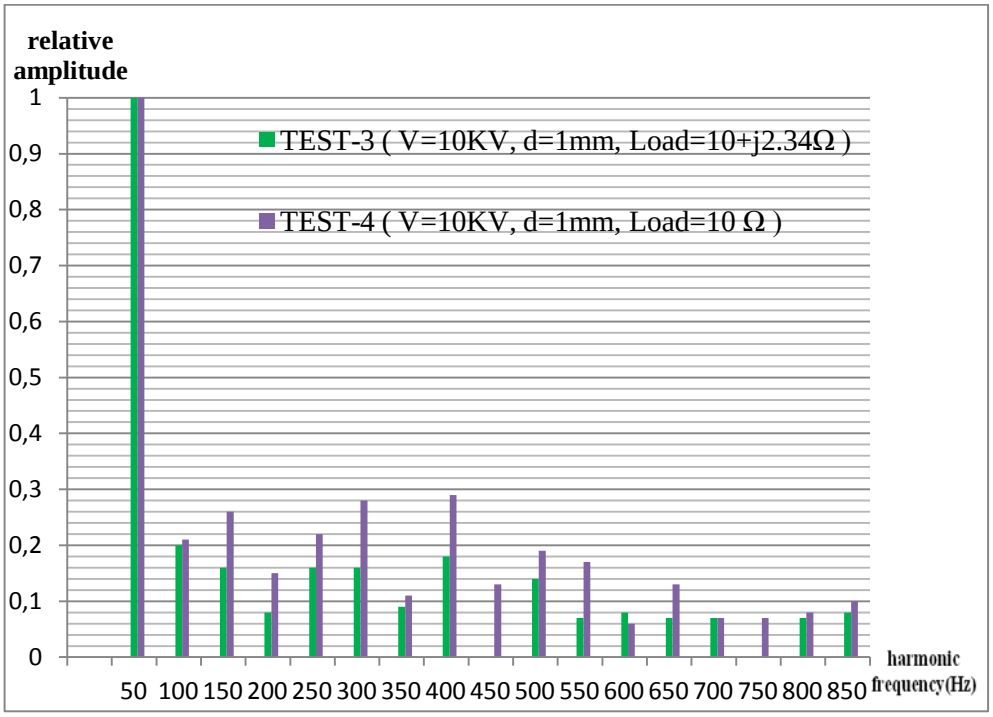

Figure 4-26 Harmonic frequency histograms of measured currents for Test-3 & 4

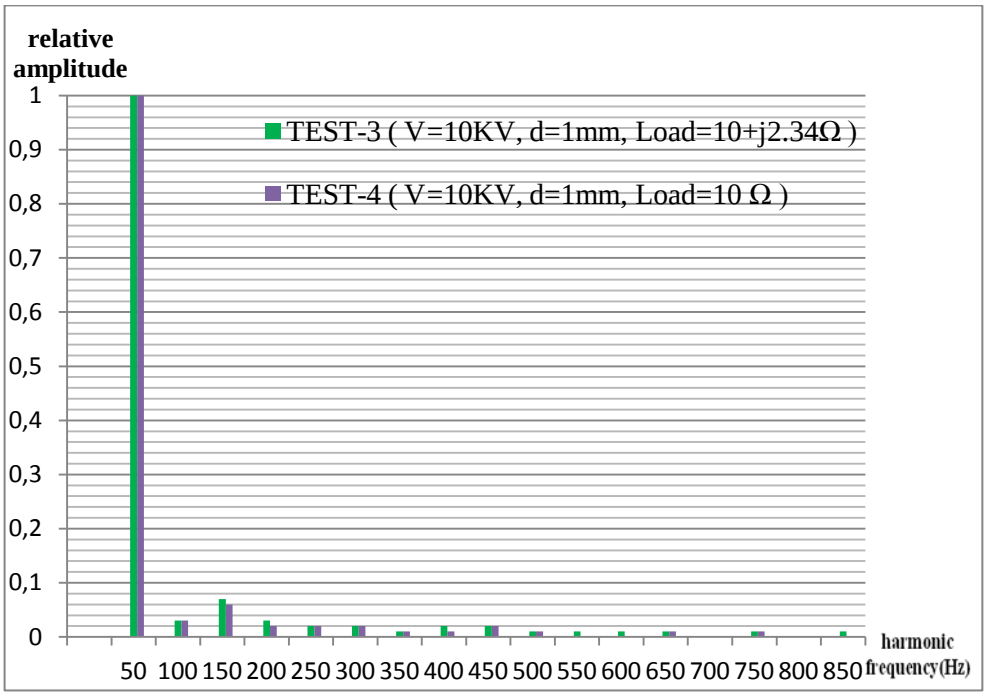

Figure 4-27 Harmonic frequency histograms of step down transformer LV output voltage for Test-3 & 4

CHAPTER 5

ARC MODELS

5.1 Introduction

Arc models were originally developed for better understanding of the current interruption process in high voltage circuit breakers and to be able to design interrupting chambers. The arc model simulates nonlinear behavior of the circuit breaker arc [23].

In this work arc models which are originally developed for circuit breakers are used to understand pantograph arcs since there is not any special model for pantograph arcing. In this chapter arc models and theories are examined in details.

5.2 Arc Modelling

Arc models can be classified in three categories:

- Black box models
- Physical models
- Parameter models

In black box models, the arc is described by a simple mathematical equation. The model gives the relation between the arc conductance and the voltage and current.

In physical arc models, the arc is described by the equations of fluid dynamics. The model obeys the laws of thermodynamics in combination of Maxwell's equations. They consist of a large number of differential equations.

Parameter models are a variation of black box models. The arc is described by more complex functions and tables. [20].

5.2.1 Black Box Arc Models

In black box arc models, the arc conductance is a function of the power supplied to the plasma channel and the power transported from the plasma channel by time;

$$g = F(P_{in}, P_{out}, t) = \frac{i_{arc}}{u_{arc}} = \frac{1}{R} \tag{5.1}$$

with

g = the arc conductance
P_{in} = the power input to the plasma channel
P_{out} = the power output from the plasma channel
t = time
i_{arc} = the arc current
u_{arc} = the arc voltage
R = the arc channel resistance

The momentary arc conductance g varies when P_{in} and P_{out} are not in equilibrium. The energy stored in the plasma channel is

$$Q = \int_0^t (P_{in} - P_{out})dt \tag{5.2}$$

Q and the momentary arc conductance can be written as

$$g = F(Q) = F[\int_0^t (P_{in} - P_{out})dt] \tag{5.3}$$

when the Equation (5.3) is differentiated

$$\frac{dg}{dt} = \frac{dF(Q)}{dQ}\frac{dQ}{dt} \tag{5.4}$$

and divided by the momentary arc conductance g

$$\frac{1}{g}\frac{dg}{dt} = \frac{1}{g}\frac{dF(Q)}{dQ}\frac{dQ}{dt} \tag{5.5}$$

Differentiation of Equation (5.2) and the result substituted with Equation (5.3) in Equation (5.5) gives us the general arc equation:

$$\frac{d[\ln(g)]}{dt} = \frac{F'(Q)}{F(Q)}(P_{in} - P_{out}) \tag{5.6}$$

To solve this general arc equation, assumptions have to be made. These assumptions, named after their authors, give the different black box models.

5.2.2 Black Box Arc Theories

5.2.2.1 Slepian Theory

It was proposed in 1928 and states that arc extension process is a race between the dielectric strength and restriking voltage. After current zero, there is a hot residual column of ionized gases. If the dielectric strength builds up quickly, so that it is always greater than the restriking voltage, the arc does not restrike. If the dielectric strength is less, the arc restrikes. The theory assumes that the restriking voltage and the build-up of dielectric strength are comparable quantities, which is not correct. Secondly, the theory does not consider energy functions in the arc extinction process [24].

5.2.2.2 Cassie's Theory

A. M. Cassie presented a differential equation describing the behavior of arc in 1939. The theory assumes a constant temperature across the arc diameter. The arc cross section varies as the current varies. However, the temperature inside the arc column is not varies with the current.

with

g_0 = the conductivity per unit of volume
P_0 = the cooling or loss of power per unit of volume
D = the arc channel diameter varying with time
Q_0 = the energy content per unit of volume
$u_0 = (P_0/g_0)^{1/2}$ the static arc voltage

The arc conductance can be written as

$$g = F(Q) = Dg_0 \tag{5.7}$$

and for the energy as a function of time

$$Q = DQ_0 \tag{5.8}$$

Combining Equations (5.7) and (5.8) results in

$$g = F(Q) = \frac{Q}{Q_0} g_0 \tag{5.9}$$

$$F'(Q) = \frac{g_0}{Q_0} \tag{5.10}$$

The dissipated power per unit of length

$$P_{out} = DP_0 = \frac{Q}{Q_0} P_0 \tag{5.11}$$

Equations (5.9), (5.10) and (5.11) substituted in the general arc equation; Equation (5.6) gives us the Cassie equation

$$\frac{d[\ln(g)]}{dt} = \frac{P_0}{Q_0}\left(\frac{u_{arc}^2}{u_0^2} - 1\right) \tag{5.12}$$

The quotient $Q_0/P_0$is called the arc time constant τ and can be calculated from the homogeneous differential Equation (5.12).

Combining equation (5.12) with τ results in

$$\frac{1}{g}\frac{d(g)}{dt} = \frac{1}{\tau}\left(\frac{u_{arc}^2}{u_0^2} - 1\right) \tag{5.13}$$

$$\frac{d[\ln(g)]}{dt} = -\frac{P_0}{Q_0} \tag{5.14}$$

A solution satisfying homogeneous Equation (5.15) is

$$g = g_0 e^{-t/\tau} \tag{5.15}$$

There is a good agreement with the model for high current region when the plasma temperature 8000 K or more, but for current-zero regions, agreement is good only for high rates of current decay.

5.2.2.3 Mayr's Theory

The theory assumes an arc column where arc diameter is constant and where arc temperature varies with time and radial dimensions. The decay of temperature of the arc is considered because of the thermal conduction, and the electrical conductivity of the arc is dependent on temperature. The conductance can be expressed as

$$g = F(Q) = ke^{Q/Q_0} \tag{5.16}$$

The power loss of the arc channel is assumed to be constant. When this is substituted in the general arc equation (Equation (5.6)),

$$\frac{d[\ln(g)]}{dt} = \frac{(u_{arc}i_{arc} - P_{0)}}{Q_0} \tag{5.17}$$

Combining equation (5.17) with τ results in

$$\frac{1}{g}\frac{d(g)}{dt} = \frac{1}{\tau}\left(\frac{u_{arc}i_{arc}}{P_0} - 1\right) \tag{5.18}$$

At the instant of current zero, the power input $u_{arc}i_{arc}$ in the arc channel is zero, and the rate of change of the conductance of the arc channel is

$$\frac{dg}{dt} = -g\frac{P_0}{Q_0} \tag{5.19}$$

This is the homogeneous differential equation of Equation (5.17) and has as a solution;

$$g = g_0 e^{-P_0/Q_0 t} \tag{5.20}$$

In this expression Q_0/P_0 is the time constant τ of the arc cooling without thermal input to the arc channel and is called the arc time constant.

The Mayr model is suited for modeling of the arc in the vicinity of current zero when the temperature of the plasma is below 8000 K.

5.2.2.4 Cassie Mayr Theory

In 1958 Browne combined both the Cassie and Mayr models and suggested the use of Cassie model before current zero and the Mayr model after zero.

CHAPTER 6

ARC MODEL SIMULATIONS

6.1 Introduction

ATP-EMTP (Alternative Transients Program version of the ElectroMagnetic Transients Program) is a universal program system for digital simulation of transient phenomena of electromagnetic as well as electromechanical nature. With this digital program, complex networks and control systems of arbitrary structure can be simulated. ATP-EMTP has extensive modeling capabilities and additional important features besides the computation of transients.

ATPDraw is a graphical, mouse-driven preprocessor for ATP-EMTP on the MS Windows platforms. Using ATPDraw, one builds a graphical picture of an electric circuit by picking objects from menus, connecting and editing objects, and keying data interactively. It supports almost all standard ATP components, TACS objects and MODELS. The user can create his own circuit objects. ATPDraw has been developed by Dr. Hans-Kristian Hoidalen.

PlotXY is a plotting program created by Massimo Ceraolo of University of Pisa to generate scientific line plots using data collected from: C-LIKE PL4 files created with the program ATP-EMTP.

Arc model simulations are used for circuit breakers. Since there is different arc models, generating a suitable model for pantograph arcing and verifying it with experimental results may be useful for power system transient analysis of the electrified trains.

In this chapter, basic arc models in EMTP-ATP are examined firstly. Later a suitable arc model for pantograph arcing is generated and validated for experimental results.

6.2 Arc Models in ATP-EMTP

6.2.1 Universal Arc Resistance Model "ZAGREB" for ATP-EMTP

In [25] the electrical arc was simulated using its conductance dependent parameters described by the Mayr arc equation:

$$\frac{dg}{dt} = \frac{1}{\tau(g)}\left(\frac{i^2}{P(g)} - g\right) \tag{6.1}$$

where g- the arc conductance
i - the arc current
$P(g)$ - the arc cooling power
$\tau\,(g)$ - the arc thermal time constant

Calculation of the arc conductance requires data on the cooling power and the thermal time constant.

Parameters P(g) and τ(g) are conductance dependent. The cooling power P and the thermal time constant τ depend on temperature and they can be defined as a function of conductance f(g).

$$P = P_0 g^{\beta} \tag{6.2}$$

$$\tau = \tau_0 g^{\alpha} \tag{6.3}$$

The differential equation (6.1) was solved numerically with the Euler method for differential equations of the first order. The solution is given in Equation (6.4).

$$g(t + \Delta t) = g(t) + \left(\frac{i^2}{P(g)} - g(t)\right)\left[1 - e^{\frac{-\Delta t}{\tau(g)}}\right] \tag{6.4}$$

In [25] writers used the test circuit given in Figure 6-1 to verify the arc model.

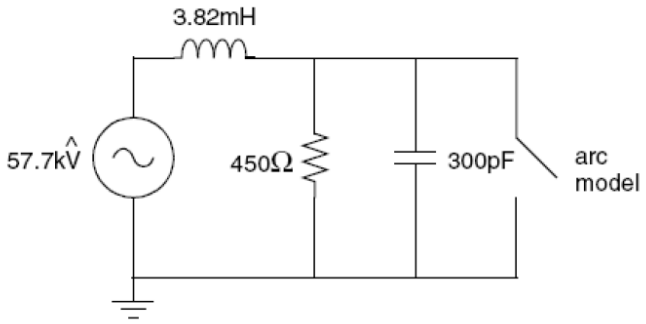

Figure 6-1 Test circuit

The supply frequency is 60 Hz and arc model parameters are as follows: $P_0 = 4MW, \beta = 0.68, \tau = 1.5\mu s \; and \; \alpha = 0.17$. The following equations are used:

$$P = P_0 g^{\beta} = 4 \; MW \; g^{0.68} \tag{6.5}$$

$$\tau = \tau_0 g^{\alpha} = 1.5 \; \mu s \; g^{0.17} \tag{6.6}$$

with an initial resistance value of 0.1 mΩ and a time step of 10 ns. Switch is opened at t = 50 ms.

The EMTP models code of the ZAGREB model is given in Appendix C.

The test circuit given in Figure 6-1 is simulated in ATP-EMTP. The circuit schematic and the simulation outputs are given in Figure 6-2 and Figure 6-3 respectively.

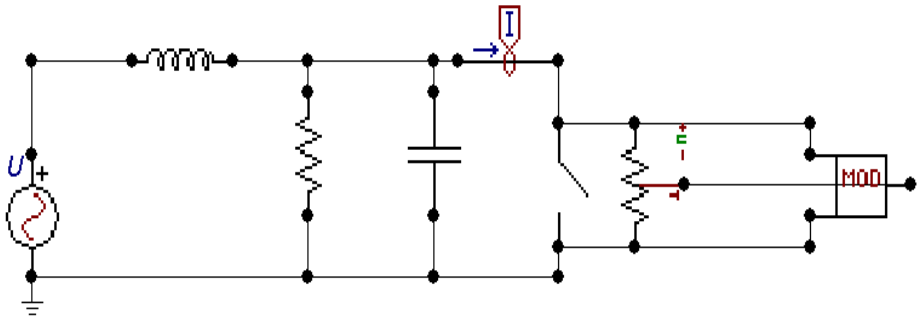

Figure 6-2 Test circuit schematic in ATP-EMTP

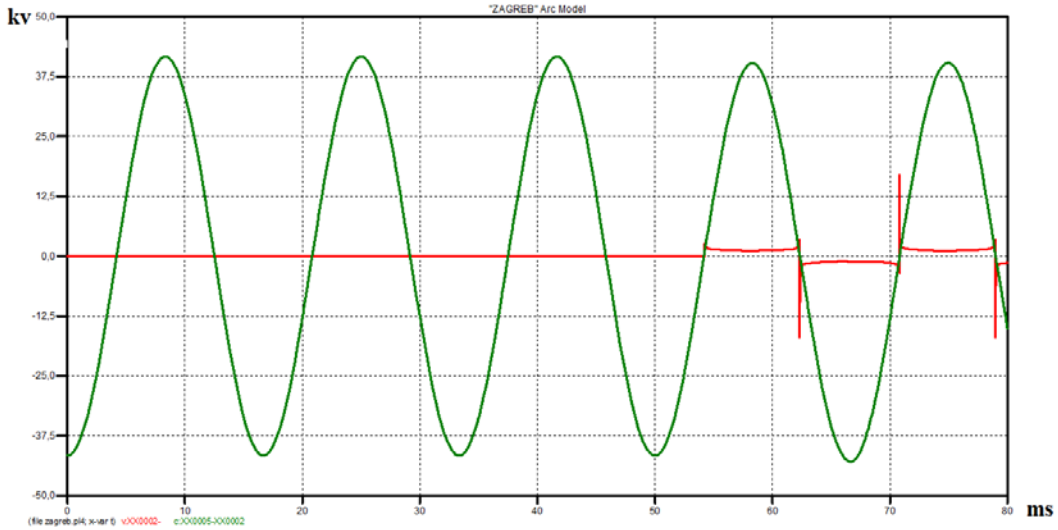

Figure 6-3 Test circuit arc voltage and current simulation in ATP-EMTP

6.2.2 Static "AirArc" EMTP Model of Long Arc in Free Air

In [26] long arcs in free air are investigated. In this study a static arc model, including the length variations was derived. The arc is modeled as a current dependent voltage source with a characteristic distorted rectangular voltage that elongates nonlinearly over time.

In [27] the arc voltage of long arc is modelled as:

$$u_{a0}(t) = \left(U_a + U_b \frac{I_0}{i_b(t)} + R_\delta |i_b(t)|\right) sgn(i_a) + \varepsilon \tag{6.7}$$

Where $u_{a0}(t)$ and $i_a(t)$ are the voltage and current of an arc having a constant length L_0

$$i_b(t) = \begin{cases} I_0 & |i_a(t)| < I_0 \\ |i_a(t)| & |i_a(t)| \geq I_0 \end{cases} \tag{6.8}$$

U_a, U_b, I_0 ($I_0 \neq 0$), R_δ and ε are all parameters defining the shape of the arc voltage. $\varepsilon(t)$ is zero-mean Gaussian noise. U_a is the product of the arc voltage gradient E_a and the length of the arc path L_a (the distance between the arc electrodes). The term $U_b \frac{I_0}{i_b(t)}$ represents the arc ignition voltage and the term $R_\delta |i_b(t)|$ is a quasilinear part determined by arc current i_a. For simplicity R_δ is called arc resistance; it is however, only part of the total arc resistance, which is mainly determined by the value of U_a.

The arc model (6.7) does not consider the elongation of the arc. In [26] the arc model which considers the elongation of the arc is given as:

$$u_{a0}(t) = u_{a0}(t)[1 + Ae^{B(t-T_i)}h(t - T_i)] \tag{6.9}$$

Where A and B are parameters determining the arc elongation dynamics, T_i is the arc inception time, h(t) is the Heaviside function.

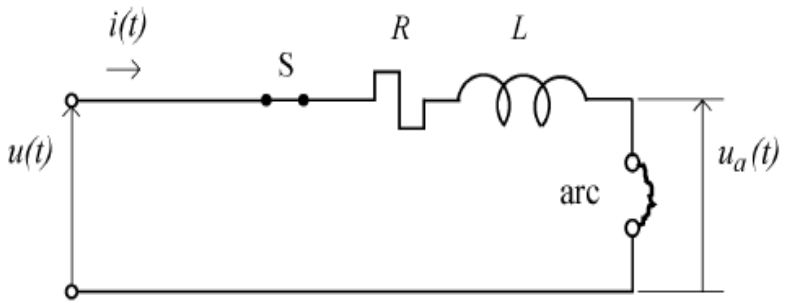

Figure 6-4 “AirArc” test circuit (adopted from [26])

Using the test circuit shown in Figure 6-4 parameters (u(t)=21 kV rms, R=0.65Ω, L=9.55 mH, C=200 pF) and arc model parameters (Ua=1.1 kV, Ub=1.2 kV, R_δ=0.015Ω, A=0.45 and B=5.25\1/s, arc inception at 0.056s) taken from [26], arc model is implemented within the ATP-EMTP environment as shown in Figure 6-5.

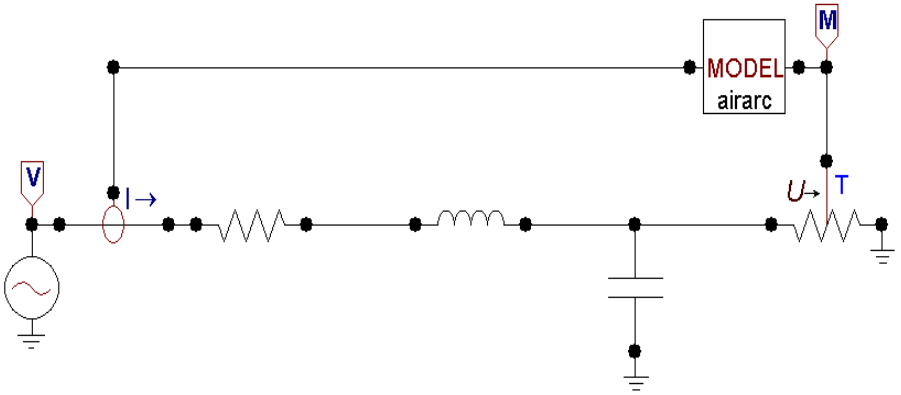

Figure 6-5 Representation of “AirArc” test circuit in ATP-EMTP

The EMTP models code of the “AirArc” model is given in Appendix D. The simulated arc current and voltages are given in Figure 6-6.

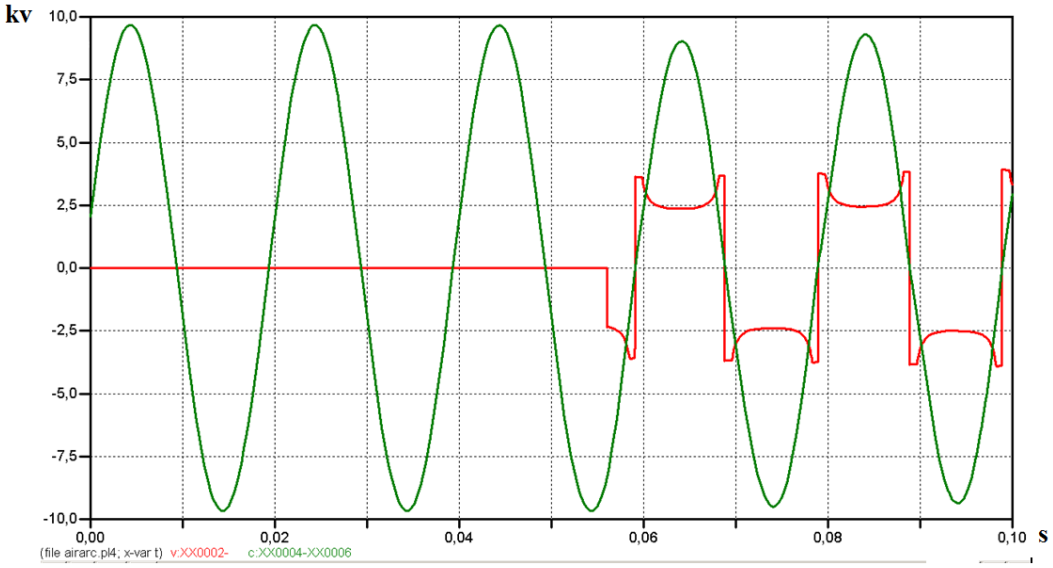

Figure 6-6 Test circuit arc voltage and current simulation in ATP-EMTP

6.3 Modeling of Pantograph Arcing Experimental Setup

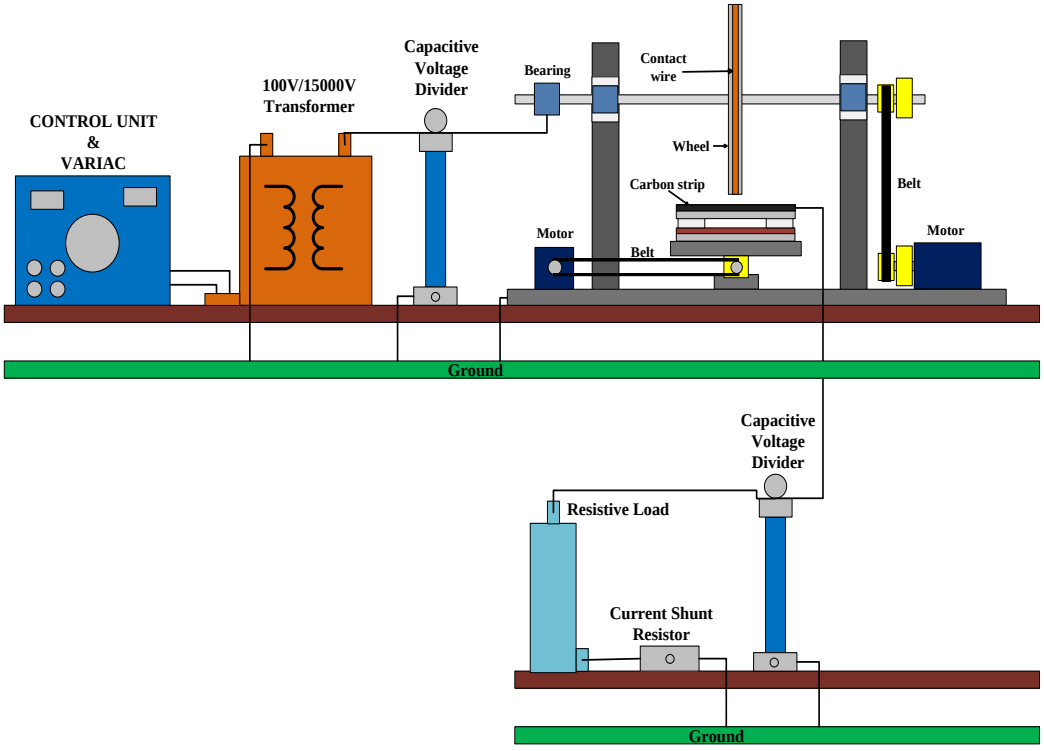

Figure 6-7 Pantograph arcing experimental setup configuration used for ATP-EMTP model

To model the pantograph arcing experimental setup in ATP-EMTP and to validate the model, the setup shown in Figure 6-7 is used. The model schematic, shown in Figure 6-8, consist of a step-up transformer, two capacitor each of them for capacitive voltage dividers, resistors for load and a nonlinear resistor for arc modeling. Arc is represented as a time varying resistance. Modeling of the circuit elements except transformer and arc modeling are straight forward. The transformer primary is adjusted so that HV side of the transformer is 4.5 KV and the load resistance is 380 k Ω. In addition, transformer and arc models are discussed in details in the followings parts.

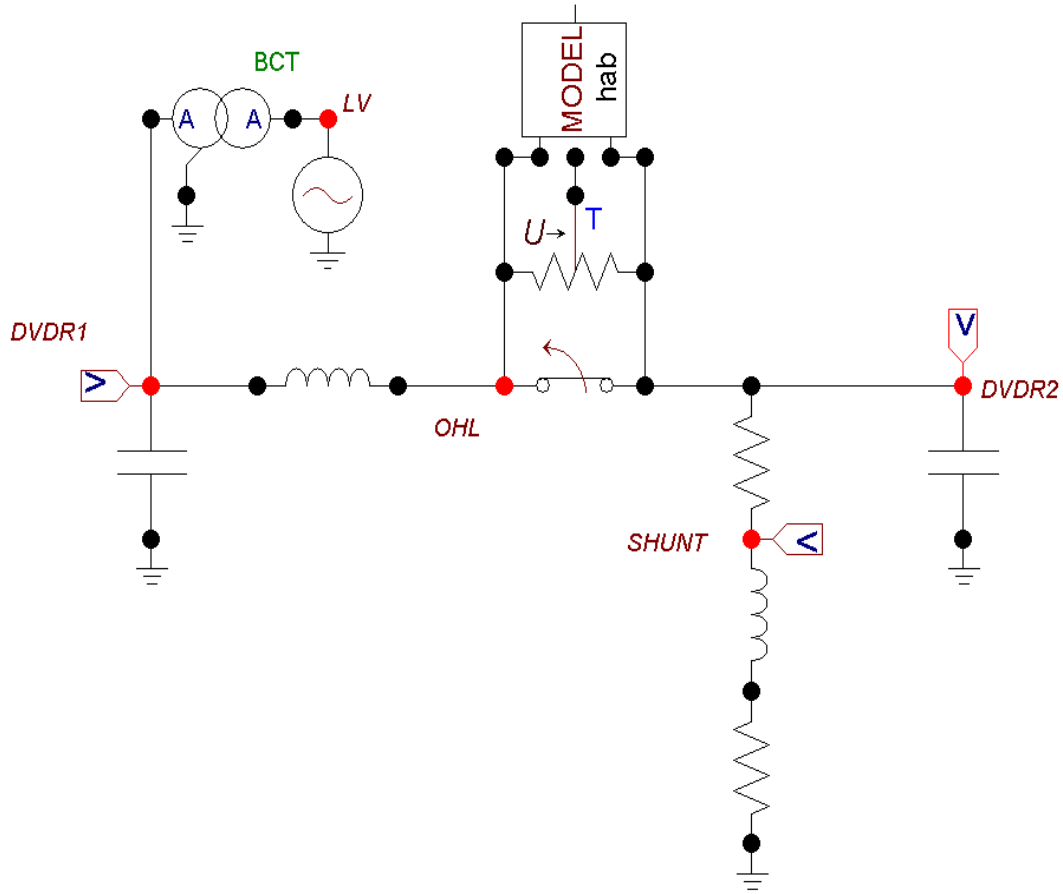

Figure 6-8 Pantograph arcing experimental setup model in ATP-EMTP

6.3.1 Transformer Parameter Tests and Transformer Model

To model the transformers which are used in the test setup in ATP-EMTP, short-circuit and open-circuit tests are conducted on the transformer. Using these test results the transformer parameters are calculated and transformer model is generated in ATP-EMTP.

The short-circuit test can be used to find the equivalent series impedance $R_{eq}+jX_{eq}$. Because the series equivalent impedance in a typical transformer is relatively small, typically an applied primary voltage on the order of 10 to 15 percent or less of rated value will result in rated current.

The equivalent circuit with transformer secondary impedance referred to the primary side and a short circuit applied to the secondary is given in Figure 6-9. The short circuit impedance Z_{SC} looking into the primary under these conditions is

$$Z_{SC} = R_1 + jX_{l1} + \frac{Z_\varphi (R_2 + jX_{l2})}{Z_\varphi + R_2 + jX_{l2}} \tag{6.10}$$

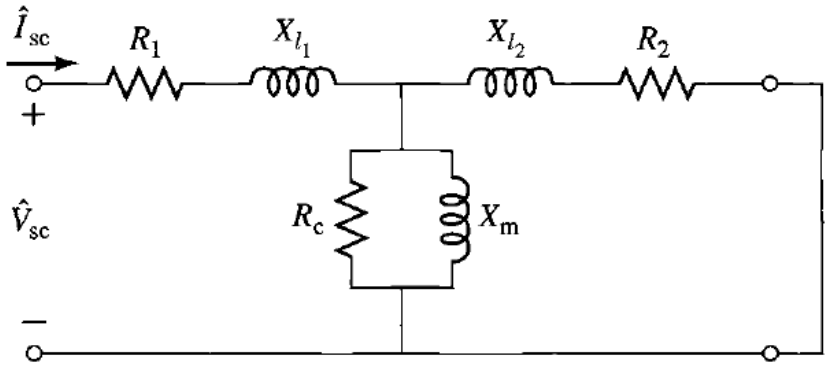

Figure 6-9 Equivalent circuit of transformer with short-circuited secondary

Z_φ of the exciting branch is much larger than that of the secondary leakage impedance. Therefore, the circuit impedance can be approximated as

$$Z_{SC} \approx R_1 + jX_{l1} + R_2 + jX_{l2} = R_{eq} + jX_{eq} \tag{6.11}$$

Applying voltage on the primary side of transformer for rated current flow and measuring applied voltage V_{SC}, the short-circuit current I_{SC} and the power P_{SC}, the equivalent resistance and reactance can be found from,

$$|Z_{eq}| = |Z_{SC}| = \frac{V_{SC}}{I_{SC}} \tag{6.12}$$

$$R_{eq} = R_{SC} = \frac{P_{SC}}{I_{SC}^2} \tag{6.13}$$

$$X_{eq} = X_{SC} = \sqrt{|Z_{SC}|^2 - R_{SC}^2} \tag{6.14}$$

The open-circuit test is performed with the secondary open-circuited and rated voltage impressed on the primary. Under this condition an exciting current of a few percent of full-load current is obtained.

The equivalent circuit with transformer secondary impedance referred to the primary side and the secondary open circuited is given in Figure 6-10. The open circuit impedance Z_{OC} looking into the primary under these conditions is

$$Z_{OC} = R_1 + jX_{l1} + Z_\varphi = R_1 + jX_{l1} + \frac{R_C(jX_m)}{R_C + jX_m} \tag{6.15}$$

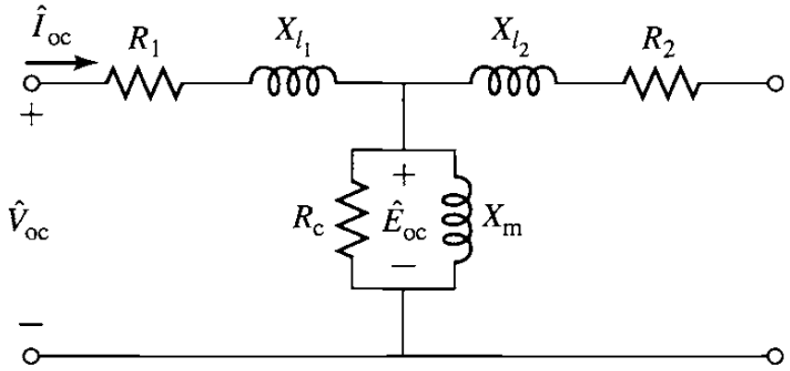

Figure 6-10 Equivalent circuit of transformer with open-circuited secondary

Because the impedance of the exciting branch is quite large, the voltage drop in the primary leakage impedance caused by the exciting current is typically negligible and the primary impressed voltage very nearly equals the EMF induced by the resultant core flux. Similarly, the primary $I_{OC}^2 R_1$ loss caused by the exciting current is negligible. For this reason, the power input P_{OC} very nearly equals the core loss E_{OC}^2/R_C. As a result, it is common to ignore the primary leakage impedance and to approximate the open-circuit impedance as being equal to the magnetizing impedance. Therefore, the circuit impedance can be approximated as

$$Z_{OC} \approx Z_\varphi = \frac{R_C(jX_m)}{R_C + jX_m} \tag{6.16}$$

Applying rated voltage on the primary side of transformer and measuring applied voltage V_{OC}, the open-circuit current I_{OC} and the power P_{OC}, the magnetizing resistance and reactance can be found from,

$$R_C = \frac{V_{OC}^2}{P_{OC}} \tag{6.17}$$

$$|Z_\varphi| = \frac{V_{OC}}{I_{OC}} \tag{6.18}$$

$$X_m = \frac{1}{\sqrt{(\frac{1}{|Z_\varphi|})^2 - (\frac{1}{R_C})^2}} \tag{6.19}$$

The rated primary current of 100V/15000V transformer which is used in the pantograph arcing experimental setup is 6 A. The short circuit and open circuit tests are conducted on this transformer to get equivalent circuit parameters. Low voltage winding of transformer is chosen as primary for both tests. The equivalent circuit parameters (referred to the primary side) given in Table 6-1 are found.

Table 6-1 Transformer measurements and equivalent circuit parameters

Short circuit test measurements	**Equivalent circuit parameters**
V_{SC} = 5.0 V	R_{eq} = 0.694 Ω
I_{SC} = 6 A	X_{eq} = 0.461 Ω
P_{SC} = 25 W	
Open circuit test measurements	
V_{OC} = 100 V	R_C = 400 Ω
P_{OC} = 25 W	X_m = 123 Ω
I_{OC} = 0.85 A	

6.3.2 Pantograph Arc Model

In the previous chapter arc modeling is discussed in details. In this part, suitable arc model for pantograph arcing is produced and validated with experimental results. First of all, Mayr's model with constants given in [25] is used for pantograph arc model. However, it is required to change the model constants and parameters. Using the Mayr's model with in the circuit given in Figure 6-8 and the arc voltage given in Figure 6-11 is obtained in ATP-EMTP. The EMTP models code of the Mayr model is given in Appendix E.

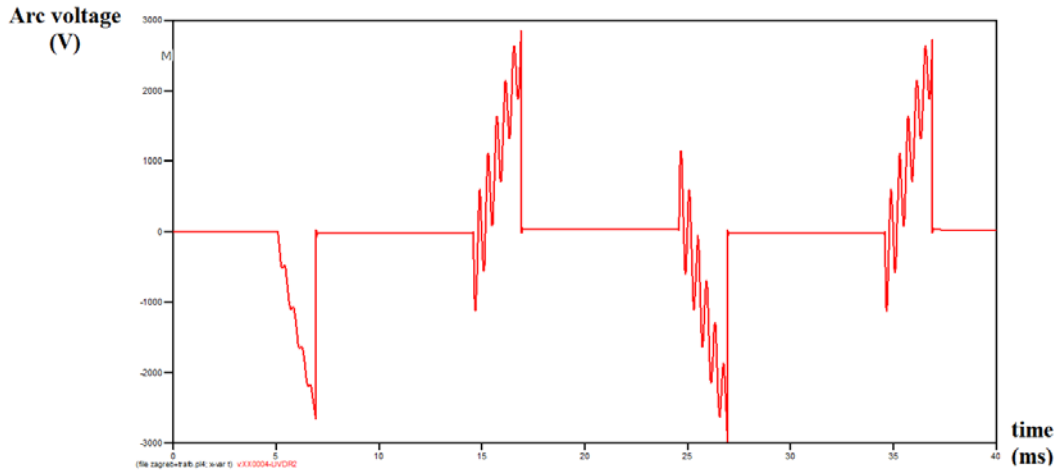

Figure 6-11 Mayr's model arc voltage in ATP-EMTP

The experimental arc voltage of the circuit given in Figure 6-7 is shown in Figure 6-12. The math function signal represents the arc voltage and has a dividing ratio of 149. When the model output is compared with the experimental result, it is shown that the model is consistent with the experimental results for current zero regions. However, for the post zero regions the model need modifications. Actually, it is also consistent with the nature of the model because Mayr's model is suited for modeling of the arc in the vicinity of current zero.

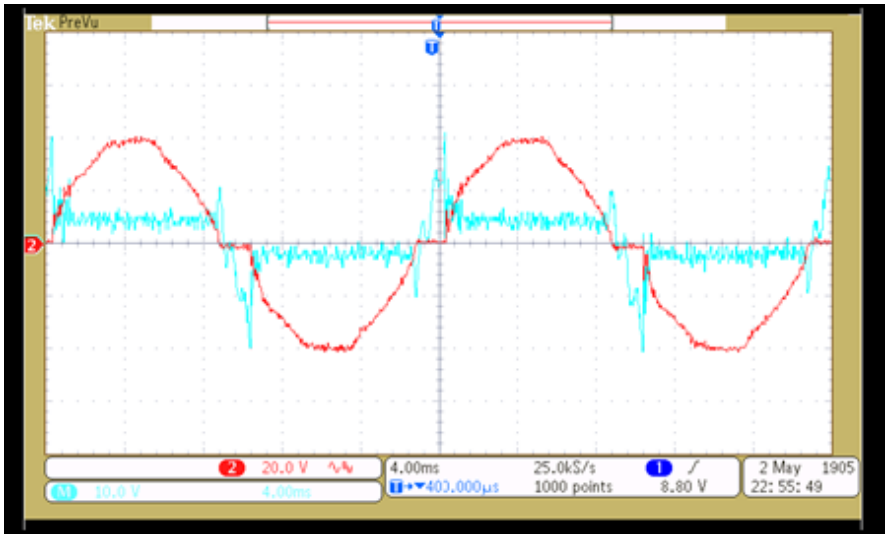

Figure 6-12 Experimental arc voltage

In contrary with the Mayr's model, for high current regions there is a good agreement with the Cassie's model. Therefore Cassie's model is used as an arc model in ATP-EMTP. The arc voltage of the simulation is given in Figure 6-13. The EMTP model code of the Cassie's model is given in Appendix F. When the model output is compared with the actual experimental result, it is shown that model output is consistent with the experimental one for high current regions. However, for the zero current regions the model needs modifications.

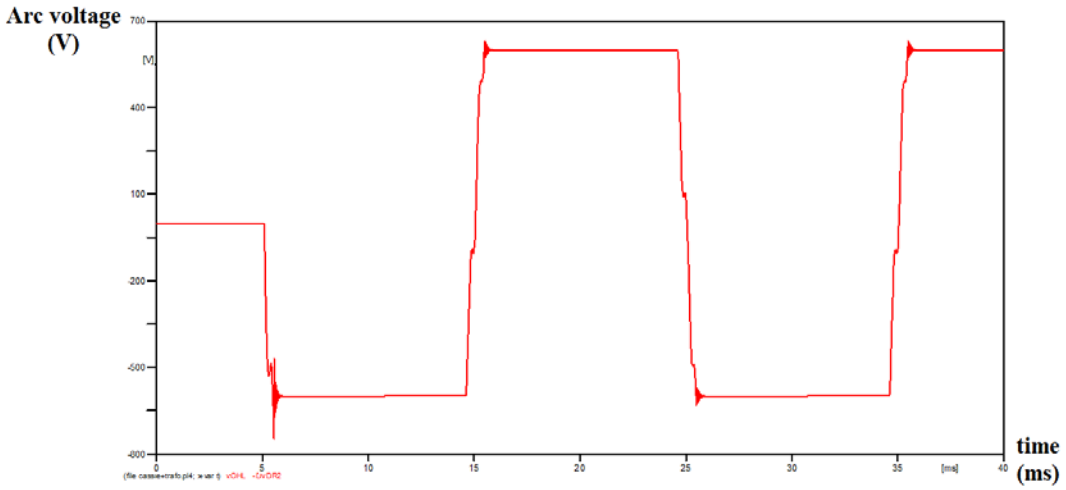

Figure 6-13 Cassie's model arc voltage in EMTP-ATP

Simulation results showed that when the Mayr's model is suitable for the zero current regions, the Cassie's model is suitable for the high current regions. Therefore a hybrid model is used for pantograph arc modeling in this thesis. The arc voltage output of the simulation is given in Figure 6-14. The EMTP model code of the hybrid model is given in Appendix G. When the model output is compared with the actual experimental result, it is shown that the model output is consistent with the experimental result for both zero current and high current regions.

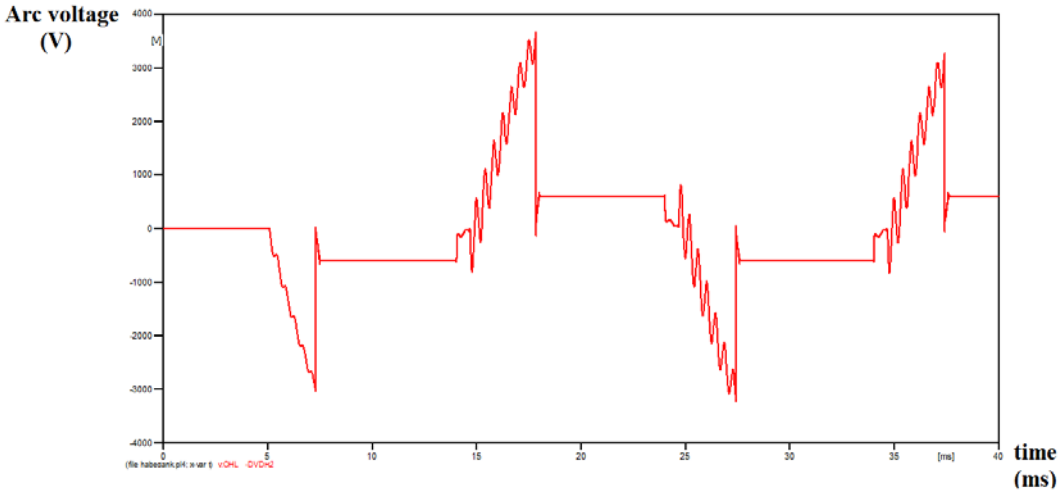

Figure 6-14 Hybrid model arc voltage in ATP-EMTP

CHAPTER 7

FUTURE OF RAIL TRANSFER

7.1 Introduction

After the presentation of the first electric railway, running at a speed of 7 km/h, in 1879, electric railways are expanded rapidly around the world. Now electric railways convey over 90% person trips of whole railway.

Needs of modern society and economy is characterized by increasing mobility of goods and persons. Therefore, railway transportation has a great future. One of main tasks of the railway transportation is transfer of the energy from main grid to the train. In previous chapters some problems of sliding contact power transfer with a pantograph and overhead contact line related with arcing are mentioned. Developments in energy transfer and storage technologies will provide opportunities in railways.

In this chapter contactless inductive power transfer and super capacitors in electric trains are discussed in details.

7.2 Contactless Inductive Power Transfer

A contactless technology for the transfer of electric power to a moving vehicle is based on the use of alternating magnetic field which is generated by a distributed primary conductor loop (power source) and a secondary coil which is called pick-up (power sink). The primary conductor loop and the secondary pick-up are magnetically coupled to ensure the inductive power transfer from the power source to the power sink. The total system acts similar to a single phase transformer which is characterized by large stray inductance and a large magnetization current due to the large air gab between the primary side and the secondary side of the inductive power transfer system [28].

By using the contactless inductive energy transmission technology, conductor rails, sliding contacts, trailing cables or slip rings can be eliminated [29]. Other advantages are; no wear and tear on the electrical contacts, no contact resistance, no sparking and no non-protected voltage-carrying contacts [29], [30].

7.2.1 Model of Magnetic System

The investigations have shown that the energy transmission parameters of contactless systems mainly depend on the dimensions of the primary and secondary systems, the existence of ferrite cores on the primary or secondary sides, length of the air gap, the number of turns on the primary and secondary sides, the secondary operation point (load) and the transmission frequency [30].

The E-shaped iron core pick-up is useful for monorail transportation systems, while the flat iron core pick-up is used for ground floor transportation systems. Due to the large air gap which is common in both designs high magnetization currents are required. Especially for the flat pick-up the high amount of stray flux leads to low magnetically coupling and high stray reactance [28].

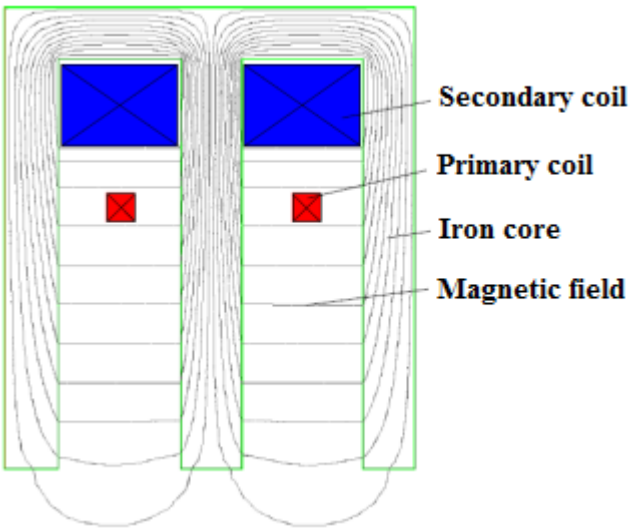

Figure 7-1 E-Shape Pick-Up (Flux Simulation)

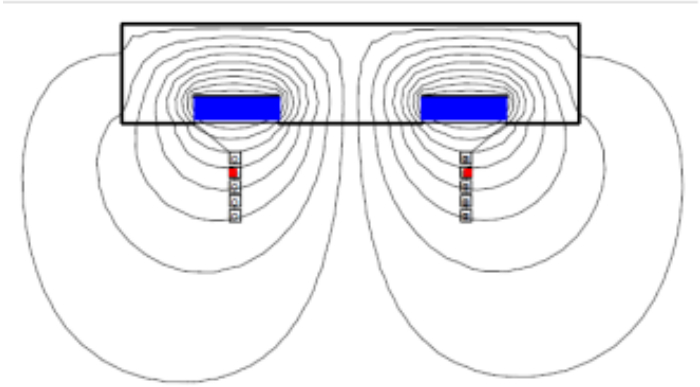

Figure 7-2 Flat Pick-Up (Flux Simulation)

7.2.2 High Frequency Inverter

The transmission frequency influences the efficiency critically. High efficiency in large air gap systems requires high transmission frequencies of at least 100 kHz [28], [29]. With a given volume of the transformer the transferred power increases proportional to the frequency. The increase in the frequency is limited with the resulting increase in the inverter switching losses. Although the size and cost of all components of the inductive power system can be reduced by increasing the frequency, it is a good and favorable practice to set the frequency in the range of 10 kHz to 30 kHz for high power ratings. The research work indicates that the switching losses of the current state IGBT-technology are limiting the frequency range which can be used [28].

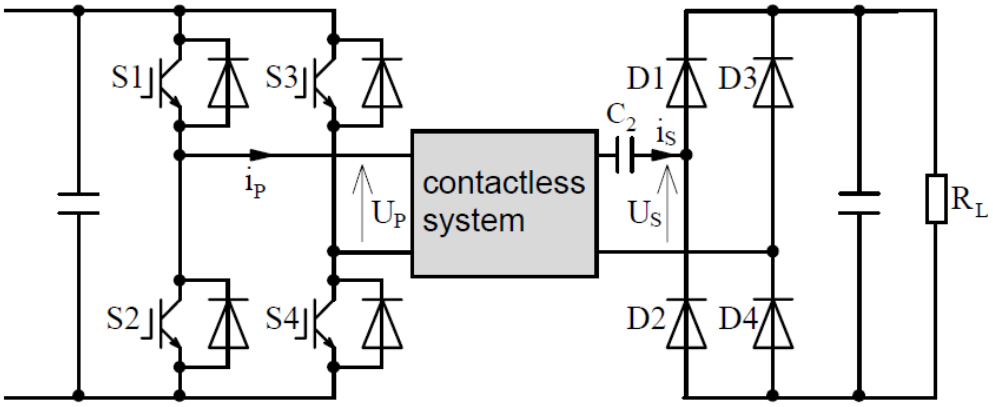

Figure 7-3 High frequency inverter for contactless energy transmission

7.2.3 Contactless Inductive Power Transferred Trains

In [32] an experimental arrangement transfers an electric power of 1 kW through an air gap of 300mm. At a 100 kHz transmission frequency, the overall efficiency, including magnetic and power electronic components, is greater than 80%.

In [33] authors have proposed the simple C core type wide air gap transformer and the experimental data on a low power prototype of the contact-less power transmission equipment are reported, in which the air gap control is installed, and the primary and secondary move at the relative speed up to 25 m/s. A power transmission efficiency of 70% was achieved. The concept of the proposed system is given in Figure 7-4.

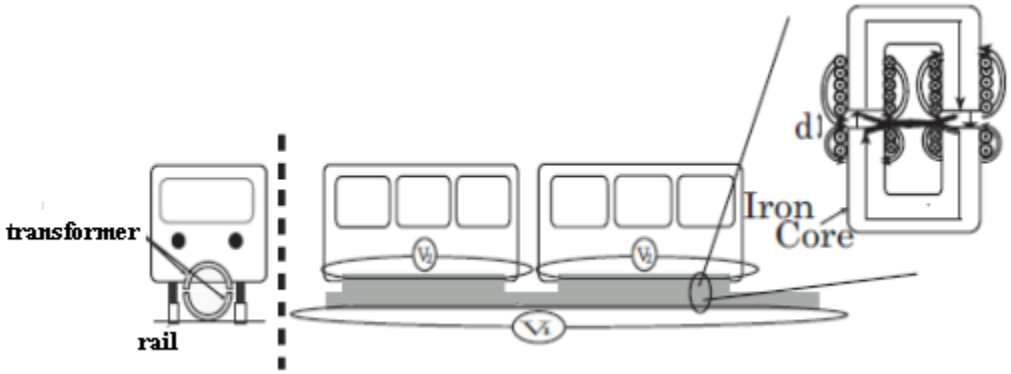

Figure 7-4 C core transformer system induction power transfer system (adopted from [33])

In [34] an inductive power transfer test system for railways is constructed with 10 cm narrow rail with. The power supply inverter uses 440 V, 3 phase input and supplies 20 kHz output current. To null the high voltages of power rail and pick-up and to transfer maximum power to vehicles, resonant capacitors are inserted to each side of the rail and the pick-up. The test results show that the maximum output power is 35 kW and the maximum efficiency is 74 % at 27 kW output. The structure of the transformer is given in Figure 7-5.

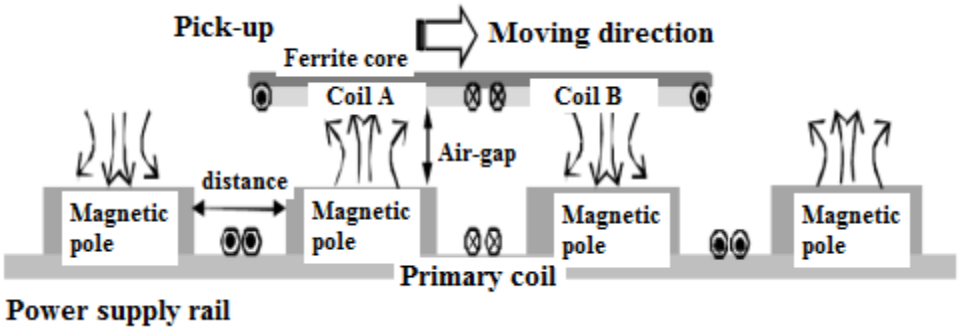

Figure 7-5 Structure of the Inductive Power Transfer Test System

Bombardier is the first company offers the catenary free and contactless commercial urban rail vehicles. The company named the system as PRIMOVE system. In [35] it is stated that 270 kW continuous output of the PRIMOVE system is designed for a typical light rail vehicle (30-42 meters long, operating at a speed of up to 50 km/h with a gradient of up to six percent). The author of [34] states that Bombardier improved the power transfer efficiency up to 92 % at 6.5 cm air gap. This system can also be used for cars and buses.

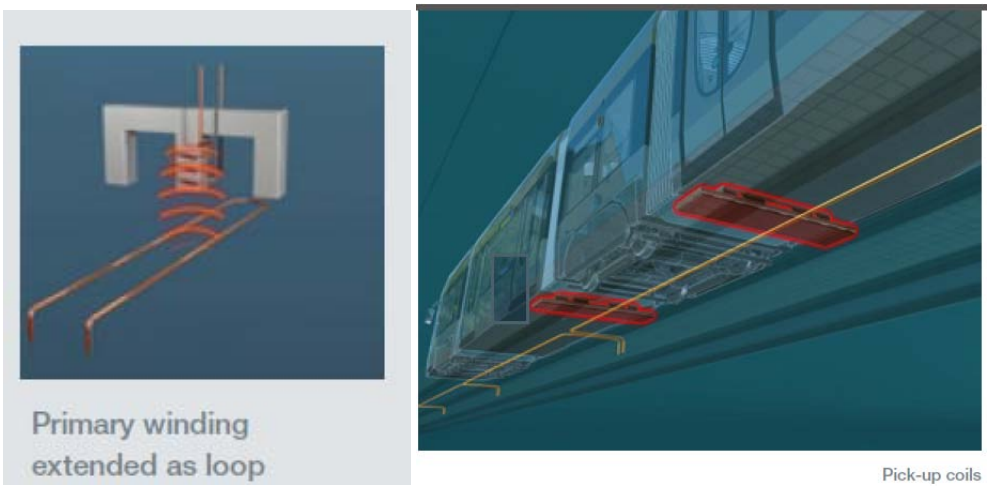

Figure 7-6 PRIMOVE system (adopted from [34])

Although the efficiency of the contactless induction power transfer systems is lower compared to a conventional pantograph catenary rail system, the overall advantages have to be taken into consideration when planning new transportation systems. Contactless power transfer system is resistant to all weather and ground conditions. Using this technology for tram and buses eliminates the overhead wires and increase the

attractiveness of the city. The improvement of this technology depends on the improvements of semiconductor and magnetic material technologies.

7.3 Super Capacitors in Trains

7.3.1 Super Capacitors in Electrical Braking

The use on board of super capacitors unit in electrical braking reduces the power peak demand up to 50%. The reduction in the peak demand provide reduction in line drop voltage up to 1% and recovering energy on board during braking operations up to 30%. [36].

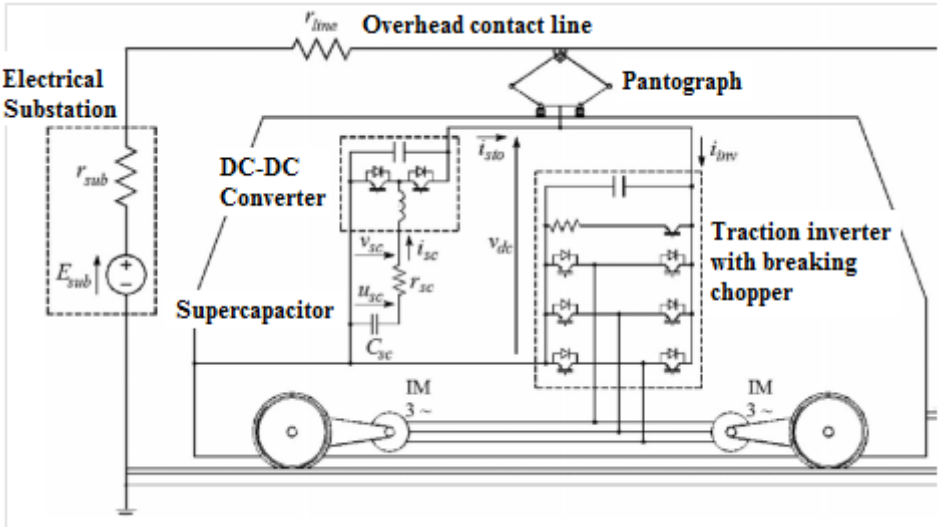

Figure 7-7 Electrical drive configuration equipped with super capacitors (adopted from [37])

7.3.2 Super Capacitor Train

A Chinese company, CSR Zhuzhou Electric Locomotive has unveiled a prototype light metro train set which uses super capacitor energy storage to operate without an external power supply. Developed in conjunction with Chinese Academy of Engineering, the train set has under floor power pick-ups which are used to charge the roof-mounted super capacitor unit from a fixed supply while the train is stood at a station. The charging time of the train set is only 30 sec and the charge can power the train for 2 km. Energy regenerated during braking is also charge the super capacitors. The train set is designed for a maximum speed of 80 km/h. The super capacitor has a greater power density than lithium-ion batteries, and wireless operation is considered as a cheaper and less visually

intrusive alternative to conventional electrification. Commercial production is planned by 2014 [38].

Figure 7-8 Chinese super capacitor light train (adopted from [38])

CHAPTER 8

CONCLUSION AND COMMENTS

8.1 Conclusion

The objective of the traction power supply is to ensure uninterrupted, reliable and safe operation of the electric traction vehicle. The sliding contact between pantograph and overhead line is a critical interface between the train and high voltage power supply in an electrified railway.

Arcing from pantograph is commonly observed throughout the year. However, factors like increasing train speed, current and especially ice formation on the lines contribute to the pantograph arcing. The ice formation on the power lines forms an insulating layer which separates it from the pantograph. However, the current will not be completely interrupted but flows through the arcs established between the pantograph and the line. On the other hand, the pantograph arcs introduce a certain distortion into the supply voltage and current waveforms.

In this thesis, pantograph arcing and some of the effects on the railway vehicle's power supply were investigated. A test setup was designed and implemented to investigate the pantograph arcing phenomena. The effects of the parameters like contact distance, load current and power factor on the pantograph arcing were studied. A pantograph arc model is generated in ATP-EMTP and validated with the experimental results.

To understand the effects of transformer on the voltage at the test setup, harmonic contents of the HV input and LV output signals of transformer is compared using FFT function of an oscilloscope. The amplitudes of harmonics are given in Table 4-3. In addition, the harmonic frequency histograms of HV input and LV output of transformer is shown in Figure 4-3. Comparing the harmonics on both sides of the transformer, it can be said that transformer has very little contribution to the harmonic content of the voltage.

The track circuit based signaling systems are operating using the dc or even harmonics of the traction power frequency. Test results shows that pantograph arcing distorts the sinusoidal current waveform. During the current zero crossings of the ac supply voltage

arc is extinguished and after the voltage reaches enough magnitude it reignites again. Between these two events current remains at zero. This causes both even and odd harmonics on the current. Therefore, pantograph arcing can cause conducted interference with the track signaling systems. False signaling in the railways may cause accidents and delays in the rail operations. Same problems are also covered in [16].

In tests, the current has peaks every half cycle due to arcing. Therefore, pantograph arcing also may cause the wrong opening of the protective circuit breakers because of the current peaks. This is another problem due to pantograph arcing. Same problem also mentioned in [41] and [42].

When the experimental results of arc voltages of the positive and negative half cycles are compared, it can be said that they are not symmetrical. The arc voltage at positive half cycle is greater than the negative half cycle in this work. The current is 10 mA in the test setup. Therefore, the line and carbon contact are at the same temperature. With the help of Richardson's law, and thermionic properties of carbon and brass, it can be said that emission current density of brass (copper) is higher than carbon. Therefore, it is easier to liberate electrons from the brass (copper). Results of pantograph arcing experiments conducted by "OHL Ice Team" in Sweden also shows asymmetry between the arc voltages. However, they found that arc voltage is greater at negative half cycle contrary to the results of this work. At negative half cycle, carbon strip is anode and copper contact line is cathode. Since copper contact is always cool, it causes a lower rate of electron emission compared to the heated carbon when it is the cathode. Therefore, it can be concluded that the arc voltage is higher when the copper contact line is the cathode. In [16], experiments conducted by "OHL Ice Team" has a supply current of order of 10 A with the help of a more powerful voltage supply. On the other end, experiments conducted with supply currents order of 10 mA in this work. Therefore, the pantograph contact (carbon) was at a much higher temperature then the copper line in their work. This may causes a higher rate of thermionic emission from the carbon when it is the cathode resulting in a higher conductivity in the arc and a lower arc voltage as observed.

Test results showed that distortion in the supply voltage and current has a linear relation with contact separation between the pantograph and over head line. When no contact distance is set between the contacts, there is relatively small distortions in the voltage and current. However, with the increase in the contact distance, distortion in the voltage and current increased. In the tests 1, 2 and 5 contact distances are changed while the other variables are kept constant. The peak values of the arc voltages are measured 1650V, 5700V and 7500V, respectively. Using the Paschen equation breakdown voltages for 1 mm and 2 mm contact distance are found 7400 V and 13240 V, respectively. As Paschen law states, breakdown voltages increases with electrode separation. The conditions in the case of re-ignition of a self-sustained discharge by an alternating potential are vastly

unlike those existing in the case of the original breakdown of the gas. In the arc plasma, the number of free ions is larger than those in the fresh gas. Therefore in the experiment reignition voltages are measured to be smaller than breakdown voltages of the gas for given contact distances. In conclusion, to reignite the arc, the required voltage increases with contact separation. These are also consistent with the train operation in summer and winter. In summer, pantograph arc is relatively slight since there is no ice between the contacts. On the other hand, at temperature below freezing point hoar frost can form on the conductors when enough moisture is in the air and wind is blowing against the lines. Also super-cooled rain and wet snow can lead to serve ice formation on the conductors. This ice layer increases the distance between the contacts. Therefore, visible arcs are realized in winters. Harmonic content of the pantograph voltage also increases with the contact separation distance. This is also related with the increase in the arc voltage.

In tests, increase in the arc current reduced the harmonic contents of both current and voltage. In the tests 2 and 4 load currents are changed with changing resistive load while the other variables are kept constant. The arc current is doubled in test 4. The peak values of the arc voltages are measured as 5700V and 4050V, respectively. An AC arc may be extinguished or reignite after zero current crossings. The arc reignition arises from the birth of a new cathodic spot after zero current crossings. In principle, the generation of a new spot is not different from a first ignition of the arc, except that the extinguished arc may create circumstances which favor new births. For example, an electrode can be considerably hotter after the arc has operated for some time than it was before the first ignition. Mechanism of the cathodic spots is purely or essentially thermo-electronic. Arc reignition is easy as long as the temperature is still above a certain threshold when the conditions favorable to the reignition of an arc are restored. As the hot spot cools down, it is observed that the reignition becomes less and less possible. Reignition at the new cathode is helped considerably by the heat liberated at the old anode since they are one and the same surface. The active portion of the electrodes will have become heated, the extent of this heating is dependent on the current of the discharge. The degree of ionization at zero current is a direct function of the arc current. In the absence of a reappearing voltage, the ionization when the current is low will quickly disappear by recombination in the gas and neutralization at the electrode surfaces. For higher values of current, the volume deionization will be slower, because in the presence of thermal ionization, deionization will proceed at a much slower rate, determined by a time constant characteristic of the gas. Obviously, in the case of small current arcs, the reapplied voltage must be very much higher or must be applied at a much higher rate than for heavy currents if deionization is to be arrested. Therefore, an increase in the arc current causes a decrease in the arc voltage.

Results of the experiments also show that adding inductance to the circuit decreases the zero current regions time so the harmonic content of the current. The magnetic energy

stored in the inductances of the load, forces the current to flow. Therefore, high voltage will appear across the arc during the extinction. In modern trains power factor of the traction unit can be arranged easily. Therefore during winter, when the visible arcs are observed, trains may be driven with a lagging power factor to reduce the arcing.

Arc models were originally developed for better understanding of the current interruption process in high voltage circuit breakers. In this thesis, different arc models are examined and evaluated to use an arc model for pantograph arcing. A hybrid model is generated from Mayr and Cassie arc models for pantograph arc simulations. Arc is represented as a time varying resistance. The pantograph arcing experimental setup model is formed in ATP-EMTP and different arc models are used in the experimental setup model. The pantograph arcing model also validated with the experimental results.

Firstly, Mayr's model is used for pantograph arc model. When the model output is compared with the experimental result, it is shown that the model is consistent with the experimental results for zero current regions. However, for the post zero regions the model needs modifications. Actually, it is also consistent with the nature of the model because Mayr's model is suited for modeling of the arc in the vicinity of zero current.

Secondly, Cassie's model is used for pantograph arc model. In contrary with the Mayr's model, for high current regions there is a good agreement with the Cassie's model. Therefore Cassie's model is used as an arc model in ATP-EMTP. When the model output is compared with the actual experimental result, it is shown that model output is consistent with the experimental one for high current regions. However, for the zero current regions the model needs modifications.

Simulation results showed that the Mayr's model is suitable for the zero current regions and the Cassie's model is suitable for the high current regions. Therefore a hybrid model is used for pantograph arc modeling in this thesis. When the hybrid model output is compared with the actual experimental result, it is shown that the model output is consistent with the experimental result for both zero current and high current regions. This model may be used in transient analysis of the railway power system network.

Needs of modern society and economy is characterized by increasing mobility of goods and persons. Therefore, railway transportation has a great future. One of main tasks of the railway transportation is transfer of the energy from main grid to the train. In this thesis some problems of sliding power transfer with a pantograph and overhead contact line is discussed. Developments in energy transfer and storage will provide opportunities in railways. Inductive contactless power transfer and energy storage with super capacitors are some of the future trends in railway industry. Prototypes of these technologies are

already on the rails. Researches and investments in new technologies in railway industry will be beneficial.

8.2 Comments

In modern trains, pantographs transfer hundreds of amperes to the vehicle. However, in the present work the pantograph arcing test setup was designed for tens of milliamperes to limit the cost of the test setup. Although the arcing tests in this thesis conducted with small current, they show similarities with the arcing tests on the DB locomotive class BR185 in Luxembourg, December 2001 conducted by “OHL Ice Team”. The main difference between the tests is the asymmetry between the arc voltages as discussed above. In the present work since the arc current is very small with respect to the real case, thermal ionization is smaller compared to the real case. For these reasons a test setup with a much more powerful high voltage supply can be more useful to understand the pantograph arcing phenomena more accurately.

It is known that pantograph arcing is a source of radiated and conducted electromagnetic interference. Pantograph arcing causes radiated interference due to the rapid changes in the current with the wireless and radio communication services. Besides the conducted interference with railway signaling systems, in the present work it is noticed that radiated electromagnetic fields couple into the step motor control systems and disturbed the operation of the motor. This problem is solved by shielding the motor cable and grounding the shield at connecter ends. This thesis focused on the conducted interference of the pantograph arcing. However, studies focuses on the radiated interference of pantograph arcing may also be very useful.

REFERENCES

[1] The Siemens tram from past to present. [Online]. Available: http://www.siemens.com/history/en/innovations/transportation.htm#content-zone (last accessed on 13 September 2013)

[2] Electrifying Trains. [Online]. Available: http://www.siemens.com/innovation/en/publikationen/publications_pof/pof_spring_2004/electric_trains_article.htm (last accessed on 13 September 2013)

[3] Uzuka, T., "Trends in high-speed railways and the implications on power electronics and power devices," Power Semiconductor Devices and ICs (ISPSD), 2011 IEEE 23rd International Symposium on, pp.6, 9, 23-26 May 2011

[4] Kiessling, F., Puschmann, R., Schmieder, A., & Schmieder, E. (2009). *Contact lines for electric railways*. (2 ed.). Erlangen, Germany: Publicis Publishing.

[5] Klontz, K.W.; Divan, D.M.; Novotny, D.W.; Lorenz, R.D., "Contactless power delivery system for mining applications," Industry Applications, IEEE Transactions on , vol.31, no.1, pp.27,35, Jan/Feb 1995

[6] Phillpotts, R., "Monitoring discontinuities in the 25 kV overhead," Condition Monitoring for Rail Transport Systems (Ref. No. 1998/501), IEE Seminar on , vol., no., pp.9/1,9/3, 10 Nov 1998

[7] Kobayasi, T., Fujihasi, Y., Tsuburaya, T. & Satoh, J. (1998). *Current collecting performance of overhead contact line-pantograph system at 425 km/h*. Electrical Engineering in Japan, 124(3), 73-81.

[8] Occoleanu, C. F., Manolea, G., & Cividjian, G. (2010). *Experimental study of contact resistance variation for pantograph-contact line contact* . In *Proceedings of the international conference on risk management, assessment and mitigation (RIMA '10)* (pp. 101-105). Bucharest, Romania: WSEAS Press.

[9] Occoleanu, C. F., Popa, I., Manolea, G., Dolan, A. I., & Vlase, S. (2009). Temperature investigation in contact pantograph - ac contact line. *International Journal of Circuits, Systems and Signal Processing*, *3*(3), 154-163.

[10] Bucca, G., & Collina, A. (2009). A procedure for the wear prediction of collector strip and contact wire in pantograph–catenary system. *Wear*, *266*(1-2), 46-59.

[11] Bucca, G., & Collina, A. (2009). A procedure for the wear prediction of collector strip and contact wire in pantograph–catenary system. Wear, 266*(1-2), 46-59.*

[12] Wang, W., Dong, A., Wu, G., Gao, G., Zhou, L., Wang, B., Cui, Y., & Liu, D. (2011, September). *Study on characterization of electrical contact between pantograph and catenary*. Paper presented at 2011 ieee 57th holm conference on electrical contacts, Minneapolis, Minnesota, USA.

[13] Tianzhi Li; Guangning Wu; Lijun Zhou; Guoqiang Gao; Wangang Wang; Bo Wang; Donglai Liu; Dajian Li, "Pantograph Arcing's Impact on Locomotive Equipments," Electrical Contacts (Holm), 2011 IEEE 57th Holm Conference on, pp.1,5, 11-14 Sept. 2011

[14] Yu-Jen Liu; Chang, G.W.; Huang, H.-M., "Mayr's Equation-Based Model for Pantograph Arc of High-Speed Railway Traction System," Power Delivery, IEEE Transactions on, vol.25, no.3, pp.2025,2027, July 2010.

[15] Bormann, D.; Midya, S.; Thottappillil, R., "DC components in pantograph arcing: mechanisms and influence of various parameters," Electromagnetic Compatibility, 2007. EMC Zurich 2007. 18th International Zurich Symposium on , vol., no., pp.369,372, 24-28 Sept. 2007.

[16] “Ice on the overhead line of AC electrified railways: Summary report from the OHL ice team”, The OHL Ice Working Group, Nov. 2003.

[17] J. M. Somerville, *The Electric Arc*. New York: John Willey & Sons Inc., 1959.

[18] M. F. Hoyaux, *Arc Physics*. New York: Springer-Verlag, 1968.

[19] J. D. Cobine and R. Burton, “The Application of Paschen’s Law to the Re-Ignition of an Arc”, *Journal of Applied Physics*, vol. 8, Apr. 1937.

[20] Lou van der Sluis, *Transients in Power Systems.* England: John Willey & Sons Ltd., 2001.

[21] Electricity 2013. *Encyclopædia Britannica Online*. Retrieved 04 October, 2013, from http://www.britannica.com/EBchecked/topic/182915/electricity.

[22] F. Cardarelli, “Miscellaneous Electrical Materials,” in *Materials Handbook: a concise desktop reference*, 2nd ed. London: Springer, 2008, ch.9, pp. 552-553.

[23] P. H. Schavemaker and L. van der Sluis, “The Arc Model Blockset”, *in Proceedings of the second IASTED International Conference on Power and Energy Systems (EuroPES)*, Crete, Greece, Jun. 2002, pp. 644-648.

[24] J. C. Das, *Transients in Electrical Systems: Analysis, Recognition and Mitigation.* The McGraw-Hill, 2010.

[25] S. Hutter and I. Uglesic, “Universal Arc Resistance Model "Zagreb" For EMTP ”, *in Proceedings of the CIRED International Conference on Electricity Distribution*, Vienna, Austria, May. 2007.

[26] Terzija, V.; Preston, G.; Popov, M.; Terzija, N., "New Static “AirArc” EMTP Model of Long Arc in Free Air," Power Delivery, IEEE Transactions on , vol.26, no.3, pp.1344,1353, July 2011.

[27] Terzija, V.V.; Koglin, H-J, "Long arc in free air: laboratory testing, modelling, simulation and model-parameters estimation," Generation, Transmission and Distribution, IEE Proceedings- , vol.149, no.3, pp.319-325, May 2002.

[28] Jurgen, M., Gunther, B., Robert, C., & Faisal, T. (2006). *Contactless inductive power supply*. Paper presented at Maglev'2006: The 19th international conference on magnetically levitated systems and linear drives, Dresden, Germany.

[29] Rathge, C., & Kuschner, D. (2009, September). *High efficient inductive energy and data transmission system with special coil geometry*. Paper presented at Power electronics and applications, 2009. EPE '09. 13th European conference, Barcelona.

[30] Mecke, R. (2001). *Contactless inductive energy transmission systems with large air gap*. Paper presented at Epe 2001

[31] Lee, D., Jang, D. U., Kim, H. C., & Jung, S. Y. (2011). Numerical analysis and design of moving contactless high power transformer. *Journal of Magnetics,16*(4), 423-426.

[32] Mecke, R., & Rathge, C. (2004). *High frequency resonant inverter for contactless energy transmission over large air gap.* Paper presented at 2004 35th annual IEEE power electronics specialists conference, Aachen, Germany.

[33] Kawamura, A., Kuroda, G., & Zhu, C. (2007). *Experimental results on contact-less power transmission system for the high-speed trains*. In *IEEE 38th Annual Power Electronics Specialists Conference* (pp. 2779-2784).

[34] Huh, J., Lee, S., Park, C., Cho, G. H., & Rim, C. T. (2010, September). *High performance inductive power transfer system with narrow rail width for on-line electric vehicles*. Paper presented at Energy conversion congress and exposition (ECCE), Atlanta, GA

[35] Primove. [Online]. Available: http://primove.bombardier.com/ (last accessed on 13 September 2013)

[36] Iannuzzi, D.; Tricoli, P., "Metro trains equipped onboard with supercapacitors: A control technique for energy saving," *Power Electronics Electrical Drives Automation and Motion (SPEEDAM), 2010 International Symposium on* , vol., no., pp.750,756, 14-16 June 2010

[37] Iannuzzi, D.; Tricoli, P., "Speed-Based State-of-Charge Tracking Control for Metro Trains With Onboard Supercapacitors," *Power Electronics, IEEE Transactions on* , vol.27, no.4, pp.2129,2140, April 2012

[38] Supercapacitor light metro train unveiled. [Online]. Available: http://www.railwaygazette.com/news/urban/single-view/view/supercapacitor-light-metro-train-unveiled.html#.UlaSiwPB91E.email (last accessed on 13 September 2013)

[39] Z. Kolacinski. “Modeling of Short Arc Re-ignition”, *Journal of Physics D: Applied Physics*, vol.26, no.11, pp1941-1947, 1993.

[40] Tcdd Hakkinda Genel Bilgi. [Online]. Available: http://www.tcdd.gov.tr/home/detail/?id=266 (last accessed on 23 October 2013)

[41] Midya, S.; Bormann, D.; Schutte, T.; Thottappillil, R., "Pantograph Arcing in Electrified Railways—Mechanism and Influence of Various Parameters—Part I: With DC Traction Power Supply," *Power Delivery, IEEE Transactions on* , vol.24, no.4, pp.1931,1939, Oct. 2009

[42] Midya, S.; Bormann, D.; Schutte, T.; Thottappillil, R., "Pantograph Arcing in Electrified Railways—Mechanism and Influence of Various Parameters—Part II: With AC Traction Power Supply," *Power Delivery, IEEE Transactions on* , vol.24, no.4, pp.1940,1950, Oct. 2009

APPENDIX A CARBON DATASHEET

MEGA — **Main brush grades — Qualités standard**

HARD GRADES

Hard grades made from amorphous carbon (retort coal, carbon black, coke) have a robust cleaning and long wearing characteristic. Normally used on commutators with flush mica and partially even with undercut mica. Grades with high electrical resistance and graphite structure are used for difficult commutation and high circumferential speed.
APPLICATION: fractional h. p. motors, electrical tools, domestic machines, up to 30 KW and up to 500 V, contacts and current collectors.

CHARBON DURS

Ils sont fabriqués à partir de carbones amorphes (de cornue, suie, coke). Ils possèdent une texture compacte, une grande dureté ainsi que des actions nettoyantes.
Pour des commutations difficiles et des vitesses circonférentielles élevées il est conseillé d'employer des qualités en charbon dur à haute résistance électrique et à structure graphitique.
APPLICATION: machines universelles, outillages électriques, appareils électroménagers, contacts et charbons de prises de courant, machines avec ou sans mica fraisé, jusqu'à env. 30 KW et 500 V.

Grade Qualité	Spec. resistance Résistance spéc. Ohm mm²/m	Bulk density Densité apparente g/cm³	Bending strength Charge de rupture N/mm²	Rockwell-Hardness HR 10/40	Admissible load Charge admissible A/cm²	Max. speed Vitesse m/s	Voltage drop Chute au contact V	Friction Frottement μ
H2	40	1,45	20	100	7	25	m	m
H4	45	1,50	24	75	8	40	n	n
H4S2	45	1,52	23	78	8	40	n	m
H6	36	1,50	38	85	8	30	n	n
H9	500	1,42	25	80	6	40	h	m
H12	800	1,55	24	80	8	45	h	s.n.
H16	500	1,34	18	30	8	45	h	s.n.
H20	100	1,52	35	90	8	40	m	m
H47	250	1,45	20	70	8	40	h	m
H67	250	1,45	18	70	8	40	h	m

GRAPHITE GRADES

Carbon graphite brushes consist of various graphite and carbon materials, having weak grinding effect due to mineral ingredients. Mica must be undercut. The brush is able to grind off burnt spots on the commutator, whilst speed and brush fire are low.
APPLICATION: machines with high speed, for turbo-alternator sliprings and D. C. machines, micro motors, fractional h. p. motors and dynamos.

CHARBONS GRAPHITIQUES

Ils sont fabriqués à partir de différents graphites et de carbones; ils ont du fait de leur composition minérale une faible action abrasive. L'isolation des lamelles devrait être approfondie. Si la vitesse circonférentielle est faible et les crachements aux balais négligeables, ces derniers peuvent enlever de légères brûlures sur le collecteur.
APPLICATION: machines à grande vitesse, turbo-alternateurs, moteurs à petite et moyenne puissance (env. 30 KW), micro moteurs, moteurs universels, dynamos d'automobiles.

				10/40	10/20				
G4	35	1,40	15	30		10	25	n	n
G6	25	1,57	12	20		10	25	n	n
G1	7	1,80	18		93	10	35	n	n
T1	12	1,48	15		80	10	45	n	n
TU	12	1,40	5		15	10	60	n	n
T3	40	1,54	7		75	10	50	n	n
G47	400	1,38	12	15		8	25	m	h
G67	250	1,41	10	10		8	20	m	n

RESIN BONDED GRADES

High resistance, high transient voltage and large ratio of vertical and horizontal resistance, all facts which influence favourably the suppression of commutating currents.
APPLICATION: Schorch and Schrage type A. C. commutator motors, D. C. up to 30 KW auxiliar brushes for cross-field exitation, 3-phase commutator machines, repulsion motors, converters, fractional h. p. motors, thyristor controlled motors etc.

BALAIS GRAPHITIQUES BAKELISES

Ils se distinguent par leur résistance et par leur chute de contact élevées ainsi que le rapport de la résistance transversale à la résistance longitudinale, agissant favorablement sur l'atténuation des courants de commutation.
APPLICATION: moteurs courant alternatif à collecteur du type Schrage et Schorch, machines CC, traction ou stationnaires, à vitesses réglables et moyennes, balais auxiliaires pour exitation du champ transversal etc.

UG	80	1,75	15	70	8	35	m	n
UG 1	450	1,70	31	80	5	35	s.h.	n
UG 2	600	1,65	37	85	5	35	s.h.	n
UG 8	120	1,75	18	70	8	40	h	n
UG 9	190	1,52	10	20	8	40	h	n
UG12	220	1,75	22	75	8	40	h	n
V12	250	1,55	25	80	8	45	h	n
UG13	180	1,80	40	90	8	40	h	n
UC 4	350	1,75	25	80	9	40	h	n
UC15	14	1,85	27	90	12	35	n	n
UG25	--	1,57	20	80	8	35	lubricating brush charbon lubrifiant	

SYMBOLS – LEGENDE:

	voltage drop – chute au contact	friction – frottement
"s.n."	– 1,0 V	– 0,15
"n"	1,0 – 1,8 V	0,15 – 0,20
"m"	1,8 – 2,5 V	0,20 – 0,26
"h"	2,5 – 3,5 V	higher/plus de 0,26
"s.h."	higher/plus de 3,5 V	

Besides the standard grades we manufacture special grades for carbon vanes, bearings, electrodes for pulse circuit machines etc. **All carbon grades can be impregnated** as to improve values such as friction, radio interference, mechanical strength etc.
Please consider the following pages as well the questionnaire in case of problems.

En plus des qualités standard nous fabriquons des qualités spéciales (vannes de pompes, coussinets en carbone, électrodes pour machines à érosion, etc.). **Toutes nos qualités peuvent subir un traitement spécial** pour améliorer le frottement, la capacité d'antiparasitage, la résistance à la rupture et la dureté.
Veuillez considerer les informations suivantes et la questionnaire en cas de problèmes.

APPENDIX B EXPERIMENT RESULTS

TEST-1								
	Step-up transformer HV output voltage		Carbon strip voltage		Current		Step-down transformer LV output voltage	
Frequency (Hz)	Amplitude (V)	Relative Amplitude	Amplitude (V)	Relative Amplitude	Amplitude (mV)	Relative Amplitude	Amplitude (V)	Relative Amplitude
50	66.12	1.00	63.17	1.00	203.8	1.00	61.95	1.00
100	0.25	< 0.01	0.80	0.01	15.3	0.08	0.80	0.01
150	1.73	0.03	2.31	0.04	9.3	0.05	2.25	0.04
200			0.53	0.01	3.1	0.02	0.46	0.01
250	0.25	< 0.01	0.38	0.01			0.86	0.01
300			0.38	0.01			0.37	0.01
350	0.84	0.01	0.59	0.01	3.2	0.02	1.27	0.02
400			0.40	0.01	1.1	0.01	0.29	0.01
450	0.75	0.01	0.77	0.01	2.2	0.01	0.28	0.01
500	0.16	< 0.01	0.30	0.01			0.28	0.01
550								
600	0.19	< 0.01	0.30	0.01			0.38	0.01
650	0.19	< 0.01					0.19	< 0.01
700							0.27	< 0.01
750							0.40	0.01

TEST-2								
	Step-up transformer HV output voltage		Carbon strip voltage		Current		Step-down transformer LV output voltage	
Frequency (Hz)	Amplitude (V)	Relative Amplitude	Amplitude (V)	Relative Amplitude	Amplitude (mV)	Relative Amplitude	Amplitude (V)	Relative Amplitude
50	65.57	1.00	58.70	1.00	160.8	1.00	57.02	1.00
100	0.29	< 0.01	1.92	0.03	44	0.27	1.78	0.03
150	2.78	0.04	4.41	0.08	125	0.78	4.50	0.08
200	0.65	0.01	2.14	0.04	99.9	0.62	2.03	0.04
250	0.65	0.01	0.94	0.02	79.6	0.50	0.97	0.02
300	0.78	0.01	2.28	0.04	111	0.69	2.18	0.04
350	0.27	< 0.01	0.62	0.01	34.51	0.22	0.60	0.01
400	0.82	0.01	1.82	0.03	71	0.44	1.73	0.03
450	0.85	0.01	0.85	0.02	32.7	0.20	0.79	0.01
500	0.77	0.01	1.48	0.03	47.2	0.29	1.40	0.03
550	0.33	0.01	0.95	0.02	20.7	0.13	0.90	0.02
600	0.52	0.01	0.77	0.01	48	0.30	0.72	0.01
650	0.75	0.01	1.00	0.02	28	0.17	0.95	0.02
700			0.43	0.01	34	0.21	0.40	0.01
750			0.66	0.01	40.3	0.25	0.65	0.01
800			0.35	0.01			0.31	0.01
850			0.51	0.01	47	0.29	0.46	0.01

TEST-3								
	Step-up transformer HV output voltage		Carbon strip voltage		Current		Step-down transformer LV output voltage	
Frequency (Hz)	Amplitude (V)	Relative Amplitude	Amplitude (V)	Relative Amplitude	Amplitude (mV)	Relative Amplitude	Amplitude (V)	Relative Amplitude
50	67.01	1.00	61.27	1.00	376.1	1,00	57.50	1.00
100	0.68	0.01	2.17	0.04	76.7	0,20	1.76	0.03
150	2.74	0.04	4.18	0.07	60.8	0,16	4.13	0.07
200	0.55	0.01	1.72	0.03	30.1	0,08	1.53	0.03
250	0.37	0.01	1.01	0.02	59.4	0,16	1.10	0.02
300	0.61	0.01	1.41	0.02	59.6	0,16	1.29	0.02
350	0.66	0.01	0.55	0.01	33.2	0,09	0.53	0.01
400	0.52	0.01	1.12	0.02	68.7	0,18	1.03	0.02
450	0.30	0.00	1.18	0.02		0,00	1.04	0.02
500	0.34	0.01	0.71	0.01	53.1	0,14	0.65	0.01
550	0.46	0.01	0.45	0.01	26.7	0,07	0.73	0.01
600			0.52	0.01	29.3	0,08	0.48	0.01
650	0.56	0.01	0.72	0.01	25.3	0,07	0.55	0.01
700				0.00	25.1	0,07		0.00
750	0.78	0.01	0.40	0.01		0,00	0.35	0.01
800				0.00	27.9	0,07		0.00
850	0.50	0.01	0.38	0.01	28.5	0,08	0.49	0.01

TEST-4								
	Step-up transformer HV output voltage		Carbon strip voltage		Current		Step-down transformer LV output voltage	
Frequency (Hz)	Amplitude (V)	Relative Amplitude	Amplitude (V)	Relative Amplitude	Amplitude (mV)	Relative Amplitude	Amplitude (V)	Relative Amplitude
50	66.22	1.00	61.12	1.00	358.0	1.00	57.33	1.00
100	0.54	0.01	2.26	0.04	75.2	0.21	1.99	0.03
150	3.32	0.05	3.59	0.06	94.3	0.26	3.64	0.06
200	0.64	0.01	1.39	0.02	53.3	0.15	1.22	0.02
250			1.15	0.02	79.0	0.22	1.13	0.02
300	0.62	0.01	1.05	0.02	99.6	0.28	0.94	0.02
350	0.35	0.01	0.66	0.01	39.7	0.11	0.58	0.01
400	0.48	0.01	0.66	0.01	103.8	0.29	0.59	0.01
450	0.48	0.01	1.19	0.02	46.8	0.13	0.99	0.02
500	0.36	0.01	0.34	0.01	68.6	0.19	0.34	0.01
550	0.7	0.01	0.28	< 0.01	59.3	0.17	0.27	< 0.01
600	0.28	0.00	0.30	< 0.01	22.9	0.06	0.24	< 0.01
650	0.61	0.01	0.60	0.01	47.9	0.13	0.53	0.01
700	0.26	< 0.01	0.39	0.01	23.8	0.07		0.00
750	0.36	0.01			26.7	0.07	0.34	0.01
800					27.3	0.08		
850					34.6	0.10		

TEST-5								
	Step-up transformer HV output voltage		Carbon strip voltage		Current		Step-down transformer LV output voltage	
Frequency (Hz)	Amplitude (V)	Relative Amplitude	Amplitude (V)	Relative Amplitude	Amplitude (mV)	Relative Amplitude	Amplitude (V)	Relative Amplitude
50	66.31	1.00	56.17	1.00	174.3	1.00	54.56	1.00
100	0.35	0.01	2.81	0.05	21.9	0.13	2.63	0.05
150	2.64	0.04	7.77	0.14	69.1	0.40	7.75	0.14
200	1.13	0.02	4.10	0.07	43.3	0.25	3.92	0.07
250	0.96	0.01	2.98	0.05	54.2	0.31	2.90	0.05
300	1.36	0.02	3.74	0.07	44.6	0.26	3.59	0.07
350	0.68	0.01	1.50	0.03	41.9	0.24	1.46	0.03
400	1.23	0.02	2.48	0.04	46.1	0.26	2.36	0.04
450	1.16	0.02	1.03	0.02	30.1	0.17	0.97	0.02
500	0.93	0.01	1.48	0.03	48.4	0.28	1.49	0.03
550			0.73	0.01	18.7	0.11	0.76	0.01
600	0.88	0.01	1.20	0.02	48.2	0.28	1.15	0.02
650	0.58	0.01	0.48	0.01	12.8	0.07		0.00
700	0.86	0.01	0.88	0.02	45.53	0.26	0.81	0.01
750	0.73	0.01			14.8	0.08		
800	0.41	0.01			40.6	0.23		
850	0.43	0.01			19.6	0.11		

APPENDIX C ZAGREB ARC MODEL

```
MODEL ZAGREB
        INPUT U1, U2
        OUTPUT RB
        VAR I, RB2, RB, G, G2, TAU
INIT
        RB:=0.0001
ENDINIT
EXEC
        I:=(U1-U2)/RB
        IF (ABS(I)>1.E-12) THEN
                G:=(1./RB)
                TAU:=(1.5E-6*(G**0.17))
                G2:=((I**2.)/(4000000.*(G**0.68))-G)*(1-1./EXP(timestep/TAU))
                RB2:=(1./ABS(G+G2))
                RB:=RB2
        ENDIF
ENDEXEC
ENDMODEL
```

APPENDIX D AIRARC ARC MODEL

```
MODEL AirArc
        CONST
                Io {val:2000.0}
                Ua {val:1100.0}
                Rohm {val:0.015}
                Ub {val:1200.0}
                AA {val:0.45}
                BB {val:5.25}
                topen {val:0.056}
        INPUT
                current
        OUTPUT
                Rarc
        VAR
                Uarc, Rarc, ib, state, p, conduc
INIT
        Uarc:=0.0; Rarc:=1.0e-6; ib:=0.1; state:=0; p:=0; conduc:=0
ENDINIT
EXEC
        IF t>topen THEN
                IF abs(current)<1.e-9 THEN
                        Rarc:=1.e-9
                        state:=1
                ELSE
                        state:=0
                ENDIF
                IF state=0 THEN
                        IF abs((current))<Io THEN
```

```
                ib:=Io
            ELSE
                ib:=abs((current))
            ENDIF
            p:=(Ua+Ub*Io/ib+Rohm*abs(ib))
            Uarc:=p*sign((current))
            IF t>topen THEN
            Uarc:=Uarc*(1+AA*exp(BB*(t-0.02)))
            ENDIF
            Rarc:=Uarc/((current))
            conduc:=1.0/Rarc
        ENDIF
    ELSE
    Rarc:=1.e-6
    ENDIF
ENDEXEC
ENDMODEL
```

APPENDIX E MAYR ARC MODEL

```
MODEL Z1

INPUT U1, U2
OUTPUT RB
VAR I, RB2, RB, G, G2, TAU

INIT
RB:=0.0001
ENDINIT

EXEC
I:=(U1-U2)/RB
IF (ABS(I)>1.E-12) THEN
        G:=(1./RB)
        TAU:=(1.5E-6*(G**0.17))
        G2:=((I**2.)/(40.*(G**0.665))-G)*(1-1./EXP(timestep/TAU))
        RB2:=(1./ABS(G+G2))
        RB:=RB2
ENDIF
ENDEXEC
ENDMODEL
```

APPENDIX F CASSIE ARC MODEL

```
MODEL CASSIE

INPUT U1, U2
OUTPUT RB
VAR I, RB2, RB, G, G2, TAU

INIT
RB:=0.0001
ENDINIT

EXEC
I:=(U1-U2)/RB
IF (ABS(I)>1.E-12) THEN
        G:=(1./RB)
        TAU:=(1.5E-6*(G**0.17))
        G2:=((I*(U1-U2))/(600*600)-G)*(1-1./EXP(timestep/TAU))
        RB2:=(1./ABS(G+G2))
        RB:=RB2
ENDIF
ENDEXEC
ENDMODEL
```

APPENDIX G HYBRID ARC MODEL

```
MODEL HYBRID

INPUT U1, U2
OUTPUT RB
VAR I, RB2, RB, G, G2, TAU, GM, GM2, GC, GC2

INIT
RB:=0.0001
GM:=10000
GC:=10000
ENDINIT

EXEC
I:=(U1-U2)/RB
IF (ABS(I)>1.E-12) AND (ABS(I)<2.E-3) THEN
        G:=(1./RB)
        TAU:=(1.5E-6*(G**0.17))
        G2:=((I**2.)/(40.*(G**0.66))-G)*(1-1./EXP(timestep/TAU))
        RB2:=(1./ABS(G+G2))
        RB:=RB2
ENDIF
IF (ABS(I)>=2.E-3) THEN
        G:=(1./RB)
        TAU:=(1.5E-6*(G**0.17))
        G2:=((I*(U1-U2))/(600*600)-G)*(1-1./EXP(timestep/TAU))
        RB2:=(1./ABS(G+G2))
        RB:=RB2
ENDIF
```

```
ENDEXEC
ENDMODEL
```